Morten Hjorth-Jensen, Maria Paola Lombardo, and Ubirajara van Kolck, Editors

An advanced course in computational nuclear physics

Bridging the scales from quarks to neutron stars

June 1, 2016

Springer

No Title Given

No Author Given

Preface

This graduate-level text collects and synthesizes nine series of lectures on the nuclear quantum many-body problem - starting from our present understanding of the underlying forces with a presentation of recent advances within the field of lattice quantum chromodynamics, via effective field theories to central many-body methods like Monte Carlo methods, coupled cluster theories, similarity renormalization group and large-scale diagonalization approaches.

In particular algorithmic and computational advances show promise for breakthroughs in predictive power including proper error estimates, a better understanding of the underlying effective degrees of freedom and of the respective forces at play.

Enabled by recent advances in theoretical, experimental and numerical techniques, the modern and state-of-the art applications considered in this volume span the entire range from our smallest components, quarks and gluons as the mediators of the strong force to the computation of the equation of state for neutron star matter.

The present lectures provide a proper exposition of the underlying theoretical and algorithmic approaches as well as strong ties to the numerical implementation of the exposed methods. Each series of lectures provides a proper link to actual numerical software. The latter will enable the reader to build upon these and develop his/her own insights about these methods, as well as using the corresponding codes for developing own programs for tackling challenging nuclear many-body problems.

Contents

Chapter 1
Motivation and overarching aims

Morten Hjorth-Jensen, Maria Paola Lombardo, and Ubirajara van Kolck

Abstract Our presentation

Nuclear physics has recently experienced several discoveries and technological advances that address the fundamental questions of the field, in particular how nuclei emerge from the strong dynamics of quantum chromodynamics (QCD). Many of these advances have been made possible by significant investments in frontier research facilities worldwide over the last two decades. Some of these discoveries are the detection of perhaps the most exotic state of matter, the quark-gluon plasma, which is believed to have existed in the very first moments of the Universe (refs). Recent experiments have validated the standard solar model and established that neutrinos have mass (refs). High-precision measurements of the quark structure of the nucleon are challenging existing theoretical understanding. Nuclear physicists have started to explore a completely unknown landscape of nuclei with extreme neutron-to-proton ratios using radioactive and short-lived ions, including rare and very neutron-rich isotopes. These experiments push us towards the extremes of nuclear stability. Moreover, these rare nuclei lie at the heart of nucleosynthesis processes in the universe and are therefore an important component in the puzzle of matter generation in the universe.

A firm experimental and theoretical understanding of nuclear stability in terms of the basic constituents is a huge intellectual endeavor. Experiments indicate that developing a comprehensive description of all nuclei and their reactions requires theoretical and experimental investigations of rare isotopes with unusual neutron-to-proton ratios that are very different from their stable counterparts. These rare nuclei are difficult to produce and study experimentally since they can have extremely short lifetimes. Theoretical approaches to these nuclei involve solving the nuclear many-body problem.

Accompanying these developments, a qualitative change has swept the nuclear theory landscape thanks to a combination of techniques that is allowing, for the first time, th direct connection between QCD and nuclear structure. This transformation has been brought by a dramatic improvement in the capability of numerical calculations both in QCD, via lattice simulations, and in the nuclear many-body problem, via "ab initio" methods for the diagonilization of non-relativistic Hamiltonians. Simultaneously, the framework of effective field

Morten Hjorth-Jensen
Department of Physics and Astronomy and National Superconducting Cyclotron Laboratory, Michigan State University, East Lansing, Michigan, USA and Department of Physics, University of Oslo, Oslo, Norway, e-mail: hjensen@msu.edu,

Maria Paola Lombardo
Name and address of institution(s), e-mail: mariapaola.lombardo@lnf.infn.it,

Ubirajara van Kolck
Name and address of institution(s), e-mail: vankolck@ipno.in2p3.fr

theories builts a bridge between the two numerical approaches, allowing to convert the results of lattice QCD into input to ab initio methods.

Now, algorithmic and computational advances hold promise for breakthroughs in predictive power including proper error estimates, enhancing the already strong links between theory and experiment. These advances include better ab initio many-body methods as well as a better understanding of the underlying effective degrees of freedom and the respective forces at play. And obviously better numerical algorithms as well as developments in high-performance computing. This will provide us with important new insights about the stability of nuclear matter and allow us to relate these novel understandings to the underlying laws of motion, the corresponding forces and the pertinent fundamental building blocks.

Important issues such as whether we can explain from first-principle methods the existence of magic numbers and their vanishing as we add more and more nucleons, how the binding energy of neutron-rich nuclei behaves, or the radii, neutron skins, and many many other probes that extract information about many-body correlations as nuclei evolve towards their limits of stability — these are all fundamental questions which, combined with recent experimental and theoretical advances, will allow us to advance our basic knowledge about the limits of stability of matter, and, hopefully, help us in gaining a better understanding of visible matter.

It is within this framework the present texts finds its rationale. This text collects and synthesizes seven series of lectures on the nuclear many-body problem, starting from our present understanding of the underlying forces with a presentation of recent advances within the field of lattice QCD, via effective field theories to central many-body methods like Monte Carlo, coupled-cluster, and large-scale diagonalization methods. The applications span from our smallest components, quarks and gluons as the mediators of the strong force to the computation of the equation of state for infinite nuclear matter and neutron star matter. The lectures provide a proper exposition of the underlying theoretical and algorithmic approaches as well as strong ties to the numerical implementation of the exposed methods. The lectures propose exercises, often providing a proper link to actual numerical software The latter will enable the reader to build upon these and develop his/her own insights about these methods, as well as using these codes for developing his/her own programs for tackling complicated many-body problems.

Chapter 2
Quantum Chromodynamics

Thomas Schäfer

Abstract We present a brief introduction to QCD, the QCD phase diagram, and non-equilibrium phenomena in QCD. We emphasize aspects of the theory that can be addressed using computational methods, in particular euclidean path integral Monte Carlo, fluid dynamics, kinetic theory, classical field theory and holographic duality.

2.1 Introduction

The goal of this chapter is to provide a brief summary of Quantum Chromodynamics (QCD) and the QCD phase diagram, and to give an introduction to computational methods that are being used to study different aspects of QCD. Quantum Chromodynamics is a remarkable theory in many respects. QCD is an almost parameter free theory. Indeed, in the context of nuclear physics QCD is completely characterized by the masses of the up, down, and strange quark, and a reasonable caricature of nuclear physics emerges in the even simpler case in which the up and down quark are taken to be massless, and the strange quark is infinitely heavy. QCD nevertheless accounts for the incredible richness of the phase diagram of strongly interacting matter. QCD describes finite nuclei, normal and superfluid states of nuclear matter, color superconductors, hadronic gases, quark gluon plasma, and many other states. This rich variety of states is reflected in the large number of computational methods that have been brought to bear on problems in QCD. This includes a large number of methods for the structure and excitations of finite Fermi systems, quantum Monte Carlo methods, and a variety of tools for equilibrium and non-equilibrium statistical mechanics.

The bulk of this book is devoted to the study of few and many nucleon systems. Summarizing everything else in one brief chapter is obviously out of the question, both because of limitations of space and because of my limited expertise. I will therefore be very selective, and focus on a number of very simple yet powerful ideas. This reflects, in part, my background, which is not primarily in computational physics. It also reflects my conviction that progress in computational physics is unfortunately often reflected in increasingly complicated codes that obscure the simplicity of the underlying methods.

Thomas Schäfer
Department of Physics, North Carolina State University, Raleigh, NC 27695, USA, e-mail: tmschaef@ncsu.edu

2.2 Path integrals and the Metropolis algorithm

Consider a simple quantum mechanical problem, the motion of a particle in a one-dimensional potential. In order to be specific I will focus on the double well potential $V(x) = \lambda(x^2-\eta^2)^2$, where η and λ are parameters. The Hamiltonian is

$$H = \frac{p^2}{2m} + \lambda(x^2-\eta^2)^2\,. \tag{2.1}$$

Using a change of variables I can set $2m = \lambda = 1$. This implies that there is only one physical parameter in this problem, the barrier separation η. The regime $\eta \gg 1$ corresponds to the limit in which the system has two almost degenerate minima that are split by semi-classical tunneling events. The energy eigenstates and wave functions are solutions of the eigenvalue problem $H|n\rangle = |n\rangle E_n$. Once the eigenstates are known I can compute all possible correlation functions

$$\Pi_n(t_1,t_2,\ldots,t_n) = \langle 0|x(t_1)x(t_2)\ldots x(t_n)|0\rangle\,, \tag{2.2}$$

by inserting complete sets of states. An alternative to the Hamiltonian formulation of the problem is the Feynman path integral [1]. The path integral for the anharmonic oscillator is given by

$$\langle x_1|e^{-iHt_f}|x_0\rangle = \int_{x(0)=x_0}^{x(t_f)=x_1} \mathscr{D}x\, e^{iS}, \qquad S = \int_0^{t_f} dt\, \left(\frac{1}{4}\dot{x}^4 - (x^2-\eta^2)^2\right). \tag{2.3}$$

This expression contains a rapidly oscillating phase factor e^{iS}, which prohibits any direct numerical attempt at computing the path integral. The standard approach is based on analytic continuation to imaginary time $\tau = it$. This is also referred to as Euclidean time, because the Minkowski interval $dx^2 - dt^2$ turns into the Euclidean expression $dx^2 + d\tau^2$. In the following I will consider the euclidean partition function

$$Z(T) = \int \mathscr{D}x\, e^{-S_E}, \qquad S_E = \int_0^{\beta} d\tau\, \left(\frac{1}{4}\dot{x}^4 + (x^2-\eta^2)^2\right), \tag{2.4}$$

where $\beta = 1/T$ is the inverse temperature. To see that equ. (2.4) we can use equ. (2.3) to show that $Z(T)$ can be expressed in terms of the eigenvalues of the Hamiltonian, $Z(T) = \sum_n \exp(-E_n/T)$. In the following I will describe numerical simulations using a discretized version of the euclidean action. For this purpose I discretize the euclidean time coordinate $\tau_j = ja, i = 1,\ldots n$ where $a = \beta/n$ is the length of time interval. The discretized action is given by

$$S = \sum_{i=1}^{n} \left\{ \frac{1}{4a}(x_i - x_{i-1})^2 + a(x_i^2-\eta^2)^2 \right\}, \tag{2.5}$$

where $x_i = x(\tau_i)$. I consider periodic boundary conditions $x_0 = x_n$. The discretized euclidean path integral is formally equivalent to the partition function of a statistical system of (continuous) "spins" x_i arranged on a one-dimensional lattice. This statistical system can be studied using standard Monte-Carlo sampling methods. In the following I will use the Metropolis algorithm [2]. Detailed numerical studies of the euclidean path integral can be found in [3–6].

The Metropolis method generates an ensemble of configurations $\{x_i\}^{(k)}$ where $i = 1,\ldots,n$ labels the lattice points and $k = 1,\ldots,N_{conf}$ labels the configurations. Quantum mechanical averages are computed by averaging observables over many configurations,

$$\langle \mathscr{O} \rangle = \lim_{N_{conf}\to\infty} \frac{1}{N_{conf}} \sum_{k=1}^{N_{conf}} \mathscr{O}^{(k)} \tag{2.6}$$

where $\mathcal{O}^{(k)}$ is the value of the classical observable $\mathcal{O}$ in the configuration $\{x_i\}^{(k)}$. The configurations are generated using Metropolis updates $\{x_i\}^{(k)} \to \{x_i\}^{(k+1)}$. The update consists of a sweep through the lattice during which a trial update $x_i^{(k+1)} = x_i^{(k)} + \delta x$ is performed for every lattice site. Here, δx is a random number. The trial update is accepted with probability

$$P\left(x_i^{(k)} \to x_i^{(k+1)}\right) = \min\left\{\exp(-\Delta S), 1\right\}, \tag{2.7}$$

where ΔS is the change in the action equ. (2.5). This ensures that the configurations $\{x_i\}^{(k)}$ are distributed according the "Boltzmann" distribution $\exp(-S)$. The distribution of δx is arbitrary as long as the trial update is micro-reversible, i. e. is equally likely to change $x_i^{(k)}$ to $x_i^{(k+1)}$ and back. The initial configuration is arbitrary. In order to study equilibration it is useful to compare an ordered (cold) start with $\{x_i\}^{(0)} = \{\eta\}$ to a disordered (hot) start $\{x_i\}^{(0)} = \{r_i\}$, where r_i is a random variable.

The advantage of the Metropolis algorithm is its simplicity and robustness. The only parameter to adjust is the distribution of δx. A simple choice is to take δx to be a Gaussian random number, and choose the width of the distribution so that the average acceptance rate for the trial updates is around 50%. Fluctuations of $\mathcal{O}$ provide an estimate in the error of $\langle\mathcal{O}\rangle$. The uncertainty is given by

$$\Delta\langle\mathcal{O}\rangle = \sqrt{\frac{\langle\mathcal{O}^2\rangle - \langle\mathcal{O}\rangle^2}{N_{conf}}}. \tag{2.8}$$

This requires some care, because the error estimate is based on the assumption that the configurations are statistically independent. In practice this can be monitored by computing the auto-correlation "time" in successive measurements $\mathcal{O}(\{x_i\}^{(k)})$.

I have written a simple fortran code that implements the Metropolis algorithm for euclidean path integrals [6]. The most important part of that code is a sweep through the lattice with a Metropolis update on every site τ_j:

```
do j=1,n-1

      nhit = nhit+1

      xpm = (x(j)-x(j-1))/a
      xpp = (x(j+1)-x(j))/a
      t = 1.0/4.0*(xpm**2+xpp**2)
      v = (x(j)**2-f**2)**2
      sold = a*(t+v)

      xnew = x(j) + delx*(2.0*ran2(iseed)-1.0)

      xpm = (xnew-x(j-1))/a
      xpp = (x(j+1)-xnew)/a
      t = 1.0/4.0*(xpm**2+xpp**2)
      v = (xnew**2-f**2)**2
      snew = a*(t+v)
      dels = snew-sold

      p = ran2(iseed)
      if (exp(-dels) .gt. p) then
        x(j) = xnew
        nacc = nacc + 1
      endif

enddo
```

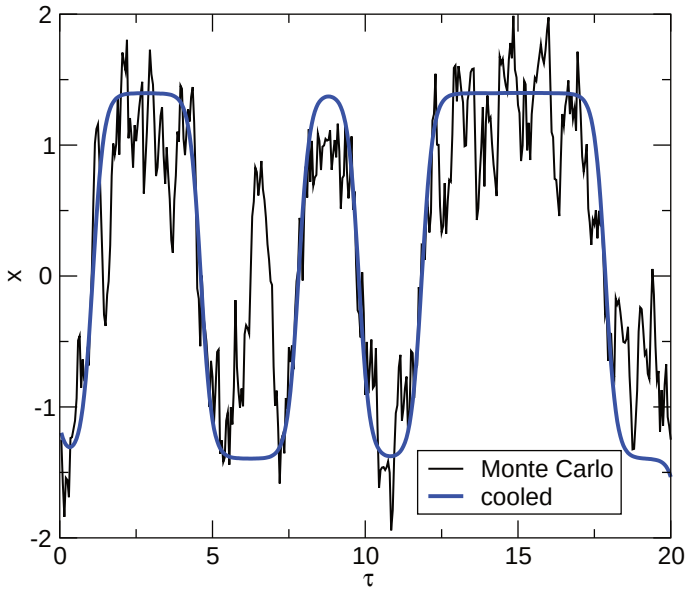

Fig. 2.1 Typical euclidean path obtained in a Monte Carlo simulation of the discretized euclidean action of the double well potential for $\eta = 1.4$. The lattice spacing in the euclidean time direction is $a = 0.05$ and the total number of lattice points is $N_\tau = 800$. The green curve shows the corresponding smooth path obtained by running 100 cooling sweeps on the original path.

Here, `sold` is the local action corresponding to the initial value of `x(j)`, and `snew` is the action after the trial update. The trial update is accepted if `exp(-dels)` is greater that the random variable `p`. The function `ran2()` generates a random number between 0 and 1, and `nacc/nhit` measures the acceptance rate. A typical path is shown in Fig. 2.1. An important feature of the paths in the double well potential is the presence of tunneling events. Indeed, in the semi-classical regime $\eta \gg 1$, a typical path can be understood as Gaussian fluctuations superimposed on a series of tunneling events (instantons).

The path integral method does not provide direct access to the eigenvalues of the Hamiltonian, but it can be used to compute imaginary time correlation functions

$$\Pi_n^E(\tau) = \langle x(\tau_1) \dots x(\tau_n) \rangle. \tag{2.9}$$

Note that the average is carried out with respect to the partition function in equ. (2.4). In the limit $\beta \to \infty$ this corresponds to the ground state expectation value. A very important observable is the two-point function $\Pi^E(\tau) \equiv \Pi_2^E(0,\tau)$. The euclidean correlation functions is related to the eigenstates of the Hamiltonian via a spectral representations. This representation is obtained by inserting a complete set of states into equ. (2.9). The result is

$$\Pi^E(\tau) = \sum_n |\langle 0|x|n\rangle|^2 \exp(-(E_n - E_0)\tau), \tag{2.10}$$

where E_n is the energy of the state $|n\rangle$. This can be written as

$$\Pi^E(\tau) = \int dE\, \rho(E) \exp(-(E - E_0)\tau), \tag{2.11}$$

where $\rho(E)$ is the spectral function. In the case of the double well potential there are only bound states and the spectral function is a sum of delta-functions. Equ. (2.10) shows that the

euclidean correlation function is easy to construct once the energy eigenvalues and eigenfunctions are known. The inverse problem is well defined in principle, but numerically much more difficult. The excitation energy of the first excited state $\Delta E_1 = E_1 - E_0$ is easy to extract from the exponential decay of the two-point functions, but higher states are more difficult to compute. A technique that can be used on order determine the spectral function from euclidean correlation functions is the maximum entropy image reconstruction method, see [7,8].

The calculation of correlation functions in a Monte Carlo simulation is very straightforward. All I need to do is multiply the values of $x(\tau_i)$ for a given path, and then average over all paths:

```
do ic=1,nc

    ncor = ncor + 1
    ip0 = int( (n-np)*ran2(iseed) )
    x0 = x(ip0)

    do ip=1,np
      x1 = x(ip0+ip)
      xcor = x0*x1
      x2cor= xcor**2
      xcor_sum(ip) = xcor_sum(ip) + xcor
      xcor2_sum(ip) = xcor2_sum(ip) + xcor**2
  enddo
enddo
```

The advantages of this method are that it is extremely robust, that it requires no knowledge (or preconceived notion) of what the wave function looks like, and that it can explore a very complicated configuration space. On the other hand, in the case of one-dimensional quantum mechanics, the Metropolis method is very inefficient. Using direct diagonalization in a finite basis it is not difficult to compute the energies of the first several states in the potential in equ. 2.1 with a very high accuracy, $\Delta E/E_0 \sim O(10^{-6})$ or better. On the other hand, using the Monte Carlo method, it is quite difficult to achieve an accuracy of $O(10^{-2})$ for observable other than $(E_1 - E_0)/E_0$. The advantage of the Monte Carlo method is that it scales much better towards high dimensional systems, such as quantum mechanics of many particles, or quantum field theory.

The Monte Carlo method also does not directly provide the ground state energy, or the partition function and free energy at finite temperature. In quantum mechanics we can compute the ground state energy from the expectation value of the Hamiltonian $\langle H \rangle = \langle T + V \rangle$ in the limit $\beta \to \infty$. The expectation value of the kinetic energy is singular as $a \to 0$, but this problem can be overcome by using the Virial theorem

$$\langle H \rangle = \left\langle \frac{x}{2} V' + V \right\rangle . \tag{2.12}$$

There is no simple analog of this method in quantum field theory. A method for computing the free energy which does generalize to quantum field theory is the adiabatic switching technique. The idea is to start from a reference system for which the free energy is known and calculate the free energy difference to the real system using Monte Carlo methods. For this purpose I write the action as

$$S_\alpha = S_0 + \alpha \Delta S, \tag{2.13}$$

where S is the full action, S_0 is the action of the reference system, ΔS is defined by $\Delta S = S - S_0$, and α is a coupling constant. The action S_α interpolates between the physical system and the reference system. Integrating the relation $\partial \log Z(\alpha)/(\partial \alpha) = -\langle \Delta S \rangle_\alpha$ I find

$$\log(Z(\alpha=1)) = \log(Z(\alpha=0)) - \int_0^1 d\alpha' \, \langle \Delta S \rangle_{\alpha'} \ , \tag{2.14}$$

where $\langle . \rangle_\alpha$ is computed using the action S_α. In the case of the anharmonic oscillator it is natural to use the harmonic oscillator as a reference system. In that case

$$Z(\alpha=0) = \sum_n \exp(-\beta E_n^0) = \frac{\exp(-\beta\omega_0/2)}{1-\exp(-\beta\omega_0)}, \tag{2.15}$$

where ω_0 is the oscillator constant. Note that the free energy of the anharmonic oscillator should be independent of the reference frequency ω_0. The integral over the coupling constant α can be calculated in a Monte Carlo simulation by slowly changing α from 0 to 1 during the simulation. Free energy calculations of this type play an important role in quantum chemistry, and more efficient methods for determining ΔF have been developed [9].

2.3 Quantumchromodynamics

2.3.1 QCD at zero temperature and density

The rich phenomenology of strong interacting matter is encoded in a deceptively simple Lagrangian. The fundamental fields in the Lagrangian are quark fields $q^c_{\alpha f}$ and gluon fields A^a_μ. Here, $\alpha = 1,\ldots,4$ is a Dirac spinor index, $c = 1,\ldots,N_c$ with $N_c = 3$ is a color index, and $f = up, down, strange, charm, bottom, top$ is a flavor index. Interactions in QCD are governed by the color degrees of freedom. The gluon field A^a_μ is a vector field labeled by an index $a = 1,\ldots,N_c^2-1$ in the adjoint representation. The N_c^2- multiplet of gluon fields can be used to construct a matrix valued field $A_\mu = A^a_\mu \frac{\lambda^a}{2}$, where λ^a is a set of traceless, Hermitian, $N_c \times N_c$ matrices. The QCD Lagrangian is

$$\mathscr{L} = -\frac{1}{4} G^a_{\mu\nu} G^a_{\mu\nu} + \sum_f^{N_f} \bar{q}_f (i\gamma^\mu D_\mu - m_f) q_f \, , \tag{2.16}$$

where $G^a_{\mu\nu}$ is the QCD field strength tensor defined by

$$G^a_{\mu\nu} = \partial_\mu A^a_\nu - \partial_\nu A^a_\mu + g f^{abc} A^b_\mu A^c_\nu \, , \tag{2.17}$$

and $f^{abc} = 4i\mathrm{Tr}([\lambda^a,\lambda^b]\lambda^c)$ are the $SU(N_c)$ structure constants. The action of the covariant derivative on the quark fields is

$$iD_\mu q = \left(i\partial_\mu + g A^a_\mu \frac{\lambda^a}{2} \right) q \, , \tag{2.18}$$

where m_f is the mass of the quarks. The terms in equ. (2.16) describe the interaction between quarks and gluons, as well as nonlinear three and four-gluon interactions. Note that, except for the number of flavors and their masses, the structure of the QCD Lagrangian is completely fixed by the local $SU(N_c)$ color symmetry.

A natural starting point for studying the phase diagram of hadronic matter is to consider the light flavors (up, down, and strange) as approximately massless, and the heavy flavors (charm, bottom, top) as infinitely massive. In this limit the QCD Lagrangian is completely characterized by two integer valued parameters, the number of colors $N_c = 3$ and flavors $N_f = 3$, and a single dimensionless coupling constant g. Quantum fluctuations cause the coupling constant to become scale dependent [10,11]. At one-loop order the running coupling constant

is

$$g^2(q^2) = \frac{16\pi^2}{b_0 \log(q^2/\Lambda_{QCD}^2)}\,, \qquad b_0 = \frac{11}{3}N_c - \frac{2}{3}N_f\,, \tag{2.19}$$

where q is a characteristic momentum and N_f is the number of active flavors. The scale dependence of the coupling implies that, as a quantum theory, QCD is not governed by a dimensionless coupling but by a dimensionful scale, the QCD scale parameter Λ_{QCD}. This phenomenon is known as dimensional transmutation [12].

A crucial aspect of the scale dependence of the coupling in QCD is that the effective interaction decreases as the energy or momentum scale is increased. This feature of QCD is called asymptotic freedom [10, 11]. It implies that high energy interactions can be analyzed using perturbative QCD. The flip side of asymptotic freedom is anti-screening, or confinement: The effective interaction between quarks increases with distance, and quarks are permanently confined into hadrons. The absence of colored states in the spectrum implies that the use of perturbation theory is subtle, even at high energy. Quantities that can be computed perturbatively either involve a sum over many hadronic states, or allow for a factorization of perturbative interactions and non-perturbative matrix elements.

If quarks are massless then QCD observables are dimensionless ratios like m_p/Λ_{QCD}, where m_p is the mass of the proton. This implies that the QCD scale is not a parameter of the theory, but reflects a choice of units. In the real world QCD is part of the standard model, quarks acquire masses by electroweak symmetry breaking, and the QCD scale is fixed by value of the coupling constant at the weak scale. Experiments determine the value of the QCD fine structure constant $\alpha_s = g^2/(4\pi)$ at the position of the Z boson pole, $\alpha_s(m_z) = 0.1184 \pm 0.0007$ [13]. The numerical value of Λ_{QCD} depends on the renormalization scheme used in computing quantum corrections to the coupling constant. Physical observables, as well as the value of b_0, are independent of this choice. In the modified minimal subtraction ($\overline{MS}$) scheme the scale parameter is $\Lambda_{QCD} \simeq 200$ MeV [13].

A schematic phase diagram of QCD is shown in Fig. 2.2. In this figure I show the phases of strongly interacting matter as a function of the temperature T and the baryon chemical potential μ. The chemical potential μ controls the baryon density ρ, defined as 1/3 times the number density of quarks minus the number density of anti-quarks. In the following I will explain that the basic structure of the phase diagram is determined by asymptotic freedom and the symmetries of QCD. For more detailed reviews see [14–16].

At small temperature and chemical potential the interaction between quarks is dominated by large distances and the effective coupling is strong. This implies that quarks and gluons are permanently confined in color singlet hadrons, with masses of order Λ_{QCD}. The proton, for example, has a mass of $m_p = 935$ MeV. A simplistic view of the structure of the proton is that it is a bound state of three constituent quarks with effective masses $m_Q \simeq m_p/3 \simeq \Lambda_{QCD}$. These masses should be compared to the bare up and down quark masses which are of the order 10 MeV.

As a consequence of strong interactions between virtual quarks and anti-quarks in the QCD ground state a vacuum condensate of $\bar{q}q$ pairs is generated, $\langle \bar{q}q \rangle \simeq -\Lambda_{QCD}^3$ [17–19]. This vacuum expectation value spontaneously breaks the approximate chiral $SU(3)_L \times SU(3)_R$ flavor symmetry of the QCD Lagrangian down to its diagonal subgroup, the flavor symmetry $SU(3)_V$. Spontaneous chiral symmetry breaking implies the existence of Goldstone bosons, massless modes with the quantum numbers of the generators of the broken axial symmetry $SU(3)_A$. The corresponding excitations in the spectrum of QCD are the π, K and η mesons. The $SU(3)_L \times SU(3)_R$ symmetry is explicitly broken by quark masses, and the mass of the charged pion is $m_\pi = 139$ MeV. This scale can be compared to the mass of the lightest non-Goldstone particle, the rho meson, which has a mass $m_\rho = 770$ MeV.

At low energy Goldstone bosons can be described in terms of an effective field theory in which composite π, K and η particles are treated as fundamental fields. The Goldstone boson

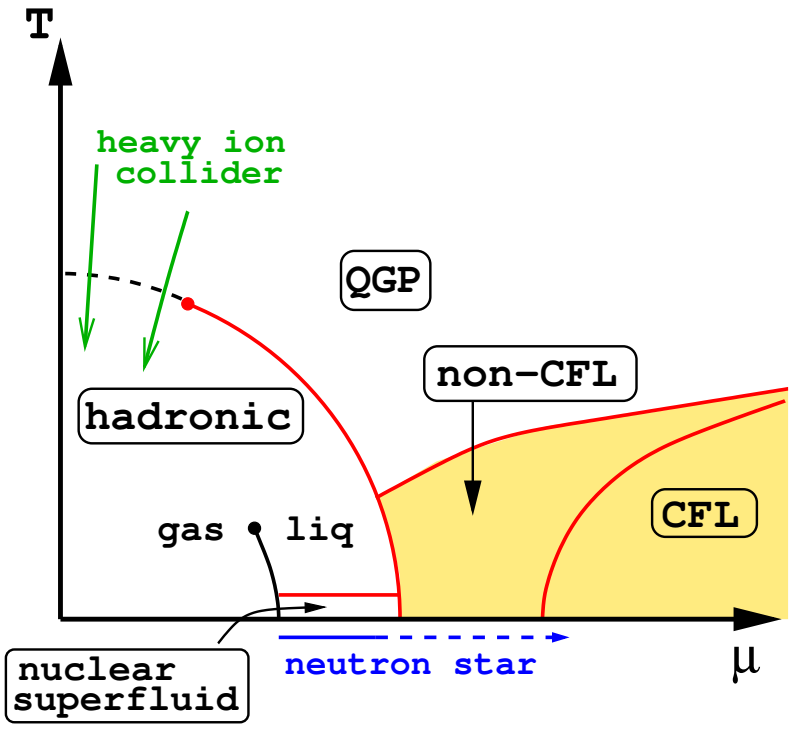

Fig. 2.2 Schematic phase diagram of QCD as a function of temperature T and baryon chemical potential μ. The quark gluon plasma phase is labeled QGP, and CFL refers to the color superconducting phase that is predicted to occur at asymptotically large chemical potential. The critical endpoints of the chiral and nuclear liquid-gas phase transitions, are denoted by red and black points, respectively. The chiral pseudo-critical line associated with the crossover transition at low temperature is shown as a dashed line. The green arrows indicate the regions of the phase diagram that can be studied by the experimental heavy ion programs at RHIC and the LHC.

field can be parametrized by unitary matrices

$$\Sigma = \exp(i\lambda^a \phi^a / f_\pi)\,, \tag{2.20}$$

where λ^a are the Gell-Mann matrices for $SU(3)$ flavor and $f_\pi = 93$ MeV is the pion decay constant. For example, $\pi^0 = \phi^3$ and $\pi^\pm = (\phi_1 \pm i\phi_2)/2$ describe the neutral and charged pion. Other components of ϕ^a describe the neutral and charged kaons, as well as the eta. The eta prime, which is the $SU(3)_F$ singlet meson, acquires a large mass because of the axial anomaly, and is not a Goldstone boson. The axial anomaly refers to the fact that the flavor singlet axial current, which is conserved in massless QCD at the classical level, is not conserved if quantum effects are taken into account. The divergence of the axial current $A_\mu = \bar{q}\gamma_\mu\gamma_5 q$ is

$$\partial_\mu A^\mu = \frac{g^2 N_f}{32\pi^2}\varepsilon^{\mu\nu\alpha\beta} G^a_{\mu\nu} G^a_{\alpha\beta}\,. \tag{2.21}$$

The right hand side is the topological charge density, which I will discuss in more detail in Sect. 2.4.3.

At low energy the effective Lagrangian for the chiral field can be organized as a derivative expansion in gradients of Σ. Higher derivative terms describe interactions that scale as either the momentum or the energy of the Goldstone boson. Since Goldstone bosons are approximately massless, the energy is of the same order of magnitude as the momentum. We will see that the expansion parameter is $p/(4\pi f_\pi)$. At leading order in (∂/f_π) there is only one

possible term which is consistent with chiral symmetry, Lorentz invariance and the discrete symmetries C,P,T. This is the Lagrangian of the non-linear sigma model

$$\mathscr{L} = \frac{f_\pi^2}{4}\mathrm{Tr}\left[\partial_\mu \Sigma \partial^\mu \Sigma^\dagger\right] + \left[B\mathrm{Tr}(M\Sigma^\dagger) + h.c.\right] + \ldots, \tag{2.22}$$

where the term proportional to B takes into account explicit symmetry breaking. Here, $M = \mathrm{diag}(m_u, m_d, m_s)$ is the quark mass matrix and B is a low energy constant that I will fix below.

First, I will show that the parameter f_π controls the pion decay amplitude. For this purpose I have to gauge the non-linear sigma model. As usual, this is achieved by promoting the derivative to a gauge covariant operator $\nabla_\mu \Sigma = \partial_\mu \Sigma + i g_w W_\mu \Sigma$ where W_μ is the charged weak gauge boson and g_w is the weak coupling constant. The gauged non-linear sigma model gives a pion-W boson interaction

$$\mathscr{L} = g_w f_\pi W_\mu^\pm \partial^\mu \pi^\mp . \tag{2.23}$$

This term contributes to the amplitude for the decay $\pi^\pm \to W^\pm \to e^\pm \nu_e$. We get $\mathscr{A} = g_w f_\pi q_\mu$, where q_μ is the momentum of the pion. This result agrees with the definition of f_π in terms of the weak axial current matrix element of the pion, $\langle 0|A_\mu^a|\pi^b\rangle = f_\pi q_\mu \delta^{ab}$.

In the ground state $\Sigma = 1$ and the ground state energy is $E_{vac} = -2B\mathrm{Tr}[M]$. Using the relation $\langle \bar{q}q\rangle = \partial E_{vac}/(\partial m)$ we find $\langle \bar{q}q\rangle = -2B$. Fluctuations around $\Sigma = 1$ determine the masses of the Goldstone bosons. The pion mass satisfies the Gell-Mann-Oaks-Renner relation (GMOR) [17]

$$m_\pi^2 f_\pi^2 = -(m_u + m_d)\langle \bar{q}q\rangle \tag{2.24}$$

and analogous relations exist for the kaon and eta masses. This result shows the characteristic non-analytic dependence of the pion mass on the quark masses, $m_\pi \sim \sqrt{m_q}$.

2.3.2 QCD at finite temperature

The structured of QCD at high temperature can be analyzed using the assumption that quarks and gluons are approximately free. We will see that this assumption is internally consistent, and that it is confirmed by lattice calculations. If the temperature is large then quarks and gluons have thermal momenta $p \sim T \gg \Lambda_{QCD}$. Asymptotic freedom implies that these particles are weakly interacting, and that they form a plasma of mobile color charges, the quark gluon plasma (QGP) [20, 21]. The pressure of a gas of quarks and gluons is

$$P = \frac{\pi^2 T^4}{90}\left(2\left(N_c^2 - 1\right) + 4N_c N_f \frac{7}{8}\right). \tag{2.25}$$

This is the Stefan-Boltzmann law, where $2(N_c^2 - 1)$ is the number of bosonic degrees of freedom, and $4N_c N_F$ is the number of fermions. The factor 7/8 takes into account the difference between Bose and Fermi statistics. The pressure of a QGP is parametrically much bigger than the pressure of a pion gas, indicating that the QGP at high temperature is thermodynamically stable.

The argument that the QGP at asymptotically high temperature is weakly coupled is somewhat more subtle than it might appear at first glance. If two quarks or gluons in the plasma interact via large angle scattering then the momentum transfer is large, and asymptotic freedom implies that the effective coupling is weak. However, the color Coulomb interaction is dominated by small angle scattering, and it is not immediately clear why the effective interaction that governs small angle scattering is weak. The basic observation is that in a high temperature plasma there is a large thermal population ($n \sim T^3$) of mobile color charges that

screen the interaction at distances beyond the Debye length $r_D \sim 1/(gT)$. We also note that even in the limit $T \gg \Lambda_{QCD}$ the QGP contains a non-perturbative sector of static magnetic color fields [22]. This sector of the theory, corresponding to energies below the magnetic screening scale $m_M \lesssim g^2 T$, is strongly coupled, but it does not contribute to thermodynamic or transport properties of the plasma in the limit $T \to \infty$.

The quark gluon plasma exhibits neither color confinement nor chiral symmetry breaking. This implies that the high temperature phase must be separated from the low temperature hadronic phase by a phase transition. The order of this transition is very sensitive to the values of the quark masses. In QCD with massless u,d and infinitely massive s,c,b,t quarks the transition is second order [23]. In the case of massless (or sufficiently light) u,d,s quarks the transition is first order. Lattice simulations show that for realistic quark masses, $m_u \simeq m_d \simeq 10$ MeV and $m_s \simeq 120$ MeV, the phase transition is a rapid crossover [24, 25]. The transition temperature, defined in terms of the chiral susceptibility, is $T_c \simeq 151 \pm 3 \pm 3$ MeV [26, 27], which is consistent with the result 154 ± 9 MeV reported in [25, 28].

The phase transition is expected to strengthen as a function of chemical potential, so that there is a critical baryon chemical potential μ at which the crossover turns into a first order phase transition [29]. This critical point is the endpoint of the chiral phase transition. Because of the fermion sign problem, which I will discuss in Sect. 2.4.4, it is very difficult to locate the critical endpoint using simulations on the lattice. Model calculations typically predict the existence of a critical point, but do not constrain its location. A number of exploratory lattice calculations have been performed [30–35], but at the time I am writing these notes it has not been demonstrated conclusively that the transition strengthens with increasing baryon chemical potential [36]. The critical endpoint is important because, with the exception of the endpoint of the nuclear liquid-gas transition, it is the only thermodynamically stable point in the QCD phase diagram at which the correlation length diverges. This means that the critical endpoint may manifest itself in heavy ion collisions in terms of enhanced fluctuation observables [37].

2.3.3 High baryon density QCD

The origin of the phase diagram, $T = \mu = 0$, corresponds to the vacuum state of QCD. If we stay on the $T = 0$ line and increase the chemical potential μ then there is no change initially. At zero temperature the chemical potential μ is the energy required to add a baryon to the system, and QCD has a large mass gap for baryonic states. The first non-vacuum state we encounter along the $T = 0$ axis of the phase diagram is nuclear matter, a strongly correlated superfluid composed of approximately non-relativistic neutrons and protons. Nuclear matter is self-bound, and the baryon density changes discontinuously at the onset transition, from $\rho = 0$ to nuclear matter saturation density $\rho = \rho_0 \simeq 0.15\,\mathrm{fm}^{-3}$. The discontinuity decreases as nuclear matter is heated, and the nuclear-liquid gas phase transition ends in a critical point at $T \simeq 18$ MeV and $\rho \simeq \rho_0/3$ [38–40]. Hot hadronic matter can be described quite accurately as a weakly interacting gas of hadronic resonances. Empirically, the density of states for both mesons and baryons grows exponentially. A system of this type is called a Hagedorn gas, and it is known that a Hagedorn gas has a limiting temperature. It is also known that an exponential density of states can be realized using the string model of hadronic resonances.

In the regime $\mu \gg \Lambda_{QCD}$ we can use arguments similar to those in the limit $T \gg \Lambda_{QCD}$ to establish that quarks and gluons are weakly coupled. At low temperature non-interacting quarks form a Fermi surface, where all states below the Fermi energy $E_F \simeq \mu/3$ are filled, and all states above the Fermi energy are empty. Interactions take place near the Fermi surface, and the corresponding interaction is weak. The main difference between cold quark matter

and the hot QGP is that the large density of states near the quark Fermi surface implies that even weak interactions can cause qualitative changes in the ground state of dense matter. In particular, attractive interactions between pairs of quarks $(\mathbf{p}_F, -\mathbf{p}_F)$ on opposite sides of the Fermi surface leads to color superconductivity and the formation of a $\langle qq \rangle$ diquark condensate.

Since quarks carry many different quantum numbers, color, flavor, and spin, a variety of superconducting phases are possible. The most symmetric of these, known as the color-flavor locked (CFL) phase, is predicted to exist at asymptotically high density [41, 42]. In the CFL phase the diquark order parameter is

$$\langle q^A_{\alpha f} q^B_{\beta g} \rangle = (C\gamma_5)_{\alpha\beta} \varepsilon^{ABC} \varepsilon_{fgh} \delta^h_C \Phi \,, \tag{2.26}$$

where $C\gamma_5$ is an anti-symmetric (spin zero) Dirac matrix, and Φ determines the magnitude of the gap near the Fermi surface. This order parameter has a number of interesting properties. It breaks the $U(1)$ symmetry associated with baryon number, leading to superfluidity, and it breaks the chiral $SU(3)_L \times SU(3)_R$ symmetry. Except for Goldstone modes the spectrum is fully gapped. Fermions acquire a BCS-pairing gap, and gauge fields are screened by the color Meissner effect. This implies that the CFL phase, even though it is predicted to occur in a very dense liquid of quarks, exhibits many properties of superfluid nuclear matter.

The CFL order parameter describes equal pair-condensates $\langle ud \rangle = \langle us \rangle = \langle ds \rangle$ of all three light quark flavors. As the density is lowered effects of the non-zero strange quark mass become important, and less symmetric phases are predicted to appear [14]. Phases that have been theoretically explored include Bose condensates of pions and kaons, hyperon matter, states with inhomogeneous quark-anti-quark or diquark condensates, and less symmetric color superconducting phases. The regimes of moderate baryon chemical potential in the phase diagram shown in Fig. 2.2 is largely conjecture. Empirical evidence shows that at low μ there is a nuclear matter phase with broken chiral symmetry and zero strangeness, and weak coupling calculations indicate that at high μ we find the CFL phase with broken chiral symmetry but non-zero strangeness. In principle the two phases could be separated by a single onset transition for strangeness [43, 44], but model calculation support a richer picture in which one or more first order transitions intervene, as indicated in Fig. 2.2.

2.4 Lattice QCD

2.4.1 The Wilson action

Symmetry arguments and perturbative calculations can be used to establish general features of the QCD phase diagram, but quantitative results can only be obtained using numerical calculations based on lattice QCD. The same is true for the masses of hadrons, their properties, and interactions. Lattice QCD is based on the euclidean path integral representation of the partition function, see [45–49] for introductions. More detailed reviews of the lattice field theory approach to hot and dense QCD can be found in [50, 51].

The euclidean partition function for QCD is

$$Z(T, \mu, V) = \int \mathscr{D}A_\mu \, \mathscr{D}q_f \, \mathscr{D}\bar{q}_f \, \exp(-S_E) \,, \tag{2.27}$$

where S_E is the euclidean action

$$S_E = -\int_0^\beta d\tau \int_V d^3x \, \mathscr{L}^E \,, \tag{2.28}$$

$\beta = T^{-1}$ is the inverse temperature and $\mathscr{L}^E$ is the euclidean Lagrangian, which is obtained by analytically continuing equ. (2.16) to imaginary time $\tau = it$. As in the quantum mechanical example in equ. (2.4) the temperature enters via the boundary condition on the fields in the imaginary time direction. Gauge fields and fermions obey periodic and anti-periodic boundary conditions, respectively. The chemical potential enters through its coupling to the conserved baryon density

$$\mathscr{L}^E(\mu) = \mathscr{L}^E(0) + \mu \bar{q}_f \gamma_0 q_f \,. \tag{2.29}$$

In his pioneering work Wilson proposed to discretize the action on a $N_\tau \times N_\sigma^3$ space-time lattice with lattice spacings a_τ and a_σ [52]. In many cases $a_\sigma = a_\tau = a$, but we will encounter an exception in Sect. 2.5.4. when we discuss the Hamiltonian formulation of the theory.

At finite temperature we have to ensure that the spatial volume is larger than the inverse temperature, $L > \beta$. Here, $\beta = N_\tau a_\tau$, $L = N_\sigma a_\sigma$, and $V = L^3$ is the volume. Thermodynamic quantities are determined by taking derivatives of the partition function. The energy and baryon density are given by

$$\mathscr{E} = -\frac{1}{V} \left. \frac{\partial \log Z}{\partial \beta} \right|_{\beta\mu} , \tag{2.30}$$

$$\rho = \left. \frac{1}{\beta V} \frac{\partial \log Z}{\partial \mu} \right|_{\beta} . \tag{2.31}$$

The discretized action for the gauge fields originally suggested by Wilson is given by

$$S_W = -\frac{2}{g^2} \sum_n \sum_{\mu<\nu} \mathrm{Re}\,\mathrm{Tr}\left[W_{\mu\nu}(n) - 1\right] \tag{2.32}$$

where $W_{\mu\nu}(n)$ is the plaquette, the product of gauge links around an elementary loop on the lattice,

$$W_{\mu\nu}(n) = U_\mu(n) U_\nu(n+\hat{\mu}) U_{-\mu}(n+\hat{\mu}+\hat{\nu}) U_{-\nu}(n+\hat{\nu}) \,. \tag{2.33}$$

Here, $n = (n_\tau, n_i)$ labels lattice sites and $\hat{\mu}$ is a unit vector in the μ-direction. The gauge links $U_\mu(n)$ are $SU(N_c)$ matrices. We can think of the gauge links as line integrals

$$U_\mu(n) = \exp(iaA_\mu(n)) \,, \tag{2.34}$$

and of the plaquettes as fluxes

$$W_{\mu\nu}(n)) = \exp(ia^2 G_{\mu\nu}(n)) \,, \tag{2.35}$$

but the fundamental variables in the path integral are the (compact) group variables U_μ, not the (non-compact) gauge potentials A_μ. In particular, the path integral in pure gauge QCD takes the form

$$Z = \int \prod_{n,\mu} dU_\mu(n) \exp(-S_W) \,, \tag{2.36}$$

where dU is the Haar measure on $SU(N_c)$. Using equ. (2.34) we can check that the Wilson action reduces to continuum pure gauge theory in the limit $a \to 0$. We note that the gauge invariance of QCD is maintained exactly, even on a finite lattice, but that Lorentz invariance is only restored in the continuum limit. We also observe that classical scale invariance implies that the massless QCD action is independent of a. The continuum limit is taken by adjusting the bare coupling at the scale of the lattice spacing according to asymptotic freedom, see equ. (2.19). In practice the lattice spacing is not small enough to ensure the accuracy of this method, and more sophisticated scale setting procedures are used [50, 51].

Monte Carlo simulations of the path integral equ. (2.36) can be performed using the Metropolis algorithm explained in Sect. 2.2:

- Initialize the link variables with random $SU(N_c)$ matrices. A simple algorithm is based on writing U in terms of N_c complex row vectors $\mathbf{u}_i$. Take each vector to be random unit vector and then use the Gram-Schmidt method to orthogonalize the different vectors, $\mathbf{u}_i \cdot \mathbf{u}_j^* = \delta_{ij}$. This ensures that U is unitary and distributed according to the $SU(N_c)$ Haar measure [53].
- Sweep through the lattice and update individual link variables. For this purpose multiply the link variable by a random $SU(N_c)$ matrix, $U_\mu \to RU_\mu$. Compute the change in the Wilson action and accept the update with probability $\exp(-\Delta S_W)$.
- Compute physical observables. The simplest observable is the average plaquette $\langle W_{\mu\nu}\rangle$, which can be related to the equation of state, see equ. (2.30). More complicated observables include the correlation function between plaquettes, and the Wilson loop

$$W(\mathscr{C}) = Tr\left[L(\mathscr{C})\right], \qquad L(\mathscr{C}) = \prod_{(n,\mu)\in\mathscr{C}} U_\mu(n), \tag{2.37}$$

  where $L(\mathscr{C})$ is the product of link variables around a closed loop. The average Wilson loop is related to the potential between two static charges in the fundamental representation

$$V(R) = -\lim_{T\to\infty} \frac{1}{T} \log\left[\langle W(\mathscr{C})\rangle\right], \tag{2.38}$$

  where $R \times T$ is the area of a rectangular loop $\mathscr{C}$.
- Tune to the continuum limit $a \to 0$ by adjusting the coupling constant according to the asymptotic freedom formula equ. (2.19). Note that the Lambda parameter for the lattice regulator is quite small, $\Lambda_{lat} = 28.8\Lambda_{\bar{M}S}$ [54]. Note that we have to increase N_σ, N_τ to keep the physical volume constant. Indeed, we have to study the infinite volume limit $V \to \infty$. This is more difficult than it appears, because $a \to 0$ ($g \to 0$) is a critical point, and simulations exhibit critical slowing down.

Metropolis simulations with the pure gauge Wilson action are very simple and robust. As an illustration we provide a simple Z_2 lattice gauge theory code written by M. Creutz in the appendix. Reasonable results for the heavy quark potential can be obtained on fairly coarse lattices, for example an 8^4 lattice with a spacing $a \simeq 0.25$ fm [55]. However, accurate results with controlled error bars require significant computational resources. In practice the perturbative relation between a and g^2 is only valid on very fine lattices, and the scale setting has to be done non-perturbatively. Also, determining the spectrum of pure gauge theory is difficult. Purely gluonic states, glueballs, are quite heavy, with masses in the range $m \simeq 1.6$ GeV and higher. This implies that gluonic correlation functions are short range, requiring a resolution $a \simeq 0.1$ fm or better. Finally, simulations on fine lattices are affected by critical slowing down. Indeed, finding an efficient method for updating gauge fields on very fine lattices, analogous to the cluster algorithms for spin models [56], is an important unsolved problem.

2.4.2 Fermions on the lattice

The main difficulty in lattice QCD is related to the presence of light fermions. The fermion action is of the form

$$S_F = a^4 \sum_{m,n} \bar{q}(m) D_{mn} q(n). \tag{2.39}$$

Formally, the integration over the fermion fields can be performed exactly, resulting in the determinant of the Dirac operator $\det(D(A_\mu,\mu))$. Several methods exist for discretizing the Dirac operator D, and for sampling the determinant. Different discretization schemes differ in the degree to which chiral symmetry is maintained on a finite lattice. The original formulation due to Wilson [52] preserves no chiral symmetry, the staggered Fermion scheme [57] maintains a subset of the full chiral symmetry, while the domain wall [58] and overlap methods [59] aim to preserve the full chiral symmetry on a discrete lattice.

The central difficulty in implementing these methods is that the fermion determinant is a very non-local object. While updating a single gauge link only requires recalculating a small number of plaquettes (6 in $d=4$ dimensions) in the Wilson action, recalculating the fermion action requires computing the determinant of a (very sparse) matrix of size $(N_\tau N_\sigma^3)\times(N_\tau N_\sigma^3)$ or larger. This is clearly impractical. Fermion algorithms rely on a number of tricks. The first is the observation that the Dirac operator has a property called γ_5-hermiticity, $\gamma_5 D\gamma_5 = D^\dagger$, which implies that $\det(D)$ is real. The determinant of a two-flavor theory is then real and positive. This allows us to rewrite the fermion determinant as a path integral over a bosonic field with a non-local action but positive action

$$\det(D_u)\det(D_d) = \det(DD^\dagger) = \int \mathscr{D}\phi\mathscr{D}\phi^\dagger \exp(-\phi^\dagger(DD^\dagger)^{-1}\phi)\,. \tag{2.40}$$

The path integral over the pseudofermion field ϕ can be sampled using a combination of deterministic methods like molecular dynamics and stochastic methods such as the Metropolis algorithm. These combined algorithms are known as Hybrid Monte Carlo (HMC) methods. Codes that implement the HMC algorithm for pseudofermions are significantly more complicated than the Metropolis algorithm for the pure gauge Wilson action discussed above, and I refer the interested reader to the more specialized literature [60]. I also note that since these algorithms involve the calculation of D^{-1} the computational cost increases as the quark masses are lowered.

The calculation of correlation functions also differs from the bosonic case. Consider, for example, an operator with the quantum numbers of a charged pion, $J_\pi(x) = \bar{u}^a(x)\gamma_5 d^a(x)$. Since the fermion action is quadratic the correlation function in a given gauge configuration can be computed exactly in terms of the fermion propagator. The full correlation function is

$$\Pi_\pi(x) = \langle J_\pi(x) J_\pi(0)\rangle = \langle \mathrm{Tr}\,[S(x,0)\gamma_5 S(0,x)\gamma_5]\rangle\,, \tag{2.41}$$

where $S(x,y) = \langle x|D^{-1}|y\rangle$ is the fermion propagator, and we have assumed exact isospin symmetry so that the propagator of the up quark is equal to the propagator of the down quark. Note that the interaction between quarks is encoded in the average over all gauge fields. The one-gluon exchange interaction, for example, corresponds to a perturbative fluctuation in the gauge field that modifies the two quark propagators. An operator with the quantum number of the proton is $\eta_\alpha(x) = \varepsilon_{abc}(u^a(x)C\gamma_\mu u^b(x))(\gamma^\mu\gamma_5 d^c(x))_\alpha$. The correlation function is

$$\Pi_{\alpha\beta}(x) = 2\varepsilon_{abc}\varepsilon_{a'b'c'}\left\langle \left(\gamma_\mu\gamma_5 S^{cc'}(0,x)\gamma_\nu\gamma_5\right)_{\alpha\beta} \mathrm{Tr}\left[\gamma_\mu S^{aa'}(0,x)\gamma_\nu C(S^{bb'}(0,x))^T C\right]\right\rangle. \tag{2.42}$$

Note that meson correlation function involves one forward and one backward going propagator, whereas the propagators in the baryon correlation function are all forward going. A difficulty arises when we consider flavor singlet $\bar{q}q$ currents such as $J_{\eta'} = (\bar{u}^a(x)\gamma_5 u^a(x) + \bar{d}^a(x)\gamma_5 d^a(x))/\sqrt{2}$, which has the quantum numbers of the η' meson. We find

$$\Pi_{\eta'}(x) = \langle J_{\eta'}(x) J_{\eta'}(0)\rangle = \langle \mathrm{Tr}\,[S(x,0)\gamma_5 S(0,x)\gamma_5] - 2\mathrm{Tr}\,[S(x,x)\gamma_5]\,\mathrm{Tr}\,[S(0,0)\gamma_5]\rangle\,, \tag{2.43}$$

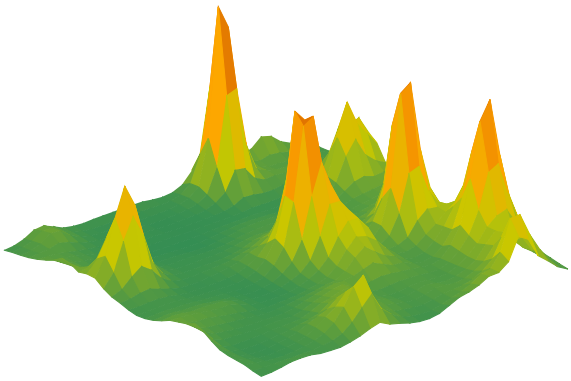

Fig. 2.3 Topological objects in lattice QCD (figure courtesy of S. Sharma, see [62]). This picture shows a slice through a low lying eigenstate of the Dirac operator in lattice QCD.

which involve propagators $S(x,x)$ that loop back to the same point. These contributions are known as quark-line disconnected diagrams, and difficult to treat numerically, see [61] for a recent discussion.

2.4.3 The QCD vacuum

It is natural to hope that lattice QCD can provide us with an intuitive picture of what the QCD vacuum looks like, similar to the picture of the quantum mechanical ground state shown in Fig. 2.1. This turns out to be more complicated, for a number of reasons. The first is that the field in QCD is a $SU(3)$ matrix, which is hard to visualize. The second, more important, problem is related to quantum fluctuations. In QCD there is no obvious separation of scales that would allow us to clearly separate perturbative fluctuations from large semi-classical fluctuations.

This has led to the idea to eliminate short range fluctuations by some kind of filtering or smoothing algorithm. The simplest of these is known as cooling [63]. In the cooling method we modify the Metropolis algorithm so that only updates that reduce the action are accepted. Since the update algorithm is local, this will tend to eliminate small structures but preserve larger objects. A modern version of cooling is gradient flow [64]. In the gradient flow method we continue the gauge fields to a 5th "time" dimension. In this direction the fields satisfy a differential equation

$$\partial_\tau A_\mu = D^\nu G_{\mu\nu}\,, \tag{2.44}$$

where $A_\mu(\tau = 0)$ is the four-dimensional gauge field and the rhs is computed from the gauge potentials evaluated at the flow time τ. The Lorentz indices remain four-dimensional. The rhs of the flow equations is the classical equation of motion, so that the gradient flow tends to drive gauge fields towards the closest classical solution. The only finite action solutions of the euclidean field equations on R^4 are instantons [65, 66]. Instantons and anti-instantons are characterized by integer values $Q_{top} = \pm 1$ of the topological charge

$$Q_{top} = \int d^4x\, q(x)\,, \qquad q(x) = \frac{g^2}{64\pi^2}\varepsilon^{\mu\nu\alpha\beta} G^a_{\mu\nu} G^a_{\alpha\beta}\,. \tag{2.45}$$

Exact higher charge solutions exist, but the QCD vacuum is dominated by configurations with both instantons and anti-instantons. These gauge field configurations are only approximate solutions of the equations of motion [66]. Under cooling or gradient flow instantons and anti-instantons will eventually annihilate and evolve to an exact multi-instantons solution with $Q_{top} = N_I - N_A$, where $N_{I,A}$ are the numbers of (anti)instantons. However, the $N_I + N_A$ topological objects are preserved for flow times that are much longer than the decay time of ordinary quantum fluctuations, and the total number of well separated instantons and anti-instantons can be determined.

The average topological charge is zero, but the pure gauge vacuum is characterized by a non-zero topological susceptibility

$$\chi_{top} = \frac{1}{V}\langle Q^2_{top}\rangle\,, \tag{2.46}$$

where V is the euclidean four-volume. The topological charge can be determined using the naive lattice discretization of equ. (2.45), but this operator is very noisy, and in general not an integer. This problem can be addressed using the cooling or gradient flow algorithms discussed above. Recent lattice calculations based on these methods give $\chi_{top} = (190 \pm 5\,\mathrm{MeV})^4$ [67, 68]. A simple picture of the QCD vacuum which is consistent with this value is the dilute instanton liquid model, which assumes that the topological susceptibility is determined by Poisson fluctuations in an ensemble of instantons and anti-instantons with an average density $(N_I + N_A)/V \simeq 1\,\mathrm{fm}^{-4}$ [66]. This is an approximate picture, and more complicated configurations involving monopoles and fractional charges are needed to understand the large N_c limit and the role of confinement [69].

Another important development is the use of fermionic methods to analyze the vacuum structure of QCD. In a given gauge configuration the quark propagator can written as

$$S(x,y) = \sum_\lambda \frac{\psi_\lambda(x)\psi^\dagger_\lambda(y)}{\lambda + im}\,, \tag{2.47}$$

where ψ_λ is an eigenvector of the Dirac operator with eigenvalue λ: $D\psi_\lambda = (\lambda + im)\psi_\lambda$. Note that this is not how propagators are typically determined in lattice QCD, because the calculation of the complete spectrum is numerically very expensive. Gamma five hermiticity implies that eigenvalues come in pairs $\pm\lambda$. The quark condensate is given by

$$\langle\bar{q}q\rangle = -i\int d^4x\, \langle \mathrm{Tr}\,[S(x,x)]\rangle = -\left\langle \sum_{\lambda>0} \frac{2m}{\lambda^2 + m^2}\right\rangle. \tag{2.48}$$

Here, I have ignored the contribution from exact zero modes because the density of zero modes is suppressed by m^{N_f}. This factor comes from the determinant in the measure. If we were to ignore the determinant (this is called the quenched approximation), then the quark condensate would diverge as $1/m$. We observe that a finite value of the quark condensate in the chiral limit $m \to 0$ requires an accumulation of eigenvalues near zero. This can be made more explicit by introducing the density of states

$$\rho(\nu) = \left\langle \sum_{\lambda\geq 0} \delta(\lambda - \nu)\right\rangle. \tag{2.49}$$

The chiral condensate in the thermodynamic and chiral limits is given by

$$\langle\bar{q}q\rangle = -\pi\rho(0)\,. \tag{2.50}$$

This is known as the Banks-Casher relation [70]. Note that is is essential to take the thermodynamic $V \to \infty$ limit before the chiral limit $m \to 0$.

Exact zero modes of the Dirac operator are related to topology. The Dirac operator has one left handed zero mode in the field of an instanton, and a right handed zero mode in the field of an anti-instanton. This is consistent with the Atiyah-Singer index theorem, which states that the topological charge is equal to the index of the Dirac operator, the difference between the number of left and right handed zero modes, $Q_{top} = N_f(n_L - n_R)$. These results suggest that it is possible to give a purely fermionic definition of the topological charge density.

On the lattice, this can be achieved for a class of Dirac operators that satisfy the Ginsparg-Wilson relation [71]

$$D\gamma_5 + \gamma_5 D = aD\gamma_5 D\,, \tag{2.51}$$

where a is the lattice spacing. In the continuum limit we recover the expected relation $D\gamma_5 + \gamma_5 D = 0$ for the massless Dirac operator. The important observation is that even on a discrete lattice

$$q_f(n) = \frac{1}{2a^3}\,\mathrm{tr}_{CD}\left[\gamma_5 D(n,n)\right]\,, \tag{2.52}$$

where tr_{CD} is a color-Dirac trace, satisfies the index theorem

$$Q_{top} = a^4 \sum_n q_f(n)\,. \tag{2.53}$$

Fig. 2.3 shows the absolute square of $q_f(x)$ constructed from lying eigenmodes of the Dirac operator. We observe that fermionic operators can indeed be used to probe the topological content of the QCD vacuum directly, without the need for filtering or smoothing.

The existence of zero mode implies that the topological susceptibility is zero if at least one quark flavor is massless. This is because the path integral measure contains the fermion determinant, which is vanishes if $m = 0$ and $Q_{top} \neq 0$. We can be more precise using the chiral lagrangian equ. (2.22). In order to keep track of topology we add to the QCD action a topological term $S_\theta = i\theta Q_{top}$. Then the topological susceptibility is given by the second derivative of the free energy with respect to θ. Since every zero mode in the Dirac operator contributes a factor $\det(M)$ to the partition function we know that θ enters the effective lagrangian in the combination $\theta + \arg(\det(M))$. The vacuum energy is determined by

$$V = -B\mathrm{Tr}\left[Me^{i\theta/N_f}\Sigma^\dagger\right] + h.c.\,, \tag{2.54}$$

and we observe that the topological susceptibility in QCD with degenerate quark masses is proportional to $m\langle\bar{q}q\rangle$. Note that equ. (2.54) is consistent with the vanishing of χ_{top} for $m_u = 0$. If $m_u = 0$ and $m_d \neq 0$ then equ. (2.54) is minimized by $\Sigma = \exp(i\phi\tau_3)$ with $\phi = \theta/2$, and the vacuum energy is independent of θ.

It is tempting to think that exact zero modes, governed by topology, and approximate zero modes, connected to chiral symmetry breaking, are related. This is the basis of the instanton liquid model [66]. In the instanton liquid model we consider an ensemble of instantons and anti-instantons with no (or small) net topology. The exact zero modes of individual instantons are lifted, and form a zero mode zone. The density of eigenvalues in the zero mode zone determines the chiral condensate via the Banks-Casher relation. This model predicts the correct order of magnitude of $\langle\bar{q}q\rangle$, but the calculation cannot be systematically improved because chiral symmetry breaking requires strong coupling. Recently, we showed that the connection of chiral symmetry breaking, instantons and monopoles can be made precise in a certain limit of QCD. The idea is to compactify QCD on $R^3 \times S_1$, where the size of the circle is much smaller than Λ_{QCD}^{-1}, and the fermions satisfy non-thermal (twisted) boundary conditions [72].

2.4.4 Lattice QCD at finite baryon density

In section 2.4.2 I discussed some of the difficulties that appear when we discretize the Dirac operator. A separate, more serious, issue with fermions is that for $\mu \neq 0$ the Dirac operator does not satisfy γ_5-hermiticity, the fermion determinant is no longer real, and that standard importance sampling methods fail. This is the "sign" problem already mentioned in Sect. 2.3.2. To understand the severity of the problem consider a generic expectation value

$$\langle \mathcal{O} \rangle = \frac{\int dU \, \det(D) \, \mathcal{O} \, e^{-S}}{\int dU \, \det(D) \, e^{-S}} \,. \tag{2.55}$$

If the determinant is complex I can write this as

$$\langle \mathcal{O} \rangle = \frac{\int dU \, |\det(D)| \, \mathcal{O} e^{i\varphi} \, e^{-S}}{\int dU \, |\det(D)| \, e^{i\varphi} e^{-S}} \equiv \frac{\langle \mathcal{O} e^{i\varphi} \rangle_{pq}}{\langle e^{i\varphi} \rangle_{pq}} \,, \tag{2.56}$$

where $\langle . \rangle_{pq}$ refers to a phase quenched average. This average can be computed using the Metropolis (or HMC) algorithm. The problem is that the average phase $\langle e^{i\varphi} \rangle_{pq}$ is very small. This follows from the fact that the average phase can be expressed as the ratio of two partition functions

$$\langle e^{i\varphi} \rangle_{pq} = \frac{\int dU \, \det(D) \, e^{-S}}{\int dU \, |\det(D)| \, e^{-S}} = \frac{Z}{Z_{pq}} = e^{-V\Delta F} \,, \tag{2.57}$$

where ΔF is the free energy density difference, and V is the volume of the system. This shows that the phase is exponentially small, and that the ratio equ. (2.56) is very difficult to compute.

As a specific example consider QCD with two degenerate flavors, up and down, and a baryon chemical potential $\mu_u = \mu_d = \mu_B/3$. Then $\det(D) = \det(D_u)\det(D_d)$ and $|\det(D)| = \det(D_u)\det(D_d)^*$, and Z_{pq} can be interpreted as the partition function of QCD with a non-zero isospin chemical potential $\mu_u = -\mu_d = \mu_I/2$. The small μ behavior of both the isospin and baryon number theories at $T = 0$ is easily understood. The isospin theory has a second order phase transition at $\mu_I = m_\pi$ which corresponds to the onset of pion condensation. The baryon theory has a first order transition at $\mu_B = m_p - B$, where $B \simeq 15$ MeV is the binding energy of infinite nuclear matter. This implies that for $\mu > m_\pi$ the partition functions Z and Z_{pq} describe very different physical systems, and the sign problem is severe.

The sign problem may manifest itself in different ways. Consider, for example, an attempt to study the correlation function of A nucleons in a QCD ensemble generated at $\mu_B = 0$. For large A this correlation function determines the binding energy of nuclear matter. There are two difficulties with this approach. The first is that the operator contains $3A$ quark fields, so that the correlator has up to $(3A)!$ contractions. This is not prohibitive, because the number of contractions can be reduced using symmetries and iterative algorithms. Indeed, correlators for medium mass nuclei have been computed [49]. The second, more serious, problem is the signal-to-noise ratio. The variance of the correlator C is

$$\mathrm{var}(C) = \langle C C^\dagger \rangle - \langle C \rangle^2 \,. \tag{2.58}$$

The A nucleon correlator C contains $3A$ forward going quark propagators, and $CC^\dagger$ consists of $3A$ forward and $3A$ backward propagators. This implies that $CC^\dagger$ couples to a state of $3A$ mesons. Since the lightest meson is the pion and the lightest baryon is the proton the signal-to-noise of an A nucleon correlation function is

$$\frac{\mathcal{S}}{\mathcal{N}} \sim \exp(-A(m_p - 3m_\pi/2)\tau) \,. \tag{2.59}$$

In order to resolve nuclear binding effects we have to go to distances of order $\tau \sim 1/B \sim 10$ fm. It may be possible to improve on this by using variationally improved sources, but even for $\tau \simeq 2$ fm the signal to noise is extremely poor for $A \gtrsim 4$. This shows that in simulations with fixed A the sign problem manifests itself as a noise problem. This is not surprising. One way to think about the sign problem is to view it as an overlap problem. The configurations that contribute to Z_{pq} have poor overlap with those that contribute to Z. The same phenomenon is at work here. Configurations generated at $\mu_B = 0$ reflect vacuum physics, and the lightest fermionic fluctuation is a pion. Large cancellations are required to explore the physics of multi-baryon states.

There are many attempts to find direct solutions to the sign problem, but at this time the only regime in which controlled calculations are feasible is the regime of small μ and high T. In this region the partition function can be expanded in a Taylor series in μ/T. The corresponding expansion coefficients are generalized susceptibilities that can be determined from lattice simulations at zero chemical potential. The susceptibilities not only determine the equation of state at finite baryon density, but also control fluctuations of conserved charges.

In addition to methods that are restricted to the regime $\mu \lesssim \pi T$, a number of proposals to explore QCD at high baryon density are being pursued. This includes new approaches, like integration over Lefshetz thimbles [73, 74], as well as novel variants of old approaches, like the complex Langevin method [75, 76], or the use of dual variables [77]. The ultimate promise of these methods is still unclear, but the central importance of the sign problem to computational physics continues to attract new ideas.

2.4.5 Real time properties

The basic trick in lattice QCD is the continuation of the path integral to imaginary time. This makes it possible to calculate the path integral by importance sampling, but it implies that we only have direct access to imaginary time correlation functions. For many observables this is not a serious problem. Thermodynamic observables, for example, are static quantities and no analytic continuation is necessary. The ground state contribution to a hadron correlation function is $\Pi(\tau) \sim e^{-m_H \tau}$ which is trivially continued to $\Pi(t) \sim e^{-im_H t}$. However, difficulties arise if one studies excited states, in particular resonances, the interaction between hadrons, or the real time response of many body systems at finite temperature and density.

Significant progress has been made in studying scattering processes, at least in the elastic regime. This is discussed in some of the later chapters of this book. Here, I will concentrate on the calculation of real time response functions. The prototypical example is the calculation of the shear viscosity of a QCD plasma using the retarded correlation function of the stress tensor T_{xy},

$$G_R^{xy,xy}(\omega,\mathbf{k}) = -i \int dt \int d^3x e^{i(\omega t - \mathbf{k}\cdot\mathbf{x})} \Theta(t) \langle [T^{xy}(\mathbf{x},t), T^{xy}(0,0)] \rangle \,, \tag{2.60}$$

The associated spectral function is defined by $\rho(\omega,\mathbf{k}) = -\,\mathrm{Im}\, G_R(\omega,\mathbf{k})$. The imaginary part of the retarded correlator is a measure of dissipation. Fluid dynamics is an effective theory of the response function in the low energy, small momentum limit [78, 79]. The static response is determined by the pressure of the fluid, and the leading energy and momentum dependence is governed by transport coefficients. These relations can be used to derive Kubo formulas, expressions for the transport coefficients in terms of retarded correlation functions. The Kubo relation for the shear viscosity is

$$\eta = \lim_{\omega\to 0} \lim_{k\to 0} \frac{\rho^{xy,xy}(\omega,\mathbf{k})}{\omega} \,, \tag{2.61}$$

and similar results hold for the bulk viscosity, the thermal conductivity, and heavy quark diffusion constants.

The spectral function contains information about the physical excitations that carry the response. The euclidean path integral does not provide direct access to the retarded correlator or the spectral function. Lattice calculations are based on the relation between the spectral function and the imaginary energy (Matsubara) correlation function

$$G_E(i\omega_n) = \int \frac{d\omega}{2\pi} \frac{\rho(\omega)}{\omega - i\omega_n}\,, \tag{2.62}$$

where $\omega_n = 2\pi nT$ is the Matsubara frequency. The imaginary time correlation function is

$$G_E(\tau) = \int \frac{d\omega}{2\pi} K(\omega,\tau)\rho(\omega)\,, \tag{2.63}$$

where the kernel $K(\omega,\tau)$ is given by

$$K(\omega,\tau) = \frac{\cosh[\omega(\tau - 1/(2T))]}{\sinh[\omega/(2T)]} = [1+n_B(\omega)]\, e^{-\omega\tau} + n_B(\omega) e^{\omega\tau}\,, \tag{2.64}$$

and $n_B(\omega)$ is the Bose distribution function. The imaginary time correlation function equ. (2.63) was studied on the lattice in [80–83]. The basic idea for calculating transport coefficients is to numerically compute $G_E(\tau)$, invert the integral transform in equ. (2.63) to obtain the spectral functions $\rho(\omega)$, and then study the limit $\omega \to 0$.

The problem is that $G_E(\tau)$ is computed on a small number of discrete lattice sites, and that the imaginary time correlator at distances on the order of $\beta/2$ is not very sensitive to the slope of the spectral function at low energy. Recent attempts to to address these problems and to obtain numerically stable spectral functions and reliable error estimates are based on Bayesian methods such as the maximum entropy method mentioned in Sect. 2.2, see [84, 85]. It is also possible to optimize the contribution from the transport peak by measuring the correlation functions of conserved charges, such as energy and momentum density, at non-zero spatial momentum [86, 87]. A possible issue with lattice calculations is that effects of poor resolution tend to favor small values of η/s. The finite temperature spectral function satisfies the sum rule [88]

$$\frac{2}{\pi}\int d\omega\, [\eta(\omega) - \eta_{T=0}(\omega)] = \frac{3}{10}\, sT\,, \tag{2.65}$$

where $\eta(\omega) = \rho(\omega)/\omega$. On the lattice it is difficult to resolve sharp features in the spectral function. I will therefore assume that the $T \neq 0$ spectral function is a Lorentzian with width πT

$$\eta(\omega) - \eta_{T=0}(\omega) \simeq \frac{\eta(0)(\pi T)^2}{\omega^2 + (\pi T)^2}\,. \tag{2.66}$$

Then the integral on the lhs is equal to $\eta(0)\pi T$, and the sum rule predicts $\eta/s \sim 3/(10\pi)$, quite close to $\eta/s = 1/(4\pi)$. The lesson is that it is easier to obtain small values of η/s, suggested by holography, and much more difficult to obtain large values of η/s, predicted by perturbative QCD [89].

The first calculation of the shear viscosity on the lattice was performed by Karsch and Wyld [80]. More recently, the problem of computing the shear and and bulk viscosity in a pure gauge plasma near T_c was revisited by Meyer [81, 87]. He obtains $\eta/s = 0.102(56)$ and $\zeta/s = 0.065(17)$ at $T = 1.24T_c$. Shear viscosity is only weakly dependent on temperature, but bulk viscosity is strongly peaked near T_c. The value of η/s is consistent with experimental results, and with the prediction from holographic duality, $\eta/s = 1/(4\pi)$ [90].

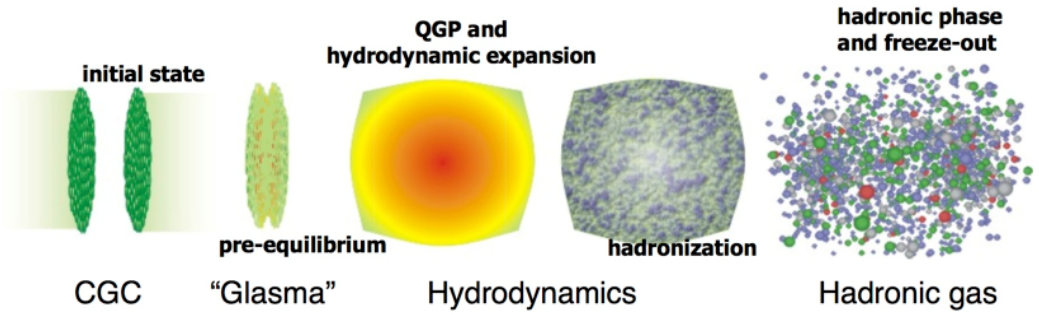

Fig. 2.4 Schematic time evolution of a heavy ion collision. Figure courtesy of S. Bass. CGC refers to the color glass condensate, a semi-classical model of the overpopulated gluon configuration in the initial state of a heavy ion collision. Glasma refers to the non-equilibrium evolution of this state into a locally equilibrated plasma. Hydrodynamics is the theory of the time evolution of a locally equilibrated fireball, and hadronic phase refers to the late time kinetic stage of the collision.

2.5 Nonequilibrium QCD

In the remainder of this chapter I will discuss a number of coarse grained approaches to the non-equilibrium dynamics of QCD. These method are relevant to the study of nuclear collisions, in particular in the ultra-relativistic regime. This regime is explored experimentally at the Relativistic Heavy Ion Collider (RHIC) at Brookhaven National Laboratory and the Large Hadron Collider (LHC) at CERN. A rough time line of a heavy ion collision is shown in Fig. 2.4. Initial nucleon-nucleon collisions release a large number of quarks and gluons. This process is described by the full non-equilibrium quantum field theory, but there are a number of approximate descriptions that may be useful in certain regimes. The first is a classical field theory description in terms of highly occupied classical gluon fields. The second is a kinetic theory in terms of quark and gluon quasi-particles. Finally, there is a new approach, which is a description in terms of a dual gravitational theory.

Theories of the initial state demonstrate that there is a tendency towards local equilibration. If local equilibrium is achieved then a simpler theory, fluid dynamics is applicable. Fluid dynamics is very efficient in the sense that it deals with a small number of variables, the conserved densities of particle number, energy and momentum, and that it has very few parameters, an equation of state and a set of transport coefficients. The fluid dynamic stage of a heavy ion collision has a finite duration. Eventually the density becomes too low and local equilibrium can no longer be maintained. At this point kinetic theory is again relevant, now formulated in terms of hadronic quasi-particles. All the theories we have mentioned, fluid dynamics, kinetic theory, classical field theory, and holography, have reached a high degree of sophistication and I will point to text books and review for detailed introductions. Nevertheless, the basic ideas are quite simple, and I will provide some examples in the following sections.

2.5.1 Fluid Dynamics

I begin with fluid dynamics, because it is the most general and in some ways the simplest non-equilibrium theory. It is important to remember, however, that fluid dynamics is a very rich framework, both mathematically and in terms of the range of phenomena that one may encounter. In the following I will focus on the non-relativistic theory. There is no fundamen-

tal difference between the relativistic and non-relativistic theories, but some simplifications appear in the non-relativistic regime. Non-relativistic fluid dynamics is used in many areas of physics, including the physics of cold atomic Fermi gases and neutron stars. The relativistic theory is relevant to high energy heavy ion collisions and supernova explosions. Introductions to relativistic fluid dynamics can be found in [91–93].

Fluid dynamics reduces the complicated non-equilibrium many-body problem to equations of motion for the conserved charges. The reason that this is possible is the separation of scales between the microscopic collision time τ_{micro}, and the relaxation time τ_{macro} of hydrodynamic variables. A generic perturbation of the system decays on a time scale on the order of τ_{micro}, irrespective of the typical length scale involved. Here, τ_{micro} is determined by microscopic time scales, such as the typical collision time between quasi-particles. A fluctuation of a conserved charge, on the other hand, cannot decay locally and has to relax by diffusion or propagation. The relevant time scale τ_{macro} increases with the length scale of the perturbation. As a consequence, when we focus on sufficiently large scales we can assume $\tau_{macro} \gg \tau_{micro}$, and focus on the evolution of conserved charges.

In a simple non-relativistic fluid the conserved charges are the mass density ρ, the momentum density π, and the energy density $\mathscr{E}$. The momentum density can be used to define the fluid velocity, $\mathbf{u} = \pi/\rho$. By Galilean invariance the energy density can then be written as the sum of the internal energy density and the kinetic energy density, $\mathscr{E} = \mathscr{E}_0 + \frac{1}{2}\rho u^2$. The conservation laws are

$$\frac{\partial \rho}{\partial t} = -\nabla \cdot \pi, \tag{2.67}$$

$$\frac{\partial \pi_i}{\partial t} = -\nabla_j \Pi_{ij}, \tag{2.68}$$

$$\frac{\partial \mathscr{E}}{\partial t} = -\nabla \cdot \mathbf{j}^{\varepsilon}. \tag{2.69}$$

In order for these equations to close we have to specify constitutive relations for the stress tensor Π_{ij} and the energy current $\mathbf{j}^{\varepsilon}$. Since fluid dynamics is an effective long wavelength theory we expect that the currents can be systematically expanded in gradients of the hydrodynamic variables ρ, $\mathbf{u}$ and $\mathscr{E}_0$. At leading order the stress tensor contains no derivatives and the structure is completely fixed by rotational symmetry and Galilean invariance. We have

$$\Pi_{ij} = \rho u_i u_j + P\delta_{ij} + \delta\Pi_{ij}\,, \tag{2.70}$$

where $P = P(\rho, \mathscr{E}_0)$ is the equation of state and $\delta\Pi_{ij}$ contains gradient terms. The approximation $\delta\Pi_{ij} = 0$ is called ideal fluid dynamics, and the equation of motion for π is known as the Euler equation. Ideal fluid dynamics is time reversal invariant and the entropy is conserved. If gradient terms are included then time reversal invariance is broken and the entropy increases. We will refer to $\delta\Pi_{ij}$ as the dissipative stresses. At first order in the gradient expansion $\delta\Pi_{ij}$ can be written as $\delta\Pi_{ij} = -\eta\sigma_{ij} - \zeta\delta_{ij}\langle\sigma\rangle$ with

$$\sigma_{ij} = \nabla_i u_j + \nabla_j u_i - \frac{2}{3}\delta_{ij}\langle\sigma\rangle\,, \qquad\qquad \langle\sigma\rangle = \nabla\cdot\mathbf{u}\,. \tag{2.71}$$

The dissipative stresses are determined by two transport coefficients, the shear viscosity η and the bulk viscosity ζ. The energy current is given by

$$\mathbf{j}^{\,\varepsilon} = \mathbf{u}w + \delta\mathbf{j}^{\varepsilon}\,, \tag{2.72}$$

where $w = P + \mathscr{E}$ is the enthalpy. At leading order in the gradient expansion

$$\delta j_i^{\varepsilon} = u_j\delta\Pi_{ij} - \kappa\nabla_i T\,, \tag{2.73}$$

where κ is the thermal conductivity. The second law of thermodynamics implies that η, ζ and κ must be positive. The equation of motion for π at first order in gradients is known as the Navier-Stokes equation, and equ. (2.73) is Fourier's law of heat conduction.

It is sometimes useful to rewrite the fluid dynamic equations using the comoving derivatives $D_t = \partial_t + \mathbf{u} \cdot \nabla$. The equations are

$$D_t \rho = -\rho \nabla \cdot \mathbf{u}\,, \tag{2.74}$$

$$D_t u_i = -\frac{1}{\rho} \nabla_j \left(\delta_{ij} P + \delta \Pi_{ij} \right), \tag{2.75}$$

$$D_t \varepsilon = -\frac{1}{\rho} \nabla_i \left(u_i P + \delta j_i^{\mathscr{E}} \right), \tag{2.76}$$

where $\varepsilon = \mathscr{E}/\rho$ is the energy per mass. This is called the Lagrangian form of the equations, in contrast to the Eulerian form given above. The Eulerian form is more naturally implemented on a fixed space-time lattice, whereas the Lagrangian form lends itself to a discretization where the computational cell is dragged along with the fluid.

2.5.2 Computational fluid dynamics

The fluid dynamic equations form a set of partial differential equations (PDEs) that can be solved in a variety of ways. I will focus here on grid based methods. The main difficulties that numerical method needs to address are: i) The existence of surfaces of discontinuity (shocks), ii) the need to implement global conservation laws exactly, even on a coarse lattice, iii) the existence of instabilities (turbulence), and the need to deal with solutions that involve many different length scales.

In the following I will discuss a numerical scheme that addresses these issues in a fairly efficient way, the PPM algorithm of Collela and Woodward [94], as implemented in the VH1 code by Blondin and Lufkin [95] and extended to viscous fluids in [96]. The first observation is that it is sufficient to construct a 1-d algorithm. Higher dimensional methods can be constructed by combining updates in different directions. Note that the coordinate system can be curvilinear, for example 3-d spherical or cylindrical coordinates, or the Milne coordinate system that is used for longitudinally expanding quark gluon plasmas.

The basic 1-d algorithm consists of a Lagrangian time step followed by a remap onto an Eulerian grid. I will denote the 1-d velocity by u and write the equation of mass conservation in terms of a mass variable m

$$\frac{\partial \tau}{\partial t} - \frac{\partial u}{\partial m} = 0\,, \tag{2.77}$$

where $\tau = \rho^{-1}$ and

$$m(r) = \int_{r_0}^{r} dr\, \rho(r)\,. \tag{2.78}$$

Here, I restrict myself to flat coordinate systems. In curvilinear coordinates equ. (2.77) and (2.78) contain suitable volume factors. Equ. (2.77) is solved by

$$\frac{dr}{dt} = u\left(m(r), t\right), \tag{2.79}$$

which is the equation for the Lagrange coordinate. In terms of the mass coordinate $m(r)$ the momentum and energy equations are

$$\frac{\partial u}{\partial t} + \frac{\partial P}{\partial m} = 0\,, \tag{2.80}$$

$$\frac{\partial \varepsilon}{\partial t} + \frac{\partial (uP)}{\partial m} = 0\,, \tag{2.81}$$

where I have only written down the ideal contributions to the stress tensor and energy current. To put these equations on a grid I focus on the mass integrated quantities

$$U_j^n = \frac{1}{\Delta m_j} \int_{m_{j-1/2}}^{m_{j+1/2}} U(m,t^n) dm \tag{2.82}$$

where U is any of the hydrodynamic variables (τ, u, ε), Δm_j is the mass contained in the cell j, and $m_{j+1/2} = \sum_k^j \Delta m_k$. We can now integrate the conservation laws (2.80,2.77). The result is

$$u_j^{n+1} = u_j^n + \frac{\Delta t}{\Delta m_j} \left(\bar{P}_{j-1/2} - \bar{P}_{j+1/2} \right)\,, \tag{2.83}$$

$$\varepsilon_j^{n+1} = \varepsilon_j^n + \frac{\Delta t}{\Delta m_j} \left(\bar{u}_{j-1/2} \bar{P}_{j-1/2} - \bar{u}_{j+1/2} \bar{P}_{j+1/2} \right)\,, \tag{2.84}$$

where I have introduced the cell face averages $\bar{u}_{j\pm1/2}$ and $\bar{P}_{j\pm1/2}$. These quantities can be obtained by parabolic interpolation from the cell integrated values. The PPM scheme introduced in [94] uses a method for constructing cell face averages which conserves the cell integrated variables.

This scheme addresses the second issue mentioned above. The first issue, the existence of shocks, can be taken into account by refining the method for calculating the cell face averages. The observation is that one can make use of exact solution of the equations of fluid dynamics in the case of piecewise constant one-dimensional flows, known as the Riemann problem. We can view $\bar{u}_{j+1/2}$ and $\bar{P}_{j+1/2}$ as the solution of a Riemann problem with left state u_j, P_j and right state u_{j+1}, P_{j+1}. The PPM code contains a simple iterative Riemann solver described in [94]. Using $\bar{u}_{j\pm1/2}$ and $\bar{P}_{j\pm1/2}$ the Lagrange step is given by:

```
do n = nmin-3, nmax+3

! density evolution. lagrangian code, so all we have to do is watch the
! change in the geometry.

  r(n) = r(n) * ( dvol1(n) / dvol(n) )
  r(n) = max(r(n),smallr)

! velocity evolution due to pressure acceleration and forces.

  uold (n) = u(n)
  u(n) = u(n) - dtbdm(n)*(pmid(n+1)-pmid(n))*0.5*(amid(n+1)+amid(n)) &
       + 0.5*dt*(fict0(n)+fict1(n))

! total energy evolution

  e(n) = e(n) - dtbdm(n)*(amid(n+1)*upmid(n+1) - amid(n)*upmid(n))
  q(n) = e(n) - 0.5*(u(n)**2+v(n)**2+w(n)**2)
  p(n) = max(r(n)*q(n)*gamm,smallp)

enddo
```

Here, `r(n)` is the density, `u(n)` is the velocity, and `e(n)` is the energy per mass. The transverse components of the velocity are `v(n)`, `w(n)`. In cartesian coordinates the volume and area factors `dvol(n)`, `amid(n)` are equal to unity, and the fictitious forces `fict(n)` vanish.

After the Lagrange step the hydrodynamic variables have to be remapped onto a fixed Eulerian grid. This can be done using the parabolic interpolation mentioned above. The advantage of the remap step is that it is simple to change the grid resolution in the process. Finally, we have to specify the time step and grid resolution. The grid resolution is determined by the requirement that $(\Delta x)\nabla_x U \ll U$, where Δx is the cell size, and U is any of the hydrodynamic variables. Note that there is no need to worry about discontinuities, because shocks are captured by the Riemann solver. Also note that the PPM scheme has at least second order accuracy, so that relatively coarse grids can be used. The time step is determined by the Courant criterion $c\Delta x \leq \Delta t$, where c is the maximum of the speed of sound and the local flow velocity. This criterion ensures that the domain of dependence of any physical variable does not exceed the cell size.

In general, modern hydro codes are very fast and efficient. The main difficulty is that $3+1$ dimensional simulations may require a lot of memory, and that some physical phenomena, such as turbulent convection and shock instabilities in supernovae, require very high resolution. One of the frontiers of numerical hydrodynamics is the problem of dealing with systems that transition from fluid dynamics to ballistic behavior at either early or late times, or systems in which the density varies by a very large factor. Problems of this type arise in the early and late time dynamics of heavy ion collisions, the dilute corona of cold atomic gases, and the transition from hydrodynamics to free streaming in the neutrino transport in a supernova explosions. Recent progress in this direction includes the development of the anisotropic hydrodynamics method [97–100], and applications of the lattice Boltzmann method to problems in nuclear and atomic physics [101, 102].

2.5.3 Kinetic theory

Fluid dynamics is based on the assumption of local thermal equilibrium and requires the mean free path to be small compared to the characteristic scales of the problem. When this condition is not satisfied a more microscopic approach to the non-equilibrium problem is required. The simplest method of this type is kinetic theory, which is based on the existence of well defined quasi-particles. This implies, in particular, that the width of a quasi-particle has to be small compared to its energy. In this case we can define the phase space density $f(\mathbf{x},\mathbf{p},t)$ of quasi-particles. In general, there can be many different kinds of quasi-particles, labeled by their spin, charge, and other quantum numbers. The phase space distribution determines the conserved densities that enter the hydrodynamic description. For example, the mass density is given by

$$\rho(\mathbf{x},t) = \int d\Gamma\, m f(\mathbf{x},\mathbf{p},t)\,, \tag{2.85}$$

where $d\Gamma = d^3p/(2\pi)^3$. The momentum density is

$$\pi(\mathbf{x},t) = \int d\Gamma\, m v_p f(\mathbf{x},\mathbf{p},t)\,, \tag{2.86}$$

where $v_p = \nabla_p E_p$ is the quasi-particle velocity and E_p is the quasi-particle energy. In general, the quasi-particle energy can be a functional of the phase distribution $f(\mathbf{x},\mathbf{p},t)$. This takes into account possible in-medium modifications of particle properties. If E_p is a functional of $f(\mathbf{x},\mathbf{p},t)$ then the total energy of the system is not just given by the integral of $E_p f(\mathbf{x},\mathbf{p},t)$. Instead, we must construct an energy density functional $\mathscr{E}[f]$ that satisfies [103]

$$E_p = \frac{\delta\mathscr{E}}{\delta f_p}\,. \tag{2.87}$$

The equation of motion for the distribution function is the Boltzmann equation

$$(\partial_t + \mathbf{v}\cdot\nabla_x - \mathbf{F}\cdot\nabla_p)\, f(\mathbf{x},\mathbf{p},t) = C[f]\,, \tag{2.88}$$

where $\mathbf{F} = -\nabla_x E_p$ is a force, and $C[f_p]$ is the collision term. For dilute systems the collision term is dominated by binary scattering and

$$C[f_p] = -\prod_{i=2,3,4}\Big(\int d\Gamma_i\Big) w(1,2;3,4)\,(f_1 f_2 - f_3 f_4)\,, \tag{2.89}$$

where $f_i = f(\mathbf{x},\mathbf{p}_i,t)$. The transition rate is given by

$$w(1,2;3,4) = (2\pi)^4 \delta\Big(\sum_i E_i\Big)\,\delta\Big(\sum_i \mathbf{p}_i\Big)\,|\mathscr{A}|^2\,, \tag{2.90}$$

where $\mathscr{A}$ is the scattering amplitude. For non-relativistic s-wave scattering $\mathscr{A} = 4\pi a/m$, where a is the scattering length.

The Boltzmann equation is a 6+1 dimensional partial integro-differential equation, and direct methods of integration, similar to those used in computational fluid dynamics, are impractical. Standard methods for solving the Boltzmann equation rely on sampling phase space using Monte Carlo methods. In nuclear physics the test particle method for solving the Boltzmann equation was popularized by Bertsch and Das Gupta [104]. Below, I will present a simple non-relativistic algorithm described by Lepers et al. [105].

The main idea is to represent the distribution as a sum of delta functions

$$f(\mathbf{x},\mathbf{p},t) = \frac{N}{N_t}\sum_{i=1}^{N_t}(2\pi)^3\delta(\mathbf{p}-\mathbf{p}_i(t))\delta(\mathbf{x}-\mathbf{x}_i(t))\,, \tag{2.91}$$

where N is the number of particles, the integral of $f(\mathbf{x},\mathbf{p},t)$ over phase space, and N_t is the number of test particles. In typical applications $N_t \gg N$, but if N is already very large it is possible to run simulations with $N_t < N$. Phase space averages can be computed as averages over test particles

$$\bar{F} = \frac{1}{N}\int d^3x \int d\Gamma\, f(\mathbf{x},\mathbf{p},t) F(\mathbf{x},\mathbf{p}) = \frac{1}{N_t}\sum_{i=1}^{N_t} F(\mathbf{x}_i,\mathbf{p}_i)\,. \tag{2.92}$$

In practice this requires some smoothing, and the delta functions are replaced by Gaussian distributions

$$\delta(\mathbf{p}-\mathbf{p}_i)\delta(\mathbf{x}-\mathbf{x}_i) \to g_{w_p}(\mathbf{p}-\mathbf{p}_i) g_{w_x}(\mathbf{x}-\mathbf{x}_i)\,, \tag{2.93}$$

where $g_w(\mathbf{x})$ is a normalized Gaussian with width w. The widths w_x and w_p are chosen such that the delta function singularities are smoothed out, but physical structures of the distribution function $f(\mathbf{x},\mathbf{p},t)$ are preserved.

If there is no collision term the equation of motion for the distribution function is Hamilton's equation for the test particle positions and momenta

$$\frac{d\mathbf{x}_i}{dt} = \frac{\mathbf{p}_i}{m}\,, \qquad \frac{d\mathbf{p}_i}{dt} = \mathbf{F}_i\,. \tag{2.94}$$

These equations can be solved with high accuracy using a staggered leapfrog algorithm

$$\mathbf{v}_i(t_{n+1/2}) = \mathbf{v}_i(t_n) + \mathbf{a}_i(t_n)\Delta t/2\,, \tag{2.95}$$

$$\mathbf{r}_i(t_{n+1}) = \mathbf{r}_i(t_n) + \mathbf{v}_i(t_{n+1/2})\Delta t\,, \tag{2.96}$$

$$\mathbf{v}_i(t_{n+1}) = \mathbf{v}_i(t_{n+1/2}) + \mathbf{a}_i(t_{n+1})\Delta t/2\,, \tag{2.97}$$

where $\mathbf{a}_i = \mathbf{F}_i/m$ is the acceleration of particle i, and $\Delta t = t_{n+1} - t_n$ is the time step of the algorithm. The size of the time step depends on the specific problem, but a good check is provided by monitoring conservation of energy.

The collision term is treated stochastically, by allowing the test particles to collide with the scaled cross section $\sigma_t = (N/N_t)\sigma$. To determine whether a collision occurs we go through all pairs of particles and compute the relative distance $\mathbf{r}_{ij} = \mathbf{r}_i - \mathbf{r}_j$ and velocity $\mathbf{v}_{ij} = \mathbf{v}_i - \mathbf{v}_j$. We then determine whether on the current trajectory the time of closest approach will be reached during the next time step. This happens if $t_{min} = t_n - \mathbf{r}_{ij} \cdot \mathbf{v}_{ij}/\mathbf{v}_{ij}^2$ satisfies $|t_{min} - t_n| \leq \Delta t/2$. In that case we compute

$$r_{min}^2 = \mathbf{r}_{ij}^2 - \frac{(\mathbf{r}_{ij} \cdot \mathbf{v}_{ij})^2}{\mathbf{v}_{ij}^2} \tag{2.98}$$

and check if $\pi r_{min}^2 < \sigma_t$. If this condition is satisfied then the collision is allowed to take place. For an s-wave elastic collision we propagate the particles to t_{min}, randomize their relative velocity $\mathbf{v}_{ij}$, and then propagate them back to t_n. Higher partial wave amplitudes are easy to implement by randomizing $\mathbf{v}_{ij}$ with suitable probability distributions. After all pairs have been checked we perform the velocity and position update in equ. (2.95-2.97).

There are a number of refinements that can be included. At low temperature Pauli-blocking has to be taken into account. This can be done by computing the phase space densities $f(\mathbf{r}_i, \mathbf{p}_i, t)$ for the collision products, and accepting the collision with probability $(1-f_i)(1-f_j)$. At higher energies relativistic effects are important. Relativistic effects in the particle propagation are easy to incorporate, but the treatment of the collision term is more subtle. The problem is that a finite collision cross section, treated geometrically, will lead to instantaneous interactions at a distance. Additional difficulties arise from the treatment of resonances, pair production and annihilation, n-body processes, etc. There are a number of codes on the market that address these issues, and that have been tuned against existing data on pp, pA and AA interactions in the relativistic regime. Examples include UrQMD [106], GiBUU [107], HSD [108], and others.

At high energies the initial pp collisions are very inelastic, and one has to rely on Monte Carlo generators developed in the high energy physics community. A possible alternative is to use a purely partonic kinetic theory that involves scattering between quark and gluon quasiparticles. There are some subtleties with this approach, having to do with the problem of how to include screening and damping of the exchanged gluons, soft gluon radiation, etc. I will not attempt to discuss these issues here, and I refer the reader to the original literature [109, 110].

2.5.4 Classical field theory

An interesting simplification occurs if the occupation numbers are large, $f \gg 1$. This is argued to happen for the gluons in the initial state of a heavy ion collision [111]. In this limit the classical kinetic theory is equivalent to a classical field theory [112]. Indeed, if the occupations numbers are non-perturbative, $f \gtrsim 1/g$, the kinetic theory no longer applies, and we have to rely on classical field theory. In general the classical action is not known, but in the weak coupling limit the bare QCD action can be used.

Classical QCD simulation have been used to study a number of issues, such as particle production from an overpopulated gluon field, and the possible approach to thermal equilibrium. Instabilities in the classical field evolution may play an important role in speeding up the equilibration process. Here, I will briefly describe a method for solving classical evolution equations on a space-time lattice, following the recent review [113].

In order to construct a Hamiltonian approach to lattice QCD I start from the Wilson action in Minkowski space with separate coupling constants β_0 and β_s in the temporal and spatial direction

$$S[U] = -\frac{\beta_0}{2N_c}\sum_x\sum_{i=1}^{3}\mathrm{Tr}\left(W_{0i}(x)+W_{0i}^\dagger(x)-2\right)+\frac{\beta_s}{2N_c}\sum_x\sum_{i<j}\mathrm{Tr}\left(W_{ij}(x)+W_{ij}^\dagger(x)-2\right), \tag{2.99}$$

In the continuum limit, we expect

$$\beta_0 = \frac{2N_c a}{g^2\Delta t}, \qquad \beta_s = \frac{2N_c\Delta t}{g^2 a}. \tag{2.100}$$

where a and Δt are spatial and temporal lattice spacings. In order to construct a Hamiltonian we have to fix the gauge freedom of the theory. Here, I will use the temporal axial gauge, $A_0 = 0$. In this case the canonical variables are the spatial gauge potentials and the conjugate momenta are the electric fields. On the lattice the gauge $A_0 = 0$ corresponds to setting all temporal gauge links to the identity, $U_0(x) = 1$. The canonical variables are given by the spatial gauge links $U_j(x)$, and the conjugate momenta are the temporal plaquettes $W_{0j}(x)$. In the continuum limit

$$A_j^a(x) = \frac{2i}{ag}\mathrm{Tr}\big[\lambda^a U_j(x)\big], \tag{2.101}$$

$$E_j^a(x) = \frac{2i}{ag\Delta t}\mathrm{Tr}\big[\lambda^a W_{0j}(x)\big]. \tag{2.102}$$

Varying the action equ. (2.99) with respect to $U_j(x)$ gives an equation of motion for E_j

$$E_j^a(t+\Delta t,\mathbf{x}) = E_j^a(t,\mathbf{x}) + \frac{i\Delta t}{ga^3}\sum_k\Big\{\mathrm{Tr}\Big[\lambda^a U_j(x)U_k(x+\hat{j})U_j^\dagger(x+\hat{k})U_k^\dagger(x)\Big] + \mathrm{Tr}\Big[\lambda^a U_j(x)U_k^\dagger(x+\hat{j}-\hat{k})U_j^\dagger(x-\hat{k})U_k(x-\hat{k})\Big]\Big\}. \tag{2.103}$$

We note that $E_j^a(t+\Delta t,\mathbf{x})$ is determined by the electric fields and the spatial gauge links at time t. Using equ. (2.102) and the electric field E_j^a at time $t+\Delta t$ we can compute the temporal plaquette $W_{0j}(x)$ at $t+\Delta t$. This result can be used to evolve the spacelike gauge links

$$U_j(t+\Delta t,\mathbf{x}) = W_{0j}(x)U_j(x). \tag{2.104}$$

Together, equ. (2.103) and equ. (2.104) describe a staggered leapfrog algorithm, similar to equ. (2.95-2.97) above. An important constraint on the numerical evolution is provided by Gauss law. Varying the lattice action with respect to U_0 before imposing temporal axial gauge gives

$$\sum_j\Big[E_j^a(x) - U_j^\dagger(x-\hat{j})E_j^a(x-\hat{j})U_j(x-\hat{j})\Big] = 0. \tag{2.105}$$

This constraint is preserved by the evolution equations.

The classical field equations are exactly scale invariant and there is no dependence on the coupling constant g. Physical quantities, like the energy momentum tensor, explicitly depend on g. In practice classical field simulations require a model for the initial conditions and the corresponding coupling. The initial conditions are typically an ensemble of gauge fields distributed according to some distribution, for example an anisotropic Gaussian in momentum space. The anisotropy is assumed to be a consequence of the strong longitudinal expansion of the initial state of a heavy ion collision. Physical observables are determined by averages the evolved fields over the initial ensemble.

Note that a purely classical field evolution does not thermalize. A thermal ensemble of classical fields would satisfy the equipartition law, and the total energy would be dominated by modes near the lattice cutoff. This is the Rayleigh-Jeans UV catastrophe. However, classical field evolution has interesting non-thermal fixed points [114], which may play a role in thermalization.

The classical field framework has been extended in a variety of ways. One direction is the inclusion of quantum fluctuations on top of the classical field [115]. Another problem is the inclusion of modes that are not highly populated. In the hard thermal loop approximation one can show that hard modes can be described as colored particles interacting with the classical field corresponding to the soft modes [116]. The equations of motion for the colored particles are known as Wong's equations [117]. Numerical studies can be found in [118].

2.5.5 Nonequilibrium QCD: Holography

A new approach to quantum fields in and out of equilibrium is provided by the AdS/CFT correspondence [119–123]. The AdS/CFT correspondence is a holographic duality. It asserts that the dynamics of a quantum field theory defined on the boundary of a higher dimensional space is encoded in boundary correlation functions of a gravitational theory in the bulk. The correspondence is simplest if the boundary theory is strongly coupled and contains a large number N of degrees of freedom. In this case the bulk theory is simply classical Einstein gravity. The partition function of the boundary quantum field theory (QFT) is

$$Z_{QFT}[J_i] = \exp\left(-S\left[\phi_i|_{\partial M} = J_i\right]\right), \tag{2.106}$$

where J_i is a set of sources in the field theory, S is the gravitational action, ϕ_i is a dual set of fields in the gravitational theory, and ∂M is the boundary of AdS_5. The fields ϕ_i satisfy classical equations of motions subject to boundary conditions on ∂M.

The original construction involves a black hole in AdS_5 and is dual to a relativistic fluid governed by a generalization of QCD known as $\mathcal{N} = 4$ super Yang-Mills theory. This theory is considered in the limit of a large number of colors N_c. The gravitational theory is Einstein gravity with additional matter fields that are not relevant here. The AdS_5 black hole metric is

$$ds^2 = \frac{(\pi T R_a)^2}{u}\left(-f(u)dt^2 + d\mathbf{x}^2\right) + \frac{R_a^2}{4u^2 f(u)}du^2, \tag{2.107}$$

where $\mathbf{x}, t$ are Minkowski space coordinates, and u is a "radial" coordinate where $u = 1$ is the location of the black hole horizon and $u = 0$ is the boundary. T is the temperature, R_a is the AdS radius, and $f(u) = 1 - u^2$.

It is instructive to check that this metric does indeed provide a solution to the Einstein equations with a negative cosmological constant. This can be done using a simple Mathematica script. I begin by defining the metric and its inverse:

```
(* metric *)
(* ------ *)
n = 5;
coord = {t, x, y, z, u};
f[u_] := 1 - u^2
metric = DiagonalMatrix[{-f[u]/u*(Pi*T*Ra)^2, (Pi*T*Ra)^2/u, (Pi*T*Ra)^2/
   u, (Pi*T*Ra)^2/u, Ra^2/(4*u^2*f[u])}]
inversemetric = Simplify[Inverse[metric]]
```

From the metric I compute the Christoffel symbols

$$\Gamma^{\mu}_{\alpha\beta} = \frac{1}{2} g^{\mu\nu} \left(\partial_\alpha g_{\nu\beta} + \partial_\beta g_{\nu\alpha} - \partial_\mu g_{\alpha\beta} \right) , \tag{2.108}$$

the Riemann tensor

$$R^{\mu}{}_{\nu\alpha\beta} = \partial_\alpha \Gamma^{\mu}_{\nu\beta} - \partial_\beta \Gamma^{\mu}_{\nu\alpha} + \Gamma^{\rho}_{\nu\beta} \Gamma^{\mu}_{\rho\alpha} - \Gamma^{\rho}_{\nu\alpha} \Gamma^{\mu}_{\rho\beta} , \tag{2.109}$$

the Ricci tensor $R_{\alpha\beta} = R^{\mu}{}_{\alpha\mu\beta}$, and the scalar curvature $R = R^{\mu}{}_{\mu}$. Finally, I compute the Einstein tensor $G_{\mu\nu} = R_{\mu\nu} - \frac{1}{2} g_{\mu\nu} R$.

```
(* Christoffel Symbols *)
(* ------------------- *)
affine := affine = Simplify[
  Table[(1/2)*
   Sum[(inversemetric[[i, s]])*(D[metric[[s, j]], coord[[k]]] +
      D[metric[[s, k]], coord[[j]]] -
      D[metric[[j, k]], coord[[s]]]), {s, 1, n}], {i, 1, n}, {j, 1,
    n}, {k, 1, n}]]

(* Riemann Tensor *)
(* -------------- *)
riemann := riemann = Simplify[Table[
   D[affine[[i, j, l]], coord[[k]]] -
    D[affine[[i, j, k]], coord[[l]]] +
    Sum[affine[[s, j, l]]*affine[[i, k, s]] -
     affine[[s, j, k]]*affine[[i, l, s]], {s, 1, n}], {i, 1, n}, {j,
    1, n}, {k, 1, n}, {l, 1, n}]]

(* Ricci Tensor *)
(* ------------ *)
ricci := ricci = Simplify[
  Table[Sum[riemann[[i, j, i, l]], {i, 1, n}], {j, 1, n}, {l, 1, n}]]

(* scalar curvature *)
(* ---------------- *)
scalar = Simplify[
 Sum[inversemetric[[i, j]]*ricci[[i, j]], {i, 1, n}, {j, 1, n}]]

(* Einstein tensor *)
(* --------------- *)
einstein = Simplify[ricci - (1/2)*scalar*metric]
```

Now I can check the equation of motion, $G_{\mu\nu} = \frac{\Lambda}{2} g_{\mu\nu}$, where the cosmological constant is determined by the AdS radius R.

```
(* Field equation with cosmological constant *)
(* ----------------------------------------- *)
lam = 12/Ra^2;
Simplify[einstein - lam/2*metric]
```

In the boundary theory the metric couples to the stress tensor $\Pi_{\mu\nu}$. Correlation functions of the stress tensor can be found by linearizing the bulk action around the AdS_5 solution, $g_{\mu\nu} = g^0_{\mu\nu} + \delta g_{\mu\nu}$. Small oscillations of the off-diagonal strain δg^y_x are particularly simple, because the equation of motion for $\phi \equiv g^y_x$ is that of a minimally coupled scalar

$$\frac{1}{\sqrt{-g}}\partial_\mu\left(\sqrt{-g}g^{\mu\nu}\partial_\nu\phi\right)=0\,. \tag{2.110}$$

The wave equation can be obtained using the metric coefficients defined above.

```
(* \sqrt{-g} g^{\mu\nu} \partial_{nu} \Phi(t,z,u) *)
(* ---------------------------------------------- *)
SqrtG = Simplify[Sqrt[-Det[metric]], {Ra > 0, T > 0, u > 0}]
dnuPhi = Table[D[Phi[t, z, u], coord[[i]]], {i, 1, n}];
DnuPhi = SqrtG*inversemetric.dnuPhi;

(* Laplacian, up to factor \sqrt{-g} *)
(* ---------------------------------- *)
DPhi = FullSimplify[Sum[D[DnuPhi[[nu]], coord[[nu]]], {nu, 1, n}]]

(* harmonic space and time dependence *)
(* ---------------------------------- *)
DPhiS =
 DPhi /. { D[Phi[t, z, u], {z, 2}] -> -k^2*fp,
   D[Phi[t, z, u], {t, 2}] -> -w^2*fp,
   D[Phi[t, z, u], {u, 2}] -> fpPP, D[Phi[t, z, u], {u, 1}] -> fpP}
```

In the case of harmonic dependence on the Minkowski coordinates $\delta g^y_x=\phi_k(u)e^{ikx-i\omega t}$ the fluctuations are governed by the wave equation

$$\phi_k''(u)-\frac{1+u^2}{uf(u)}\phi_k'(u)+\frac{\omega^2-k^2f(u)}{(2\pi T)^2uf(u)^2}\phi_k(u)=0\,. \tag{2.111}$$

This differential equation has two linearly independent solutions. The retarded correlation function corresponds to picking a solution that is purely infalling at the horizon [120]. The retarded correlation function $G_R(\omega,k)$ defined in equ. (2.60) is determined by inserting the solution into the Einstein-Hilbert action, and then computing the variation with respect to the boundary value of δg^y_x.

The infalling solution can be expressed as

$$\phi_k(u)=(1-u)^{-i\mathfrak{w}/2}F_k(u) \tag{2.112}$$

where $\mathfrak{w}=\omega/(2\pi T)$ and the first factor describes the near horizon behavior. The function $F_k(u)$ can be obtained as an expansion in $\mathfrak{w}$ and $\mathfrak{k}=k/(2\pi T)$. At second order in $O(\mathfrak{w}$ and $\mathfrak{k}$ the solution is [124]

$$F_k(u)=1-\frac{i\mathfrak{w}}{2}\log\left(\frac{1+u}{2}\right)+\frac{\mathfrak{w}^2}{8}\left\{\left[8-\frac{8\mathfrak{k}^2}{\mathfrak{w}^2}+\log\left(\frac{1+u}{2}\right)\right]\log\left(\frac{1+u}{2}\right)-4Li_2\left(\frac{1-u}{2}\right)\right\}. \tag{2.113}$$

In the opposite limit, $\mathfrak{w}\gg 1$, the wave equation can be solved using a WKB approximation [125]. For $\mathfrak{k}=0$ the result is

$$\phi_k(u)=\pi\mathfrak{w}^2\frac{u}{\sqrt{1-u^2}}\left[iJ_2\left(2\mathfrak{w}\sqrt{u}\right)-Y_2\left(2\mathfrak{w}\sqrt{u}\right)\right]. \tag{2.114}$$

In the intermediate regime the wave equation can be solved numerically. A standard method is to start from the near horizon result given in equ. (2.112) and integrate outwards towards the boundary. The retarded correlation function is given by the variation of the boundary action with respect to the field. For this purpose we consider the quadratic part of the Einstein-Hilbert action and use the AdS/CFT correspondence to express Newton's constant in terms of gauge theory parameters. We find

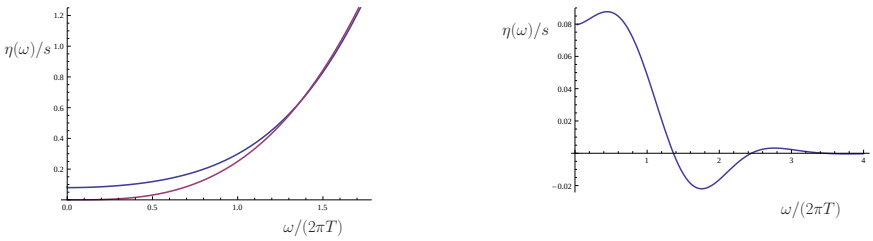

Fig. 2.5 Viscosity spectral function in a $\mathcal{N}=4$ SUSY Yang Mills plasma. The spectral function is computed in the large N_c limit of a strongly coupled plasma using the AdS/CFT correspondence. The figure in the left panel shows $\eta(\omega)/s$ (blue) and the zero temperature counterpart $\eta_{T=0}(\omega)/s$ (red) as a function of ω. The figure in the right panel shows the finite temperature part $[\eta(\omega)-\eta_{T=0}(\omega)]/s$. The figures were generated using the script described below equ. (2.116).

$$S=-\frac{\pi^2N^2T^4}{8}\int du\int d^4x\,\frac{f(u)}{u}\,(\partial_u\phi)^2+\ldots. \tag{2.115}$$

The boundary action follows after an integration by parts. The retarded Green function is determined by the second variational derivative with respect to the boundary value of the field [124, 126],

$$G_R(\mathfrak{w},\mathfrak{k})=-\frac{\pi^2N^2T^4}{4}\left[\frac{f(u)\partial_u\phi_k(u)}{u\phi_k(u)}\right]_{u\to 0}. \tag{2.116}$$

Finally, the spectral function is given by $\eta(\omega,k)=-\omega^{-1}ImG_R(\omega,k)$. Below is a short Mathematica script that determines the spectral function numerically.

```
(* equation of motion for minimally coupled scalar *)
(* with harmonic space and time dependence *)
(* ------------------------------------------------ *)
f[u_] := 1 - u^2
EomPhi = phi''[u] - (1 + u^2)/(u f[u]) phi'[u]
  + (w^2 - q^2 f[u])/(u f[u]^2) phi[u]

(* boundary solution *)
(* ----------------- *)
phiHorizon[u_] := (1-u)^(-I*w/2)

(* numerically integrate from Horizon to boundary *)
(* ---------------------------------------------- *)
SolPhi[omega_, qq_] := Block[{w = omega, q = qq},
  NDSolve[
   {0 == EomPhi,
    phi[epsH] == phiHorizon[epsH],
```

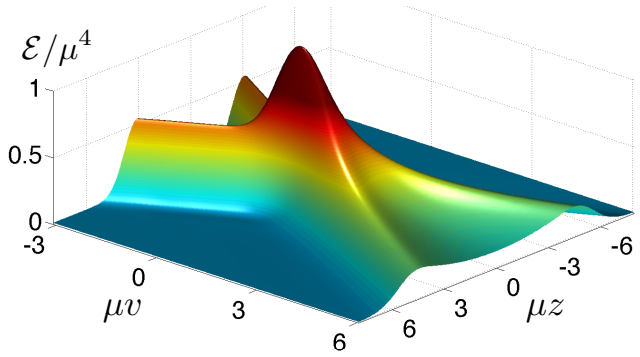

Fig. 2.6 Energy density of colliding shock waves in AdS_5 space [127]. The figure shows the energy density $\mathscr{E}/\mu^4$ on the boundary of AdS_5 as a function of the time coordinate v and the longitudinal direction z. The shocks are infinitely extended in the transverse direction. The parameter μ sets the overall scale.

```
    phi'[epsH] == phiHorizon'[epsH]},
   phi[u],
   {u, epsB, epsH}]][[1, 1, 2]]

(* retarded correlator from boundary action *)
(* ---------------------------------------- *)
Gret[omega_, qq_] := (f[u]/u D[solPhi[omega, qq], u]/solPhi[omega, qq] )
 /. {u -> epsB}
```

The spectral function for $k = 0$ is shown in Fig. 2.5. This is an interesting result because it represent a systematic calculation of a real time observable in the strong coupling limit of a quantum field theory. As explained in Sect. 2.4.5 the corresponding lattice calculation is very difficult, and existing results are difficult to improve upon. We also note that the result is quite different from expectations at weak coupling. At weak coupling we expect the spectral function to show a narrow transport peak at zero energy [79].

So far we have only considered calculations very close to equilibrium, corresponding to small perturbations of the AdS_5 Schwarzschild solution. In order to address the problem of initial state dynamics and thermalization we have to consider initial conditions that mimic colliding nuclei. Recent work focuses on colliding shock waves in asymptotically AdS_5 spaces. In the strong coupling limit the evolution of the shock waves is a problem in numerical relativity. Special methods have been developed to deal with problems in AdS space [128]. These methods are quite different from the techniques employed in connection with black hole or neutron star mergers in asymptotically flat Minkowski space time. A typical result is shown in Fig. 2.6. The calculations demonstrate fast “hydrodynamization”, that means a rapid decay of non-hydrodynamic modes. At somewhat longer time scales thermal equilibration is achieved. This corresponds to the formation of an event horizon in the bulk. In general, it was realized that there is a fluid-gravity correspondence, an equivalence between dynamic space times containing a horizon and solutions of the Navier-Stokes equation [129]. This correspondence can be used to study, both analytically and numerically, difficult problems in fluid dynamics.

2.6 Outlook and acknowledgments

I hope this brief review provides a flavor of the breadth of computational problems that are related QCD. This includes many issues that are at the forefront of computational physics, like

the sign problem in euclidean QCD at finite baryon density, and the challenge to extract real time correlation functions from the euclidean path integral. It also includes many problems that are of great interest to mathematicians. Both the Yang-Mills existence and mass gap as well as the Navier-Stokes existence and smoothness problems are among the Clay Millenium Prize problems [130, 131]. Interesting work on the Boltzmann equation was recently recognized with a Field medal [132], and gradient flow plays an important role in the proof of the Poincare conjecture [133].

Acknowledgements The euclidean path integral simulation in quantum mechanics is described in [6], and the programs are available at `https://www.physics.ncsu.edu/schaefer/physics/`. A simple Z_2 lattice gauge code can be found in the Appendix. You should be able to extend this code to $SU(2)$ and $SU(3)$. Modern lattice QCD tools can be found on the chroma website `http://github.com/JeffersonLab/chroma`. The VH1 hydro code is described in [95] and can be downloaded at `http://wonka.physics.ncsu.edu/pub/VH-1/`. Dissipative and anisotropic versions are available on request. There are a number of relativistic hydro codes on the web. An example is the VISHNU code [134] which is available at `https://u.osu.edu/vishnu/`. Both UrQMD `http://urqmd.org/` and GiBUU `https://gibuu.hepforge.org/` are also available online.

The mathematica notebooks in Sect. 2.5.5 are adapted from notebooks available on Jim Hartle's website `http://web.physics.ucsb.edu/~gravitybook/`. Much more sophisticated tensor packages are easily found on the web. The simple script for solving the wave equation in AdS_5 is adapted from a notebook written by Matthias Kaminski. A set of lecture notes and mathematica notebooks for solving the Einstein equations numerically on asymptotically AdS spaces can be found on Wilke van der Schee's website `https://sites.google.com/site/wilkevanderschee/ads-numerics`. T. S. work is supported by the US Department of Energy grant DE-FG02-03ER41260.

Appendix: Z_2 gauge theory

This is a simple Monte Carlo program for Z_2 gauge theory written by M. Creutz [135].

```
/* Z_2 lattice gauge simulation */
/* Michael Creutz <creutz@bnl.gov> */
/* http://thy.phy.bnl.gov/~creutz/z2.c */

#include <stdio.h>
#include <stdlib.h>
#include <math.h>

/* the lattice is of dimensions SIZE**4 */
#define SIZE 6
int link[SIZE][SIZE][SIZE][SIZE][4]; /* last index gives link direction */

/* utility functions */
void moveup(int x[],int d) {
  x[d]+=1;
  if (x[d]>=SIZE) x[d]-=SIZE;
  return;
}
void movedown(int x[],int d) {
  x[d]-=1;
  if (x[d]<0) x[d]+=SIZE;
  return;
}
void coldstart(){ /* set all links to unity */
  int x[4],d;
  for (x[0]=0;x[0]<SIZE;x[0]++)
    for (x[1]=0;x[1]<SIZE;x[1]++)
      for (x[2]=0;x[2]<SIZE;x[2]++)
        for (x[3]=0;x[3]<SIZE;x[3]++)
```

```
        for (d=0;d<4;d++)
    link[x[0]][x[1]][x[2]][x[3]][d]=1;
  return;
}
/* for a random start: call coldstart() and then update once at beta=0 */

/* do a Monte Carlo sweep; return energy */
double update(double beta){
  int x[4],d,dperp,staple,staplesum;
  double bplus,bminus,action=0.0;
  for (x[0]=0; x[0]<SIZE; x[0]++)
   for (x[1]=0; x[1]<SIZE; x[1]++)
    for (x[2]=0; x[2]<SIZE; x[2]++)
     for (x[3]=0; x[3]<SIZE; x[3]++)
      for (d=0; d<4; d++) {
       staplesum=0;
       for (dperp=0;dperp<4;dperp++){
        if (dperp!=d){
         /* move around thusly:
            dperp     6--5
            ^         | |
            |         1--4
            |         | |
            -----> d  2--3 */
         /* plaquette 1234 */
         movedown(x,dperp);
         staple=link[x[0]][x[1]][x[2]][x[3]][dperp]
           *link[x[0]][x[1]][x[2]][x[3]][d];
         moveup(x,d);
         staple*=link[x[0]][x[1]][x[2]][x[3]][dperp];
         moveup(x,dperp);
         staplesum+=staple;
         /* plaquette 1456 */
         staple=link[x[0]][x[1]][x[2]][x[3]][dperp];
         moveup(x,dperp);
         movedown(x,d);
         staple*=link[x[0]][x[1]][x[2]][x[3]][d];
         movedown(x,dperp);
         staple*=link[x[0]][x[1]][x[2]][x[3]][dperp];
         staplesum+=staple;
        }
    }
        /* calculate the Boltzmann weight */
        bplus=exp(beta*staplesum);
        bminus=1/bplus;
        bplus=bplus/(bplus+bminus);
        /* the heatbath algorithm */
        if ( drand48() < bplus ){
         link[x[0]][x[1]][x[2]][x[3]][d]=1;
         action+=staplesum;
        }
        else{
         link[x[0]][x[1]][x[2]][x[3]][d]=-1;
         action-=staplesum;
        }
       }
  action /= (SIZE*SIZE*SIZE*SIZE*4*6);
  return 1.-action;
}

/****************************/
```

```
int main(){
  double beta, dbeta, action;
  srand48(1234L); /* initialize random number generator */
  /* do your experiment here; this example is a thermal cycle */
  dbeta=.01;
  coldstart();
  /* heat it up */
  for (beta=1; beta>0.0; beta-=dbeta){
    action=update(beta);
    printf("%g\t%g\n",beta,action);
  }
  printf("\n\n");
  /* cool it down */
  for (beta=0; beta<1.0; beta+=dbeta){
    action=update(beta);
    printf("%g\t%g\n",beta,action);
  }
  printf("\n\n");
  exit(0);
}
```

Chapter 3
Lattice quantum chromodynamics approach to nuclear physics

Tetsuo Hatsuda

Abstract Each chapter should be preceded by an abstract (10–15 lines long) that summarizes the content. The abstract will appear *online* at `www.SpringerLink.com` and be available with unrestricted access. This allows unregistered users to read the abstract as a teaser for the complete chapter. As a general rule the abstracts will not appear in the printed version of your book unless it is the style of your particular book or that of the series to which your book belongs.

Please use the 'starred' version of the new Springer `abstract` command for typesetting the text of the online abstracts (cf. source file of this chapter template `abstract`) and include them with the source files of your manuscript. Use the plain `abstract` command if the abstract is also to appear in the printed version of the book.

3.1 General Introduction

3.2 Continuum quantum chromodynamics: basics

3.3 Lattice quantum chromodynamics: basics

3.4 Lattice quantum chromodynamics: applications

3.5 Hadron interactions: basics

Acknowledgements If you want to include acknowledgments of assistance and the like at the end of an individual chapter please use the `acknowledgement` environment – it will automatically render Springer's preferred layout.

Tetsuo Hatsuda
Name of institution and address, e-mail: `name@email.address`

Appendix

References

1. First reference

Chapter 4
Theoretical aspects of few-body systems and effective field theories

Hans-Werner Hammer

Abstract Each chapter should be preceded by an abstract (10–15 lines long) that summarizes the content. The abstract will appear *online* at `www.SpringerLink.com` and be available with unrestricted access. This allows unregistered users to read the abstract as a teaser for the complete chapter. As a general rule the abstracts will not appear in the printed version of your book unless it is the style of your particular book or that of the series to which your book belongs.

Please use the 'starred' version of the new Springer `abstract` command for typesetting the text of the online abstracts (cf. source file of this chapter template `abstract`) and include them with the source files of your manuscript. Use the plain `abstract` command if the abstract is also to appear in the printed version of the book.

4.1 General Introduction

4.2 More stuff

Acknowledgements If you want to include acknowledgments of assistance and the like at the end of an individual chapter please use the `acknowledgement` environment – it will automatically render Springer's preferred layout.

Hans-Werner Hammer
Name of institution and address, e-mail: `name@email.address`

Chapter 5
Lattice methods and effective field theory

Amy Nicholson

Abstract Each chapter should be preceded by an abstract (10–15 lines long) that summarizes the content. The abstract will appear *online* at `www.SpringerLink.com` and be available with unrestricted access. This allows unregistered users to read the abstract as a teaser for the complete chapter. As a general rule the abstracts will not appear in the printed version of your book unless it is the style of your particular book or that of the series to which your book belongs.

Please use the 'starred' version of the new Springer `abstract` command for typesetting the text of the online abstracts (cf. source file of this chapter template `abstract`) and include them with the source files of your manuscript. Use the plain `abstract` command if the abstract is also to appear in the printed version of the book.

5.1 Introduction

5.2 Basics of lattice effective field theory

5.3 Calculating Observables

5.4 Systematic errors and improvement

5.5 Beyond simple leading order effective field theory

Acknowledgements If you want to include acknowledgments of assistance and the like at the end of an individual chapter please use the `acknowledgement` environment – it will automatically render Springer's preferred layout.

Amy Nicholson
Name of institution and address, e-mail: `name@email.address`

Chapter 6
Lattice methods and the nuclear few- and many-body problem

Dean Lee

Abstract This chapter builds upon the review of lattice methods and effective field theory of the previous chapter. We begin with a brief overview of lattice calculations using chiral effective field theory. We then describe several methods for computing scattering on the lattice. After that we focus on the main goal, explaining the theory and algorithms relevant to lattice simulations of nuclear few- and many-body systems. We discuss the exact equivalence of four different lattice formalisms, the Grassmann path integral, transfer matrix operator, Grassmann path integral with auxiliary fields, and transfer matrix operator with auxiliary fields. Along with our analysis we include several coding examples and a number of exercises for the calculations of few- and many-body systems at leading order in chiral effective field theory.

6.1 Introduction

Effective field theory (EFT) provides a theoretical framework for organizing low-energy interactions in powers of particle momenta. Chiral effective field theory applies this framework to the low-energy interactions of protons and neutrons while explicitly including the interactions of pions [136–144]. Pions are qualitatively different from other mesons since they become massless in the limit of massless quarks, thereby producing long-range exchange interactions. The low-energy expansion of chiral EFT is organized in powers of Q, where Q denotes the typical momentum of the nucleons as well as explicit factors of the pion mass. The most important interactions are called leading order (LO) or $O(Q^0)$. The next most important contributions are next-to-leading order (NLO) or $O(Q^2)$. The terms after this are next-to-next-to-leading order (NNLO) or $O(Q^3)$, and so on.

Lattice EFT refers generally to lattice simulations based upon the framework of effective field theory. There are a few reviews in the literature which discuss current methods used in lattice effective field theory [145, 146] as well as the discussion in the previous chapter of this volume. Many different phenomena can be studied in lattice EFT using the same lattice action. In principle all systematic errors are introduced up front when defining the low-energy effective theory, as opposed to the particular computational scheme used to calculate observables.

Lattice EFT has been aided by efficient lattice methods developed for lattice QCD and condensed matter applications. The methods include Markov Chain Monte Carlo techniques,

Dean Lee
Department of Physics, North Carolina State University, Raleigh, NC 27695, USA, e-mail: dean_lee@nscu.edu

auxiliary fields [147, 148], pseudofermion methods [149], and non-local updating schemes such as the hybrid Monte Carlo algorithm [150–152]. Lattice EFT was first used in studies of infinite nuclear matter [153] and infinite neutron matter with and without explicit pions [154–157]. The method has also been used to study light nuclei in pionless EFT [158] and chiral EFT at leading order [159]. There have been further studies of neutron matter [160–162] and light nuclei [163, 164], and there have been several applications to nuclear structure and nuclear clustering [165–170] as well as recent work on nuclear scattering and reactions [171–173].

6.2 Scattering on the lattice

At any given order in the chiral EFT expansion, there will be short-range interaction coefficients which depend on the chosen regularization of the large-momentum divergences. On the lattice this regularization is provided by the lattice spacing, unless some additional regularization is applied to the lattice interactions. In order to set the values of the short-range two-nucleon interaction coefficients, we make a comparison of nucleon-nucleon scattering on the lattice with experimental scattering data. The extension to three-nucleon interaction coefficients is also required at NNLO, and that procedure on the lattice has been discussed in Ref. [163]

As discussed in the previous chapter, Lüscher [174–176] has shown that the finite-volume energy levels for a two-body system in a periodic cubic box are related to the infinite-volume scattering matrix. While the method is very useful at low momenta, it can become less accurate at higher momenta and higher orbital angular momenta. Also spin-orbit coupling and partial-wave mixing are difficult to measure accurately using Lüscher's method due to scattering artifacts produced by the cubic periodic boundary. An alternative approach has been developed to measure phase shifts for particles on the lattice using a spherical wall boundary [177, 178].

In this approach, a hard spherical wall boundary is imposed on the relative separation between the two particles. This wall is placed at some chosen radius $R_{\rm wall}$, and it removes copies of the interactions produced by the periodic lattice. Working in the center-of-mass frame, we solve the time-independent Schrödinger equation as a function of the relative separation between the particles and compute spherical standing waves which vanish at $r = R_{\rm wall}$. At values of r beyond the range of the interaction, the spherical standing waves can be written as a superposition of products of spherical harmonics and spherical Bessel functions,

$$[\cos\delta_\ell \cdot j_\ell(kr) - \sin\delta_\ell \cdot y_\ell(kr)]\, Y_{\ell,\ell_z}(\theta,\phi). \tag{6.1}$$

Here k is the relative momentum between the scattering particles, and δ_ℓ is the phase shift for partial wave L. We can extract k from the energy of the standing wave, and the phase shift δ_ℓ is determined by setting the wave function in Eq. (6.1) to zero at the wall boundary.

When the total intrinsic spin of the two nucleons is nonzero, spin-orbit coupling generates mixing between partial waves. In this case the standing wave at the wall boundary is decomposed into spherical harmonics and coupled-channel equations are solved to extract the phase shifts and mixing angles. The spherical wall method was used to calculate phase shifts and mixing angle for low-energy nucleon-nucleon scattering [160]. Recently the spherical wall approach has been improved in accuracy and computational efficiency [179]. In the improved approach one projects onto spherical harmonics Y_{ℓ,ℓ_z} with angular momentum quantum numbers ℓ, ℓ_z. In this manner one constructs radial position states for a given partial wave,

$$|r\rangle^{\ell,\ell_z} = \sum_{\mathbf{r}'} Y_{\ell,\ell_z}(\hat{\mathbf{r}}')\delta_{r,|\mathbf{r}'|}|\mathbf{r}'\rangle. \tag{6.2}$$

We require that r is less than half the box length $L/2$. Using this technique we are essentially constructing a radial lattice Hamiltonian for each partial wave.

It is also useful to introduce auxiliary potentials in the region lying just in front of the spherical wall boundary [179]. We use the auxiliary potential to tune the energy of the scattering wave. This auxiliary potential is a spherical attractive well positioned in front of the spherical wall boundary. We can tune to any scattering energy by adjusting the depth of the well. For systems with partial wave mixing due to spin-orbit coupling, we also include a Hermitian but imaginary off-diagonal auxiliary potential for the two coupled channels. This breaks time reversal symmetry, and the resulting standing wave solutions now have both real and imaginary parts that are linearly independent. From the real and imaginary solutions one can determine the scattering phase shifts and mixing angle at any given value of the scattering energy.

This spherical wall approach has been used together with a technique called the adiabatic projection method to study nuclear scattering and reactions on the lattice. The adiabiatic projection method [170, 173, 180–182] is a general framework that produces a low-energy effective theory for clusters of particles which becomes exact in the limit of large projection time. For the case of two-cluster scattering, we consider a set of two cluster states $|\mathbf{R}\rangle$ labeled by the spatial separation vector $\mathbf{R}$. The initial wave functions are wave packets which, for large $|\mathbf{R}|$, factorize into a product of two individual clusters,

$$|\mathbf{R}\rangle = \sum_{\mathbf{r}} |\mathbf{r}+\mathbf{R}\rangle_1 \otimes |\mathbf{r}\rangle_2. \tag{6.3}$$

The summation over $\mathbf{r}$ is required to produce states with total momentum equal to zero. We bin the initial cluster states together according to radial distance and angular momentum. In this manner, we form radial position states with projected angular momentum quantum numbers, which we label $|R\rangle^{J,J_z}$.

The next step is to multiply by powers of the transfer matrix in order to form "dressed" cluster states. This produces states that approximately span the set of low-energy cluster-cluster scattering states in our periodic box. We discuss the transfer matrix formalism in detail later in this chapter. After n_t time steps, we have the dressed cluster states

$$|R\rangle_{n_t}^{J,J_z} = M^{n_t}|R\rangle^{J,J_z}. \tag{6.4}$$

These dressed cluster states are then used to compute matrix elements of the transfer matrix M,

$$[M_{n_t}]_{R',R}^{J,J_z} = {}_{n_t}^{J,J_z}\langle R'|M|R\rangle_{n_t}^{J,J_z}. \tag{6.5}$$

Since such states are not orthogonal, we also compute a norm matrix

$$[N_{n_t}]_{R',R}^{J,J_z} = {}_{n_t}^{J,J_z}\langle R'|R\rangle_{n_t}^{J,J_z}. \tag{6.6}$$

The "radial adiabatic transfer matrix" is defined as the matrix product

$$\left[M_{n_t}^a\right]_{R',R}^{J,J_z} = \left[N_{n_t}^{-\frac{1}{2}} M_{n_t} N_{n_t}^{-\frac{1}{2}}\right]_{R',R}^{J,J_z}, \tag{6.7}$$

and the scattering phase shifts can then be determined from the standing waves of the radial adiabatic transfer matrix.

6.3 Lattice formalisms

Throughout our discussion of the lattice formalism we use dimensionless parameters and operators corresponding with physical values times the appropriate power of the spatial lattice spacing a. In our notation the three-component integer vector $\mathbf{n}$ labels the lattice sites of a three-dimensional periodic lattice with dimensions L^3. The spatial lattice unit vectors are denoted $\hat{\mathbf{l}} = \hat{1}, \hat{2}, \hat{3}$. We use n_t to label lattice steps in the temporal direction, and L_t denotes the total number of lattice time steps. The temporal lattice spacing is given by a_t, and $\alpha_t = a_t/a$ is the ratio of the temporal to spatial lattice spacing. We also define $h = \alpha_t/(2m)$, where m is the nucleon mass in lattice units. In Fig. 6.1 we show a diagram of the four different but exactly equivalent lattice formulations that we discuss, the Grassmann path integral, transfer matrix operator, Grassmann path integral with auxiliary fields, and transfer matrix operator with auxiliary fields.

6.3.1 Grassmann path integral

We define the lattice action starting from the lattice Grassmann path integral action without auxiliary fields. This is the simplest formulation in which to derive the lattice Feynman rules. We let c and c^* be anticommuting Grassmann fields for the nucleons. In our notation c is a column vector composed of the spin-isospin nucleon degrees of freedom c_i, while c^* is a row vector of the components c_i^*. The Grassmann fields are periodic with respect to the spatial extent of the L^3 lattice,

$$c_i(\mathbf{n}+L\hat{1},n_t) = c_i(\mathbf{n}+L\hat{2},n_t) = c_i(\mathbf{n}+L\hat{3},n_t) = c_i(\mathbf{n},n_t), \tag{6.8}$$

$$c_i^*(\mathbf{n}+L\hat{1},n_t) = c_i^*(\mathbf{n}+L\hat{2},n_t) = c_i^*(\mathbf{n}+L\hat{3},n_t) = c_i^*(\mathbf{n},n_t), \tag{6.9}$$

and antiperiodic along the temporal direction,

$$c_i(\mathbf{n},n_t+L_t) = -c_i(\mathbf{n},n_t), \tag{6.10}$$

$$c_i^*(\mathbf{n},n_t+L_t) = -c_i^*(\mathbf{n},n_t). \tag{6.11}$$

We write $DcDc^*$ as shorthand for the integral measure,

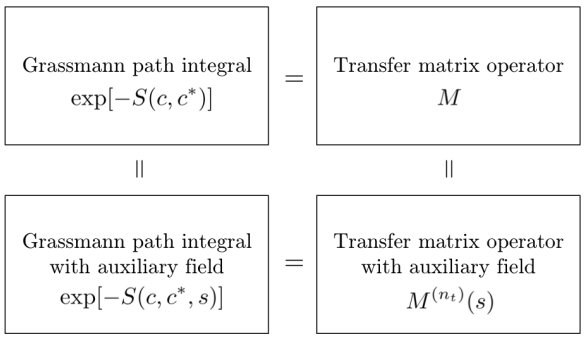

Fig. 6.1 A schematic diagram of the different lattice formulations, namely, the Grassmann path integral, transfer matrix operator, Grassmann path integral with auxiliary fields, and transfer matrix operator with auxiliary fields.

$$DcDc^* = \prod_{\mathbf{n},n_t,i} dc_i(\mathbf{n},n_t)dc_i^*(\mathbf{n},n_t). \tag{6.12}$$

We use the usual convention for Grassmann integration,

$$\int dc_i(\mathbf{n},n_t) = \int dc_i^*(\mathbf{n},n_t) = 0, \tag{6.13}$$

$$\int dc_i(\mathbf{n},n_t)c_i(\mathbf{n},n_t) = \int dc_i^*(\mathbf{n},n_t)c_i^*(\mathbf{n},n_t) = 1 \ \text{ (no sum on } i\text{)}. \tag{6.14}$$

We consider the Grassmann path integral

$$\mathscr{Z} = \int DcDc^* \exp\left[-S(c^*,c)\right], \tag{6.15}$$

where the lattice action can be broken into a free part and interacting part,

$$S(c^*,c) = S_{\text{free}}(c^*,c) + S_{\text{int}}(c^*,c). \tag{6.16}$$

The free part is the free non-relativistic nucleon action, which is

$$S_{\text{free}}(c^*,c) = \sum_{\mathbf{n},n_t} c^*(\mathbf{n},n_t)\left[c(\mathbf{n},n_t+1) - c(\mathbf{n},n_t)\right] + \alpha_t \sum_{n_t} K^{(n_t)}(c^*,c), \tag{6.17}$$

where

$$K^{(n_t)}(c^*,c) = \sum_{k=0,1,2,\cdots} (-1)^k \frac{w_k}{2m} \sum_{\mathbf{n},\hat{\mathbf{l}}} c^*(\mathbf{n},n_t)\left[c(\mathbf{n}+k\hat{\mathbf{l}},n_t) + c(\mathbf{n}-k\hat{\mathbf{l}},n_t)\right], \tag{6.18}$$

and the hopping coefficients w_k correspond to a hopping parameter expansion of the squared momentum,

$$P^2(\mathbf{p}) = 2\sum_{k=0,1,2,\cdots} \sum_{l=1,2,3} (-1)^k w_k \cos\left(kp_l\right). \tag{6.19}$$

The hopping coefficients can be chosen to match the continuum relation

$$P^2(\mathbf{p}) = \mathbf{p}^2, \tag{6.20}$$

up to some chosen level of lattice discretization error. The hopping coefficients w_k for a few different lattice actions are shown in Table 6.1.

Table 6.1 Hopping coefficients w_k for several lattice actions

coefficient	standard	$O(a^2)$-improved	$O(a^4)$-improved
w_0	1	5/4	49/36
w_1	1	4/3	3/2
w_2	0	1/12	3/20
w_3	0	0	1/90

6.3.2 Transfer matrix operator

Let $a_i(\mathbf{n})$ and $a_i^\dagger(\mathbf{n})$ denote fermion annihilation and creation operators for the nucleon component i at lattice site $\mathbf{n}$. The shorthand $a(\mathbf{n})$ represents a column vector of nucleon components $a_i(\mathbf{n})$, and $a^\dagger(\mathbf{n})$ represents a row vector of components $a_i^\dagger(\mathbf{n})$. We can write any Grassmann path integral with instantaneous interactions as the trace of a product of operators using the identity [183, 184]

$$\begin{aligned}
&\mathrm{Tr}\left\{ :F_{L_t-1}\left[a^\dagger(\mathbf{n}'),a(\mathbf{n})\right]: \times\cdots\times :F_0\left[a^\dagger(\mathbf{n}'),a(\mathbf{n})\right]: \right\} \\
&= \int DcDc^* \exp\left\{ \sum_{n_t=0}^{L_t-1} \sum_{\mathbf{n},i} c_i^*(\mathbf{n},n_t)\left[c_i(\mathbf{n},n_t)-c_i(\mathbf{n},n_t+1)\right] \right\} \\
&\qquad \times \prod_{n_t=0}^{L_t-1} F_{n_t}\left[c^*(\mathbf{n}',n_t),c(\mathbf{n},n_t)\right],
\end{aligned} \tag{6.21}$$

where $c_i(\mathbf{n},L_t) = -c_i(\mathbf{n},0)$.

Let us define the free non-relativistic lattice Hamiltonian

$$H_{\mathrm{free}}(a^\dagger,a) = \sum_{k=0,1,2,\cdots} (-1)^k \frac{w_k}{2m} \sum_{\mathbf{n},\hat{\mathbf{l}}} a^\dagger(\mathbf{n})\left[a(\mathbf{n}+k\hat{\mathbf{l}})+a(\mathbf{n}-k\hat{\mathbf{l}})\right]. \tag{6.22}$$

We write the interaction term as $H_{\mathrm{int}}(a^\dagger,a)$, so that our total Hamiltonian is

$$H(a^\dagger,a) = H_{\mathrm{free}}(a^\dagger,a) + H_{\mathrm{int}}(a^\dagger,a). \tag{6.23}$$

Using the correspondence Eq. (6.21), we can rewrite the path integral $\mathscr{Z}$ defined in Eq. (6.15) as a transfer-matrix partition function,

$$\mathscr{Z} = \mathrm{Tr}\left(M^{L_t}\right), \tag{6.24}$$

where M is the normal-ordered transfer matrix operator

$$M =: \exp\left[-H(a^\dagger,a)\alpha_t\right]: . \tag{6.25}$$

Roughly speaking, the transfer matrix operator is the exponential of the Hamiltonian operator over one Euclidean lattice time step. In order to satisfy the identity Eq. (6.21), the exact definition of the transfer matrix is the normal-ordered exponential as defined in Eq. (6.25).

In this transfer matrix formalism, one can do simulations of nucleons using Monte Carlo, and this would essentially be a lattice version of diffusion or Green's function Monte Carlo [185]. Visually one can view the nucleons as interacting with each other while diffusing in space with each time step, as indicated in Fig. 6.2. At leading order in chiral effective field theory, the interactions include two independent S-wave contact interactions and the exchange of pions. We discuss these interactions in detail in the following.

6.3.3 Grassmann path integral with auxiliary field

We now assume that there exists an integral relation that allows us to write $\exp\left[-S_{\mathrm{int}}(c^*,c)\right]$ as an integral over auxiliary fields. The purpose of the auxiliary field transformation is to decouple the interactions among the nucleons. Instead the interactions will be between the nucleons and the auxiliary fields.

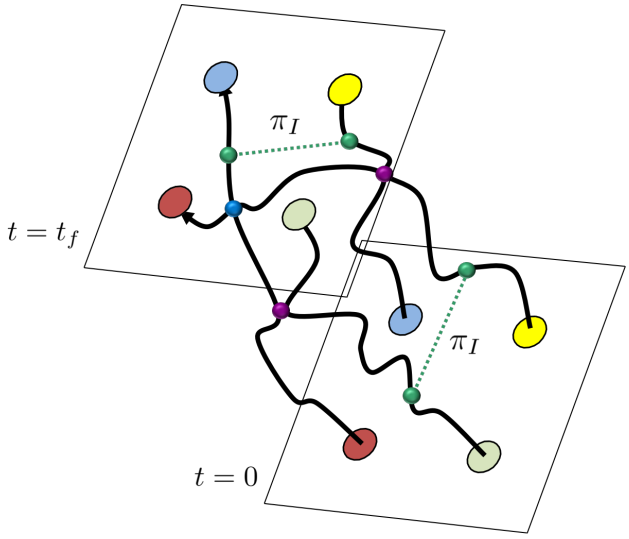

Fig. 6.2 A sketch showing nucleons which evolve with each time step. At leading order in chiral effective field theory, the interactions include two contact interactions and the exchange of pions.

We now illustrate using the interactions that appear at leading order in chiral effective field theory. For pedagogical purposes we discuss the simplest possible implementation of the leading order action on the lattice. We first consider a zero-range contact interaction which is independent of nucleon spin and isospin. The action has the form

$$S_{\rm int}^{C}(c^*,c) = \alpha_t \frac{C}{2} \sum_{\mathbf{n},n_t} \left[c^*(\mathbf{n},n_t)c(\mathbf{n},n_t)\right]^2 . \tag{6.26}$$

We can write this as

$$\exp\left[-S_{\rm int}^{C}(c^*,c)\right] = \int Ds\, \exp\left[-S_{ss}(s) - S_s(c^*,c,s)\right] \tag{6.27}$$

for auxiliary field $s(\mathbf{n},n_t)$, where

$$S_{ss}(s) = \frac{1}{2} \sum_{\mathbf{n},n_t} s^2(\mathbf{n},n_t), \tag{6.28}$$

$$S_s(c^*,c,s) = \sqrt{-C\alpha_t} \sum_{\mathbf{n},n_t} s(\mathbf{n},n_t)c^*(\mathbf{n},n_t)c(\mathbf{n},n_t). \tag{6.29}$$

In our definition of the integration measure Ds, we include a factor of $1/\sqrt{2\pi}$ for each degree of freedom.

Next we consider an isospin-dependent contact interaction

$$S_{\rm int}^{C'}(c^*,c) = \alpha_t \frac{C'}{2} \sum_{\mathbf{n},n_t,I} \left[c^*(\mathbf{n},n_t)\tau_I c(\mathbf{n},n_t)\right]^2, \tag{6.30}$$

where τ_I for $I = 1,2,3$ are the Pauli matrices in isospin space. Then we can use

$$\exp\left[-S_{\rm int}^{C'}(c^*,c)\right] = \int \prod_I Ds_I \exp\left[-S_{s_I s_I}(s_I) - S_{s_I}(c^*,c,s_I)\right] \tag{6.31}$$

for auxiliary fields $s_I(\mathbf{n},n_t)$ where

$$S_{s_I s_I}(s_I) = \frac{1}{2} \sum_{\mathbf{n},n_t,I} s_I^2(\mathbf{n},n_t), \tag{6.32}$$

$$S_{s_I}(c^*,c,s_I) = \sqrt{-C'\alpha_t} \sum_{\mathbf{n},n_t,I} s_I(\mathbf{n},n_t) c^*(\mathbf{n},n_t) \tau_I c(\mathbf{n},n_t). \tag{6.33}$$

Finally we work with the one-pion exchange potential (OPEP). In this case the pion acts much like the auxiliary fields. However there are also spatial correlations in the quadratic part of the pion action and a gradient coupling between the pions and nucleons. The one-pion exchange interaction on the lattice can written as

$$\exp\left[-S_{\rm int}^{\rm OPEP}(c^*,c)\right] = \int \prod_I D\pi_I \exp\left[-S_{\pi_I\pi_I}(\pi_I) - S_{\pi_I}(c^*,c,\pi_I)\right]. \tag{6.34}$$

The free pion action is

$$S_{\pi_I\pi_I}(\pi_I) = \frac{1}{2}\alpha_t m_\pi^2 \sum_{\mathbf{n},n_t,I} \pi_I^2(\mathbf{n},n_t) \tag{6.35}$$

$$+ \frac{1}{2}\alpha_t \sum_{k=0,1,2,\cdots} (-1)^k w_k \sum_{\mathbf{n},n_t,I,\hat{\mathbf{l}}} \pi_I(\mathbf{n},n_t) \left[\pi_I(\mathbf{n}+k\hat{\mathbf{l}},n_t) + \pi_I(\mathbf{n}-k\hat{\mathbf{l}},n_t)\right], \tag{6.36}$$

with the coefficient w_k as defined in Table 6.1 and m_π is the pion mass. At leading order we do not consider any isospin-breaking effects. The pion coupling to the nucleon is

$$S_{\pi_I}(c^*,c,\pi_I) = \frac{g_A\alpha_t}{2f_\pi} \sum_{\mathbf{n},n_t,l,I} \Delta_k \pi_I(\mathbf{n},n_t) c^*(\mathbf{n},n_t) \sigma_k \tau_I c(\mathbf{n},n_t), \tag{6.37}$$

where σ_l for $l = 1,2,3$ are the Pauli matrices in spin space and

$$\Delta_l \pi_I(\mathbf{n},n_t) = \frac{1}{2} \sum_{k=1,2,\cdots} (-1)^{k-1} o_k \left[\pi_I(\mathbf{n}+k\hat{\mathbf{l}},n_t) - \pi_I(\mathbf{n}-k\hat{\mathbf{l}},n_t)\right], \tag{6.38}$$

with coefficients o_k corresponding to a hopping parameter expansion of the momentum,

$$P(p_l) = \sum_{k=1,2,\cdots} (-1)^{k-1} o_k \sin(k p_l). \tag{6.39}$$

Here g_A is the axial-vector coupling constant, and f_π is the pion decay constant. The hopping coefficients can be chosen to match the continuum result

$$P(p_l) = p_l. \tag{6.40}$$

The hopping coefficients o_k for a few different lattice actions are shown in Table 6.2.

Table 6.2 Hopping coefficients o_k for several lattice actions.

coefficent	standard	$O(a^2)$-improved	$O(a^4)$-improved
o_1	1	4/3	3/2
o_2	0	1/6	3/10
o_3	0	0	1/30

6.3.4 Transfer matrix operator with auxiliary field

Using the equivalence in Eq. (6.21), we can write $\mathscr{Z}$ as the trace of a product of transfer matrix operators which depend on the auxiliary field,

$$\mathscr{Z} = \int Ds \prod_I (Ds_I D\pi_I)\ \exp[-S_{ss}(s) - S_{s_I s_I}(s_I) - S_{\pi_I \pi_I}(\pi_I)] \mathrm{Tr}\left\{ M^{(L_t-1)} \cdots M^{(0)} \right\}. \tag{6.41}$$

The transfer matrix at time step n_t is given by

$$M^{(n_t)} =: \exp\left[-H^{(n_t)}(a^\dagger, a, s, s_I, \pi_I)\alpha_t \right] : , \tag{6.42}$$

where

$$H^{(n_t)}(a^\dagger, a, s, s_I, \pi_I)\alpha_t = H_{\mathrm{free}}(a^\dagger, a)\alpha_t + S_s^{(n_t)}(a^\dagger, a, s) + S_{s_I}^{(n_t)}(a^\dagger, a, s_I) + S_{\pi_I}^{(n_t)}(a^\dagger, a, \pi_I), \tag{6.43}$$

and

$$S_s^{(n_t)}(a^\dagger, a, s) = \sqrt{-C\alpha_t} \sum_{\mathbf{n}} s(\mathbf{n}, n_t) a^\dagger(\mathbf{n}) a(\mathbf{n}), \tag{6.44}$$

$$S_{s_I}^{(n_t)}(a^\dagger, a, s_I) = \sqrt{-C'\alpha_t} \sum_{\mathbf{n}, I} s_I(\mathbf{n}, n_t) a^\dagger(\mathbf{n}) \tau_I a(\mathbf{n}), \tag{6.45}$$

$$S_{\pi_I}^{(n_t)}(a^\dagger, a, \pi_I) = \frac{g_A \alpha_t}{2 f_\pi} \sum_{\mathbf{n}, k, I} \Delta_k \pi_I(\mathbf{n}, n_t) a^\dagger(\mathbf{n}) \sigma_k \tau_I a(\mathbf{n}). \tag{6.46}$$

6.4 Projection Monte Carlo

Let us consider a system with A nucleons. We can create a general single-nucleon state using creation operators acting on the vacuum with coefficient function $f(\mathbf{n})$. We write $f(\mathbf{n})$ as a column vector in the space of nucleon spin and isospin components, and the single-nucleon state can be written as

$$|f\rangle = \sum_{\mathbf{n}} a^\dagger(\mathbf{n}) f(\mathbf{n}) |0\rangle . \tag{6.47}$$

For our projection Monte Carlo calculation we take our A-body initial state to be a Slater determinant of single nucleon states,

$$|f_1, \cdots, f_A\rangle = \left[\sum_{\mathbf{n}} a^\dagger(\mathbf{n}) f_1(\mathbf{n}) \right] \cdots \left[\sum_{\mathbf{n}} a^\dagger(\mathbf{n}) f_A(\mathbf{n}) \right] |0\rangle . \tag{6.48}$$

We use the same construction for the A-body final state.

For the purposes of coding the projection Monte Carlo calculation, it is convenient to view the identical nucleons as having a hidden index $j = 1, \cdots, A$ that makes all of the nucleons distinguishable. If we antisymmetrize all physical states over this extra index then all physical observables are exactly recovered. So our initial state $|f_1, \cdots, f_A\rangle$ becomes

$$\begin{aligned} &\frac{1}{\sqrt{A!}} \sum_P \left[\sum_{\mathbf{n}} a^\dagger_{[P(1)]}(\mathbf{n}) f_1(\mathbf{n}) \right] \cdots \left[\sum_{\mathbf{n}} a^\dagger_{[P(A)]}(\mathbf{n}) f_A(\mathbf{n}) \right] |0\rangle \\ &\quad = \frac{1}{\sqrt{A!}} \sum_{P'} \mathrm{sgn}(P') \left[\sum_{\mathbf{n}} a^\dagger_{[1]}(\mathbf{n}) f_{P'(1)}(\mathbf{n}) \right] \cdots \left[\sum_{\mathbf{n}} a^\dagger_{[A]}(\mathbf{n}) f_{P'(A)}(\mathbf{n}) \right] |0\rangle , \end{aligned} \tag{6.49}$$

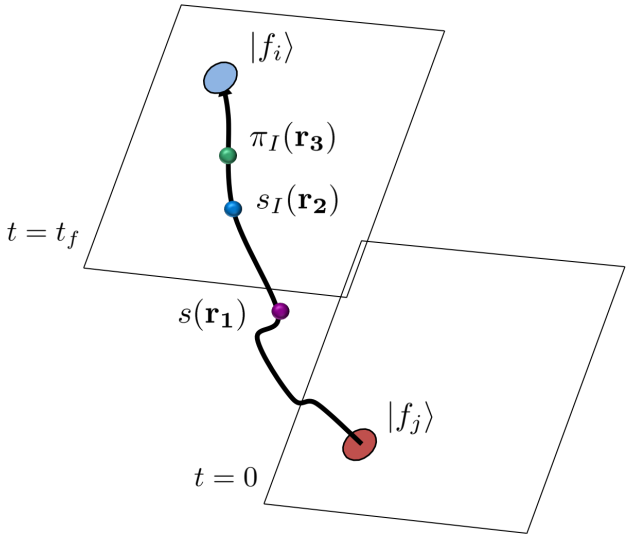

Fig. 6.3 A sketch showing the worldline for a single nucleon with a background of pion fields and auxiliary fields.

where the summations are over all permutations P, and sgn is the sign of the permutation. With these hidden indices our normal-ordered auxiliary-field transfer matrix $M^{(n_t)}$ becomes

$$\left[1 - H^{(n_t)}(a^\dagger_{[1]}, a_{[1]}, s, s_I, \pi_I)\alpha_t\right] \cdots \left[1 - H^{(n_t)}(a^\dagger_{[A]}, a_{[A]}, s, s_I, \pi_I)\alpha_t\right] \tag{6.50}$$

We see that the higher-order powers of the exponential vanish due to normal ordering.

In the projection Monte Carlo calculation we compute the amplitude

$$Z(n_t) = \langle f_1, \cdots, f_A | M^{(n_t-1)} \cdots M^{(0)} | f_1, \cdots, f_A \rangle \tag{6.51}$$

for $n_t = L_t$ and $n_t = L_t - 1$. In the limit of large L_t the amplitudes will be dominated by the state with the lowest energy E_0 and nonzero overlap with $|f_1, \cdots, f_A\rangle$. In this limit the ratio $Z(n_t)/Z(n_t - 1)$ will converge to $\exp(-E_0\alpha_t)$ from above.

Each nucleon evolves as a particle in a fluctuating background of auxiliary fields and pion fields. The original interactions are reproduced after integrating over the fluctuating auxiliary and pion fields. For a simulation with A nucleons, the amplitude for a given configuration of pion and auxiliary fields is proportional to the determinant of an $A \times A$ matrix $\mathbf{M}$. The entries of $\mathbf{M}_{ij}$ are single nucleon worldline amplitudes for a nucleon starting at state $|f_j\rangle$ at $t = 0$ and ending at state $|f_i\rangle$ at $t = t_f = L_t\alpha_t$. This is shown in Fig. 6.3.

In Fig. 6.4, we show a sample code which calculates the auxiliary-field transfer matrix multiplications on the left starting from the single-nucleon initial states. We only show the terms which arise from the free-nucleon transfer matrix and the auxiliary field s. Similarly, in Fig. 6.5, we show a sample code which calculates the auxiliary-field transfer matrix multiplications on the right starting from the single-nucleon final states. Again we present only the terms arising from the free-nucleon transfer matrix and the auxiliary field s. In Fig. 6.6 we show how these transfer matrix product multiplications are implemented as functions or subroutines (specific to Fortran as programming language) and used to compute the determinant and inverse of the matrix of single-nucleon amplitudes $\mathbf{M}$.

6.5 Importance sampling

We do importance sampling according to the positive measure

```
DO nt = nt1+1, nt2
   DO np = 0,num-1
      DO nz = 0,L-1; DO ny = 0,L-1; DO nx = 0,L-1
         DO ni = 0,1; DO ns = 0,1

            zvecs(nx,ny,nz,nt,ns,ni,np) = zvecs(nx,ny,nz,nt-1,ns,ni,np) &
                 * (1.D0-6.D0*w0_N*h+CDSQRT(-c0*atovera*(1.D0,0.D0))*s(nx,ny,nz,nt-1))

            zvecs(nx,ny,nz,nt,ns,ni,np) = zvecs(nx,ny,nz,nt,ns,ni,np) &
                 + w1_N*h*zvecs(MOD(nx+1,L),ny,nz,nt-1,ns,ni,np) &
                 + w1_N*h*zvecs(MOD(nx-1+L,L),ny,nz,nt-1,ns,ni,np) &
                 + w1_N*h*zvecs(nx,MOD(ny+1,L),nz,nt-1,ns,ni,np) &
                 + w1_N*h*zvecs(nx,MOD(ny-1+L,L),nz,nt-1,ns,ni,np) &
                 + w1_N*h*zvecs(nx,ny,MOD(nz+1,L),nt-1,ns,ni,np) &
                 + w1_N*h*zvecs(nx,ny,MOD(nz-1+L,L),nt-1,ns,ni,np)

            IF (improveN >= 1) THEN
               zvecs(nx,ny,nz,nt,ns,ni,np) = zvecs(nx,ny,nz,nt,ns,ni,np) &
                    - w2_N*h*zvecs(MOD(nx+2,L),ny,nz,nt-1,ns,ni,np) &
                    - w2_N*h*zvecs(MOD(nx-2+L,L),ny,nz,nt-1,ns,ni,np) &
                    - w2_N*h*zvecs(nx,MOD(ny+2,L),nz,nt-1,ns,ni,np) &
                    - w2_N*h*zvecs(nx,MOD(ny-2+L,L),nz,nt-1,ns,ni,np) &
                    - w2_N*h*zvecs(nx,ny,MOD(nz+2,L),nt-1,ns,ni,np) &
                    - w2_N*h*zvecs(nx,ny,MOD(nz-2+L,L),nt-1,ns,ni,np)
            END IF

            IF (improveN == 2) THEN
               zvecs(nx,ny,nz,nt,ns,ni,np) = zvecs(nx,ny,nz,nt,ns,ni,np) &
                    + w3_N*h*zvecs(MOD(nx+3,L),ny,nz,nt-1,ns,ni,np) &
                    + w3_N*h*zvecs(MOD(nx-3+L,L),ny,nz,nt-1,ns,ni,np) &
                    + w3_N*h*zvecs(nx,MOD(ny+3,L),nz,nt-1,ns,ni,np) &
                    + w3_N*h*zvecs(nx,MOD(ny-3+L,L),nz,nt-1,ns,ni,np) &
                    + w3_N*h*zvecs(nx,ny,MOD(nz+3,L),nt-1,ns,ni,np) &
                    + w3_N*h*zvecs(nx,ny,MOD(nz-3+L,L),nt-1,ns,ni,np)
            END IF

         END DO; END DO
      END DO; END DO; END DO
   END DO
```

Fig. 6.4 Sample code which calculates the auxiliary-field transfer matrix multiplications on the left starting from the single-nucleon initial states. We only show the terms which arise from the free-nucleon transfer matrix and the auxiliary field s.

$$|Z(L_t)| \exp\left[-S_{ss}(s) - S_{s_I s_I}(s_I) - S_{\pi_I \pi_I}(\pi_I)\right], \tag{6.52}$$

and use hybrid Monte Carlo to do global updates of the auxiliary and pion fields. The hybrid Monte Carlo (HMC) algorithm [150–152] is efficient in quickly generating decorrelated configurations for each auxiliary and pion field. Here we describe the updating algorithm for the s field. The updating of the s_I and π_I fields proceed in a very similar fashion. In general terms, the HMC algorithm can be described by means of a probability weight $P(s)$

$$P(s) \propto \exp[-V(s)], \tag{6.53}$$

where $V(s)$ is in general a non-local function of the field $s(\mathbf{n}, n_t)$, and a molecular dynamics (MD) Hamiltonian,

$$H(s,p) \equiv \frac{1}{2} \sum_{\mathbf{n}, n_t} [p_s(\mathbf{n}, n_t)]^2 + V(s). \tag{6.54}$$

Classical Hamiltonian dynamics is introduced by defining the momentum $p_s(\mathbf{n}, n_t)$ conjugate to $s(\mathbf{n}, n_t)$.

```
DO nt = nt2,nt1+1,-1

   DO np = 0,num-1
      DO nz = 0,L-1; DO ny = 0,L-1; DO nx = 0,L-1
         DO ni = 0,1; DO ns = 0,1

            zdualvecs(nx,ny,nz,nt-1,ns,ni,np) = zdualvecs(nx,ny,nz,nt,ns,ni,np) &
                 * (1.D0-6.D0*w0_N*h+CDSQRT(-c0*atovera*(1.D0,0.D0))*s(nx,ny,nz,nt-1))

            zdualvecs(nx,ny,nz,nt-1,ns,ni,np) = zdualvecs(nx,ny,nz,nt-1,ns,ni,np) &
                 + w1_N*h*zdualvecs(MOD(nx+1,L),ny,nz,nt,ns,ni,np) &
                 + w1_N*h*zdualvecs(MOD(nx-1+L,L),ny,nz,nt,ns,ni,np) &
                 + w1_N*h*zdualvecs(nx,MOD(ny+1,L),nz,nt,ns,ni,np) &
                 + w1_N*h*zdualvecs(nx,MOD(ny-1+L,L),nz,nt,ns,ni,np) &
                 + w1_N*h*zdualvecs(nx,ny,MOD(nz+1,L),nt,ns,ni,np) &
                 + w1_N*h*zdualvecs(nx,ny,MOD(nz-1+L,L),nt,ns,ni,np)

            IF (improveN >= 1) THEN
               zdualvecs(nx,ny,nz,nt-1,ns,ni,np) = zdualvecs(nx,ny,nz,nt-1,ns,ni,np) &
                    - w2_N*h*zdualvecs(MOD(nx+2,L),ny,nz,nt,ns,ni,np) &
                    - w2_N*h*zdualvecs(MOD(nx-2+L,L),ny,nz,nt,ns,ni,np) &
                    - w2_N*h*zdualvecs(nx,MOD(ny+2,L),nz,nt,ns,ni,np) &
                    - w2_N*h*zdualvecs(nx,MOD(ny-2+L,L),nz,nt,ns,ni,np) &
                    - w2_N*h*zdualvecs(nx,ny,MOD(nz+2,L),nt,ns,ni,np) &
                    - w2_N*h*zdualvecs(nx,ny,MOD(nz-2+L,L),nt,ns,ni,np)
            END IF

            IF (improveN == 2) THEN
               zdualvecs(nx,ny,nz,nt-1,ns,ni,np) = zdualvecs(nx,ny,nz,nt-1,ns,ni,np) &
                    + w3_N*h*zdualvecs(MOD(nx+3,L),ny,nz,nt,ns,ni,np) &
                    + w3_N*h*zdualvecs(MOD(nx-3+L,L),ny,nz,nt,ns,ni,np) &
                    + w3_N*h*zdualvecs(nx,MOD(ny+3,L),nz,nt,ns,ni,np) &
                    + w3_N*h*zdualvecs(nx,MOD(ny-3+L,L),nz,nt,ns,ni,np) &
                    + w3_N*h*zdualvecs(nx,ny,MOD(nz+3,L),nt,ns,ni,np) &
                    + w3_N*h*zdualvecs(nx,ny,MOD(nz-3+L,L),nt,ns,ni,np)
            END IF

         END DO; END DO
      END DO; END DO; END DO
   END DO
END DO
```

Fig. 6.5 Sample code which calculates auxiliary-field transfer matrix multiplications on the right starting from the single-nucleon final states. We only show terms involving the free-nucleon transfer matrix and the auxiliary field s.

Fig. 6.6 Sample code showing how the transfer matrix product multiplications are called as functions or subroutines and used to compute the determinant and inverse of the matrix of single-nucleon amplitudes.

```
CALL getzvecs(s,sI,zvecs,zwave,Lt,0, &
     pion,ztau2x2,n_f)
CALL getzdualvecs(s,sI,zdualvecs,zdualwave, &
     Lt,0,pion,ztau2x2,n_f)
CALL getinvcorr(zvecs,zdualvecs,zldeter, &
     zcorrmatrix,zcorrinv,Lt)
aldeterabs = DBLE(zldeter)
zdeterphase = CDEXP((0.D0,1.D0)*DIMAG(zldeter))
act = bose - aldeterabs
```

Given an arbitrary initial configuration $s^0(\mathbf{n},n_t)$, the conjugate momentum is chosen from a random Gaussian distribution according to

$$P[p_s^0(\mathbf{n},n_t)] \propto \exp\left\{-\frac{1}{2}\left[p_s^0(\mathbf{n},n_t)\right]^2\right\}, \tag{6.55}$$

after which the Hamiltonian equations of motion are integrated numerically with a small but nonzero step size $\varepsilon_{\rm step}$. This method begins with a "half-step" forward in the conjugate momentum,

$$\tilde{p}_s^0(\mathbf{n},n_t) = p_s^0(\mathbf{n},n_t) - \frac{\varepsilon_{\text{step}}}{2}\left[\frac{\partial V(s)}{\partial s(\mathbf{n},n_t)}\right]_{s=s^0}, \tag{6.56}$$

followed by repeated updates of s and $\tilde{p}_s$ according to

$$s^{i+1}(\mathbf{n},n_t) = s^i(\mathbf{n},n_t) + \varepsilon_{\text{step}}\tilde{p}_s^i(\mathbf{n},n_t), \qquad \tilde{p}_s^{i+1}(\mathbf{n},n_t) = \tilde{p}_s^i(\mathbf{n},n_t) - \varepsilon_{\text{step}}\left[\frac{\partial V(s)}{\partial s(\mathbf{n},n_t)}\right]_{s=s^{i+1}}, \tag{6.57}$$

for a specified number of steps N_{step}. This is followed by an additional half-step backward in $\tilde{p}_s$ given by

$$p_s^{N_{\text{step}}}(\mathbf{n},n_t) = \tilde{p}_s^{N_{\text{step}}}(\mathbf{n},n_t) + \frac{\varepsilon_{\text{step}}}{2}\left[\frac{\partial V(s)}{\partial s(\mathbf{n},n_t)}\right]_{s=s^0}. \tag{6.58}$$

The length of such an MD "trajectory" should be taken large enough to ensure significant decorrelation between successive configurations of the auxiliary field. The evolved configuration is then subjected to a "Metropolis test" against a random number $r \in [0,1)$. The new configuration is accepted if

$$r < \exp\left[-H(s^{N_{\text{step}}}, p_s^{N_{\text{step}}}) + H(s^0, p_s^0)\right]. \tag{6.59}$$

It should be noted that although H is in principle conserved in the MD evolution, the truncation error of the leapfrog method introduces a systematic error. The Metropolis test eliminates the need for extrapolation in $\varepsilon_{\text{step}}$.

In our case $\exp[-V(s)]$ has the form

$$|Z(L_t)| \exp\left[-S_{ss}(s) - S_{s_I s_I}(s_I) - S_{\pi_I \pi_I}(\pi_I)\right], \tag{6.60}$$

where $Z(L_t)$ is the determinant of an $A \times A$ matrix of single-nucleon amplitudes $\mathbf{M}$. The derivative of V is then computed using

$$\begin{aligned}
\frac{\partial V(s)}{\partial s(\mathbf{n},n_t)} &= \frac{\partial S_{ss}(s)}{\partial s(\mathbf{n},n_t)} - \frac{\partial \text{Re}\left[\ln(\det \mathbf{M})\right]}{\partial s(\mathbf{n},n_t)} \\
&= \frac{\partial S_{ss}(s)}{\partial s(\mathbf{n},n_t)} - \text{Re}\left[\frac{1}{\det \mathbf{M}} \sum_{k,l} \frac{\partial \det \mathbf{M}}{\partial \mathbf{M}_{kl}} \frac{\partial \mathbf{M}_{kl}}{\partial s(\mathbf{n},n_t)}\right] \\
&= \frac{\partial S_{ss}(s)}{\partial s(\mathbf{n},n_t)} - \text{Re}\left[\sum_{k,l} \mathbf{M}^{-1}_{lk} \frac{\partial \mathbf{M}_{kl}}{\partial s(\mathbf{n},n_t)}\right].
\end{aligned} \tag{6.61}$$

In Fig. 6.7 we show a sample code calculating the quadratic part of the action due to the auxiliary fields and pion fields,

$$\frac{1}{2}\sum_{\mathbf{n},n_t}[p_s(\mathbf{n},n_t)]^2 + \frac{1}{2}\sum_{\mathbf{n},n_t,I}[p_{s_I}(\mathbf{n},n_t)]^2 + \frac{1}{2}\sum_{\mathbf{n},n_t,I}[p_{\pi_I}(\mathbf{n},n_t)]^2 + S_{ss}(s) + S_{s_I s_I}(s_I) + S_{\pi_I \pi_I}(\pi_I). \tag{6.62}$$

In the code we have found it convenient to rescale the pion field by a factor of $\sqrt{q_\pi}$ where

$$q_\pi = \alpha_t\left(m_\pi^2 + 6w_0\right). \tag{6.63}$$

In Fig. 6.8 we show a sample code which calculates

$$\left[\frac{\partial V(s)}{\partial s(\mathbf{n},n_t)}\right]_{s=s^0} \tag{6.64}$$

and uses it to compute the half-step forward in the conjugate momentum,

```
bose = 0.D0
DO nt = 0,Lt-1
   DO nz = 0,L-1; DO ny = 0,L-1; DO nx = 0,L-1
      bose = bose &
           + s(nx,ny,nz,nt)**2.D0/2.D0 &
           + p_s(nx,ny,nz,nt)**2.D0/2.D0
      DO iso = 1,3
         bose = bose &
              + sI(nx,ny,nz,nt,iso)**2.D0/2.D0 &
              + p_sI(nx,ny,nz,nt,iso)**2.D0/2.D0 &
              + pion(nx,ny,nz,nt,iso)**2.D0/2.D0 &
              + atovera/qpi3*pion(nx,ny,nz,nt,iso)*( &
              - w1_P*pion(MOD(nx+1,L),ny,nz,nt,iso) &
              - w1_P*pion(nx,MOD(ny+1,L),nz,nt,iso) &
              - w1_P*pion(nx,ny,MOD(nz+1,L),nt,iso) &
              + w2_P*pion(MOD(nx+2,L),ny,nz,nt,iso) &
              + w2_P*pion(nx,MOD(ny+2,L),nz,nt,iso) &
              + w2_P*pion(nx,ny,MOD(nz+2,L),nt,iso) &
              - w3_P*pion(MOD(nx+3,L),ny,nz,nt,iso) &
              - w3_P*pion(nx,MOD(ny+3,L),nz,nt,iso) &
              - w3_P*pion(nx,ny,MOD(nz+3,L),nt,iso)) &
              + p_pion(nx,ny,nz,nt,iso)**2.D0/2.D0
      END DO
   END DO; END DO; END DO
END DO
```

Fig. 6.7 Sample code calculating the quadratic part of the action due to the auxiliary fields and pion fields.

```
      DO npart1 = 0,n_f-1; DO npart2 = 0,n_f-1
         zdcorrmatrix(npart2,npart1) = 0.D0
         DO ni = 0,1; DO ns = 0,1
            zdcorrmatrix(npart2,npart1) = &
                 zdcorrmatrix(npart2,npart1) + &
                 zdualvecs(nx,ny,nz,nt+1,ns,ni,npart2) &
                 *zvecs(nx,ny,nz,nt,ns,ni,npart1) &
                 *CDSQRT(-c0*atovera*(1.D0,0.D0))/L**3
         END DO; END DO
      END DO; END DO

      dVds(nx,ny,nz,nt) = s(nx,ny,nz,nt)
      DO npart1 = 0,n_f-1; DO npart2 = 0,n_f-1
         dVds(nx,ny,nz,nt) = dVds(nx,ny,nz,nt) &
              - DBLE(zdcorrmatrix(npart2,npart1) &
              *zcorrinv(npart1,npart2))
      END DO; END DO

      p_sHMC(nx,ny,nz,nt,0) = &
           p_s(nx,ny,nz,nt) - 0.5D0*eHMC*dVds(nx,ny,nz,nt)
```

Fig. 6.8 Sample code which computes the derivative of the potential $V(s)$ with respect to the auxiliary field $s(\mathbf{n},n_t)$ and uses it to compute the half-step forward in the conjugate momentum.

$$\tilde{p}_s^0(\mathbf{n},n_t) = p_s^0(\mathbf{n},n_t) - \frac{\varepsilon_{\rm step}}{2}\left[\frac{\partial V(s)}{\partial s(\mathbf{n},n_t)}\right]_{s=s^0}. \tag{6.65}$$

In Fig. 6.9 we show an example code which performs the Metropolis test against a random number $r \in [0,1)$, with the new configuration being accepted if

$$r < \exp\left[-H(s^{N_{\rm step}}, p_s^{N_{\rm step}}) + H(s^0, p_s^0)\right]. \tag{6.66}$$

Although importance sampling uses only the absolute volume, the complex phase of the determinant is treated as an observable and is collected with each configuration of the auxiliary and pion fields.

```
IF (ntrial .eq. 1 .or. grnd() .lt. DEXP(-actnew+act)) THEN

   accept = accept + 1.

   DO nt = 0,Lt-1
      DO nz = 0,L-1; DO ny = 0,L-1; DO nx = 0,L-1
         s(nx,ny,nz,nt) = snew(nx,ny,nz,nt)
      END DO; END DO; END DO
   END DO
   DO nt = 0,Lt-1
      DO nz = 0,L-1; DO ny = 0,L-1; DO nx = 0,L-1
         DO iso = 1,3
            sI(nx,ny,nz,nt,iso) = sInew(nx,ny,nz,nt,iso)
            pion(nx,ny,nz,nt,iso) = pionnew(nx,ny,nz,nt,iso)
         END DO
      END DO; END DO; END DO
   END DO
   aldeterabs = aldeternewabs
   zdeterphase = zdeternewphase

END IF
```

Fig. 6.9 Sample code showing the Metropolis condition used to determine whether the new configuration is accepted or rejected.

6.6 Exercises

6.1. Write a lattice hybrid Monte Carlo code involving only the quadratic part of the action due to the auxiliary fields and pions,

$$\frac{1}{2}\sum_{\mathbf{n},n_t}[p_s(\mathbf{n},n_t)]^2+\frac{1}{2}\sum_{\mathbf{n},n_t,I}[p_{s_I}(\mathbf{n},n_t)]^2+\frac{1}{2}\sum_{\mathbf{n},n_t,I}[p_{\pi_I}(\mathbf{n},n_t)]^2+S_{ss}(s)+S_{s_Is_I}(s_I)+S_{\pi_I\pi_I}(\pi_I). \tag{6.67}$$

Verify that the change in the action produced by the hybrid Monte Carlo update is scaling quadratically in the step size, $\varepsilon_{\text{step}}$, in the limit $\varepsilon_{\text{step}} \to 0$ with $N_{\text{step}}\varepsilon_{\text{step}}$ held fixed.

6.2. Write a function (subroutine) that generates the single-nucleon states on the lattice corresponding to the Slater-determinant state of four nucleons — proton spin-up, proton spin-down, neutron spin-up, and neutron spin-down — each with zero momentum.

6.3. Write a (function) subroutine that extends the sample code in Fig. 6.4 to repeatedly multiply the auxiliary-field transfer matrix on the left starting from some initial single-nucleon wave functions. Include the contributions from the auxiliary fields s and s_I as well as the pion field π_I.

6.4. Write a function (subroutine) that extends the sample code in Fig. 6.5 to repeatedly multiply the auxiliary-field transfer matrix on the right starting from some final single-nucleon wave functions. Include the contributions from the auxiliary fields s and s_I as well as the pion field π_I.

6.5. Use the Slater-determinant state constructed in Prob. 6.2 as the initial and final states. Apply the functions (subroutines) written in Prob. 6.3 and Prob. 6.4 with all coupling constants set to zero. Verify that this state is the ground state of the non-interacting system with energy equal to zero.

6.6. Use the Slater-determinant state constructed in Prob. 6.2 as the initial and final states. Then implement the functions (subroutines) written in Prob. 6.3 and Prob. 6.4 and extend the sample code in Fig. 6.8 to compute the derivatives of $V(s)$ with respect to $s(\mathbf{n},n_t)$, $s_I(\mathbf{n},n_t)$, and $\pi_I(\mathbf{n},n_t)$.

6.7. Take the code you have written for Prob. 6.6 and complete the remaining steps needed to do hybrid Monte Carlo updates for s, s_I, and π_I. Verify that the change in the action produced

by the hybrid Monte Carlo update is scaling quadratically in $\varepsilon_{\rm step}$ in the limit $\varepsilon_{\rm step} \to 0$ with $N_{\rm step}\varepsilon_{\rm step}$ held fixed.

6.8. Take the code you have written for Prob. 6.7 and complete the remaining steps needed to calculate the energy of the four-nucleon ground state by computing the ratio of the amplitudes $Z(L_t)/Z(L_t-1)$.

Acknowledgements The author is grateful for discussions with Amy Nicholson and Morten Hjorth-Jensen. He is also greatly indebted to his collaborators Jose Alarcón, Dechuan Du, Serdar Elhatisari, Evgeny Epelbaum, Nico Klein, Hermann Krebs, Timo Lähde, Ning Li, Bing-nan Lu, Thomas Luu, Ulf-G. Meißner, Alexander Rokash, and Gautam Rupak. Partial financial support provided by the U.S. Department of Energy (DE-FG02-03ER41260). Computational resources were provided by the Jülich Supercomputing Centre.

Chapter 7
From few to many nucleons and methods for nuclear reactions

Giuseppina Orlandini

Abstract Each chapter should be preceded by an abstract (10–15 lines long) that summarizes the content. The abstract will appear *online* at `www.SpringerLink.com` and be available with unrestricted access. This allows unregistered users to read the abstract as a teaser for the complete chapter. As a general rule the abstracts will not appear in the printed version of your book unless it is the style of your particular book or that of the series to which your book belongs.

Please use the 'starred' version of the new Springer `abstract` command for typesetting the text of the online abstracts (cf. source file of this chapter template `abstract`) and include them with the source files of your manuscript. Use the plain `abstract` command if the abstract is also to appear in the printed version of the book.

7.1 The Nuclear few- and many-body problem

7.2 Methods for bound states based on the variational principle I:The No Core Shell Model (NCSM)

7.3 Methods for bound states based on the variational principle II:The Hyperspherical Harmonics (HH) method

7.4 Methods for reactions involving continuum states I:Perturbation induced reactions and integral transforms

7.5 Methods for reactions involving continuum states II:The continuum state problem reduced to a bound state problem

Acknowledgements If you want to include acknowledgments of assistance and the like at the end of an individual chapter please use the `acknowledgement` environment – it will automatically render Springer's preferred layout.

Giuseppina Orlandini
Name of institution and address, e-mail: `name@email.address`

Chapter 8
High-performance computing Many-body methods and infinite nuclear matter

Justin G. Lietz, Samuel Novario, Gustav R. Jansen, Gaute Hagen, and Morten Hjorth-Jensen,

Abstract We present a computational approach to infinite nuclear matter employing Hartree-Fock theory, many-body perturbation theory and coupled cluster theory. These lectures are closely linked with those in chapters **??**, **??** and **??** and serve as input for the correlation functions employed in Monte Carlo calculations in chapter **??**, the in-medium similarity renormalization group theory of dense fermionic systems of chapter chapter **??** and the Green's function approach in chapter **??**. We provide extensive code examples and benchmark calculations, allowing thereby an eventual reader to start writing her/his own codes. We start with an object-oriented serial code and end with in-depth discussions on strategies for porting the code to present and planned high-performance computing facilities.

8.1 Introduction

Studies of infinite nuclear matter play an important role in nuclear physics. The aim of this part of the lectures is to provide the necessary ingredients for perfoming studies of neutron star matter (or matter in β-equilibrium) and symmetric nuclear matter. We will mainly focus on pure neutron matter, but the framework and formalism can easily be extended to other dense and homogeneous fermionic systems such as the electron gas in two and three dimensions. The introductory material we present here forms also the basis for the next three chapters, starting with the definition of the single-particle basis and our Hamiltonians as well

Justin G. Lietz
Department of Physics and Astronomy and National Superconducting Cyclotron Laboratory, Michigan State University, East Lansing, Michigan, USA, e-mail: lietz@nscl.msu.edu,

Samuel Novario
Department of Physics and Astronomy and National Superconducting Cyclotron Laboratory, Michigan State University, East Lansing, Michigan, USA, e-mail: novarios@nscl.msu.edu,

Gustav R. Jansen
Oak Ridge National Laboratory, Physics Division, Oak Ridge, Tennessee, USA and Department of Physics and Astronomy, University of Tennessee, Knoxville, Tennessee, USA, e-mail: jansen@ornl.gov,

Gaute Hagen
Oak Ridge National Laboratory, Physics Division, Oak Ridge, Tennessee, USA and Department of Physics and Astronomy, University of Tennessee, Knoxville, Tennessee, USA, e-mail: hageng@ornl.gov,

Morten Hjorth-Jensen
Department of Physics and Astronomy and National Superconducting Cyclotron Laboratory, Michigan State University, East Lansing, Michigan, USA and Department of Physics, University of Oslo, Oslo, Norway, e-mail: hjensen@msu.edu

as Hartree-Fock theory. For infinite matter, due to the translational invariance of the Hamiltonian, the single-particle basis, in terms of plane waves, unchanged under Hartree-Fock calculations.

Studies of dense baryonic matter are of central importance to our basic understanding of the stability of nuclear matter, spanning from matter at high densities and temperatures to matter as found within dense astronomical objects like neutron stars.

Neutron star matter at densities of 0.1 fm^{-3} and greater, is often assumed to be made of mainly neutrons, protons, electrons and muons in beta equilibrium. However, other baryons like various hyperons may exist, as well as possible mesonic condensates and transitions to quark degrees of freedom at higher densities [**?**]. In these notes we limit ourselves to matter composed of neutrons only. Furthermore, we will also consider matter at temperatures much lower than the typical Fermi energies.

In the next section we present some of the basic quantities that enter the different many-body methods discussed in this and the three subsequent chapters. All these methods start with some single-particle basis states, normally obtained via the solution of mean-field approaches like Hartree-Fock theory. Contributions from correlations beyond such a mean-field basis to selected observables, are then obtained via a plethora of many-body methods. These methods represent different mathematical algorithms used to solve either Schrödinger's or Dirac's equations for many interacting fermions. After the definitions of our basis states, we derive the Hartree-Fock equations in the subsequent section and move on with many-body perturbation theory, full configuration interaction theory and coupled cluster theory. Monte Carlo methods, Green's function theory approaches and Similarity Renormlization group approaches are discussed in the subsequent three chapters.

The strengths and weaknesses of these methods are discussed throughout these chapters, with applications to either a simple pairing model and/or pure neutron matter. Our focus will be on pure neutron matter, starting with a simple model for the interaction between nucleons. This allows us to focus on the pedagogical and algorithmic aspects of the various many-body methods, avoiding thereby the full complexity of nuclear forces. If properly written however, the codes can easily be extended to include models of the nuclear interactions based on effective field theory [**?**] and other baryon species than just neutrons. In our conclusions we point back to models for nuclear forces and their links to the underlying theory of the strong interaction discussed in the first chapters of this book, bridging thereby the gap between the theory of nuclear Hamiltonians and many-body methods.

8.2 Single-particle basis, Hamiltonians and models for the nuclear force

Although our focus here and in the coming chapters is on neutron matter only, our formalism lends itself easily to studies of nuclear matter with a given proton fraction and electrons. In this section we outline some of the background details, with a focus on the calculational basis and the representation of a nuclear Hamiltonian.

Neutron star matter is not composed of only neutrons. Rather, matter is composed of various baryons and leptons in chemical and charge equilibrium. The equilibrium conditions are governed by the weak processes (normally referred to as the processes for β-equilibrium)

$$b_1 \rightarrow b_2 + l + \bar{\nu}_l \qquad b_2 + l \rightarrow b_1 + \nu_l, \tag{8.1}$$

where b_1 and b_2 refer to different types of baryons, for example a neutron and a proton. The symbol l is either an electron or a muon and $\bar{\nu}_l$ and ν_l their respective anti-neutrinos and

neutrinos. Leptons like muons appear at a density close to nuclear matter saturation density, the latter being

$$n_0 \approx 0.16 \pm 0.02 \qquad \text{fm}^{-3},$$

with a corresponding energy per baryon $\mathscr{E}_0$ for symmetric nuclear matter at saturation density of

$$\mathscr{E}_0 = B/A = -15.6 \pm 0.2 \qquad \text{MeV}.$$

The energy per baryon is the central quantity in the present studies. From the energy per baryon, we can define the pressure P which counteracts the gravitional forces and hinders the gravitational collapse of neutron start. The pressure is defined through the relation

$$P = n^2 \frac{\partial \mathscr{E}}{\partial n} = n \frac{\partial \varepsilon}{\partial n} - \varepsilon. \tag{8.2}$$

Similarly, the chemical potential for particle species i is given by

$$\mu_i = \left(\frac{\partial \varepsilon}{\partial n_i} \right). \tag{8.3}$$

In calculations of properties of neutron star matter in β-equilibrium, we need to calculate the energy per baryon $\mathscr{E}$ for e.g. several proton fractions x_p. The proton fraction corresponds to the ratio of protons as compared to the total nucleon number (Z/A). It is defined as

$$x_p = \frac{n_p}{n}, \tag{8.4}$$

where $n = n_p + n_n$, the total baryonic density if neutrons and protons are the only baryons present. If this is the case, the total Fermi momentum k_F and the Fermi momenta k_{Fp}, k_{Fn} for protons and neutrons are related to the total nucleon density n by

$$\begin{aligned} n =& \frac{2}{3\pi^2} k_F^3 \\ =& x_p n + (1 - x_p) n \\ =& \frac{1}{3\pi^2} k_{Fp}^3 + \frac{1}{3\pi^2} k_{Fn}^3. \end{aligned} \tag{8.5}$$

The energy per baryon will thus be labelled as $\mathscr{E}(n, x_p)$. The quantity $\mathscr{E}(n, 0)$ refers then to the energy per baryon for pure neutron matter (PNM) while $\mathscr{E}(n, \frac{1}{2})$ is the corresponding value for SNM. Furthermore, in this work, subscripts n, p, e, μ will always refer to neutrons, protons, electrons and muons, respectively.

Since the mean free path of a neutrino in a neutron star is bigger than the typical radius of such a star (~ 10 km), we will throughout assume that neutrinos escape freely from the neutron star, see for example the work of Prakash et al. for a discussion on trapped neutrinos. Eq. (8.1) yields then the following conditions for matter in β equilibrium with for example nucleonic degrees freedom only

$$\mu_n = \mu_p + \mu_e, \tag{8.6}$$

and

$$n_p = n_e, \tag{8.7}$$

where μ_i and n_i refer to the chemical potential and number density in fm^{-3} of particle species i. If muons are present as well, we need to modify the equation for charge conservation, Eq. (8.7), to read

$$n_p = n_e + n_\mu,$$

and require that $\mu_e = \mu_\mu$.

An important ingredient in the discussion of the EoS and the criteria for matter in β-equilibrium is the so-called symmetry energy $\mathscr{S}(n)$, defined as the difference in energy for symmetric nuclear matter and pure neutron matter

$$\mathscr{S}(n) = \mathscr{E}(n, x_p = 0) - \mathscr{E}(n, x_p = 1/2). \tag{8.8}$$

If we expand the energy per baryon in the case of nucleonic degrees of freedom only in the proton concentration x_p about the value of the energy for SNM ($x_p = \frac{1}{2}$), we obtain,

$$\mathscr{E}(n, x_p) = \mathscr{E}(n, x_p = \frac{1}{2}) + \frac{1}{2}\frac{d^2\mathscr{E}}{dx_p^2}(n)\,(x_p - 1/2)^2 + \ldots, \tag{8.9}$$

where the term $d^2\mathscr{E}/dx_p^2$ is to be associated with the symmetry energy $\mathscr{S}(n)$ in the empirical mass formula. If we assume that higher order derivatives in the above expansion are small (we will see examples of this in the next subsection), then through the conditions for β-equilbrium of Eqs. (8.6) and (8.7) and Eq. (8.3) we can define the proton fraction by the symmetry energy as

$$\hbar c \left(3\pi^2 n x_p\right)^{1/3} = 4\mathscr{S}(n)\,(1 - 2x_p), \tag{8.10}$$

where the electron chemical potential is given by $\mu_e = \hbar c k_F$, i.e. ultrarelativistic electrons are assumed. Thus, the symmetry energy is of paramount importance for studies of neutron star matter in β-equilibrium. One can extract information about the value of the symmetry energy at saturation density n_0 from systematic studies of the masses of atomic nuclei. However, these results are limited to densities around n_0 and for proton fractions close to $\frac{1}{2}$. Typical values for $\mathscr{S}(n)$ at n_0 are in the range $27 - 38$ MeV. For densities greater than n_0 it is more difficult to get a reliable information on the symmetry energy, and thereby the related proton fraction.

We begin our discussion

$$\Phi_{AS}(\alpha_1, \ldots, \alpha_A; x_1, \ldots x_A) = \frac{1}{\sqrt{A}}\sum_{\hat{P}}(-1)^P \hat{P}\prod_{i=1}^{A}\psi_{\alpha_i}(x_i),$$

which is equivalent with $|\alpha_1 \ldots \alpha_A\rangle = a^\dagger_{\alpha_1} \ldots a^\dagger_{\alpha_A}|0\rangle$. We have also

$$a_p^\dagger|0\rangle = |p\rangle, \quad a_p|q\rangle = \delta_{pq}|0\rangle$$

$$\delta_{pq} = \left\{a_p, a_q^\dagger\right\},$$

and

$$0 = \left\{a_p^\dagger, a_q\right\} = \left\{a_p, a_q\right\} = \left\{a_p^\dagger, a_q^\dagger\right\}$$

$$|\Phi_0\rangle = |\alpha_1 \ldots \alpha_A\rangle, \quad \alpha_1, \ldots, \alpha_A \leq \alpha_F$$

$$\left\{a_p^\dagger, a_q\right\} = \delta_{pq}, p, q \leq \alpha_F$$

$$\left\{a_p, a_q^\dagger\right\} = \delta_{pq}, p, q > \alpha_F$$

with $i, j, \ldots \leq \alpha_F$, $a, b, \ldots > \alpha_F$, $p, q, \ldots -$ any

$$a_i|\Phi_0\rangle = |\Phi_i\rangle, \qquad a_a^\dagger|\Phi_0\rangle = |\Phi^a\rangle$$

and

$$a_i^\dagger|\Phi_0\rangle = 0 \qquad a_a|\Phi_0\rangle = 0$$

The one-body operator is defined as

$$\hat{F} = \sum_{pq} \langle p|\hat{f}|q\rangle a_p^\dagger a_q$$

while the two-body opreator is defined as

$$\hat{V} = \frac{1}{4}\sum_{pqrs} \langle pq|\hat{v}|rs\rangle_{AS} a_p^\dagger a_q^\dagger a_s a_r$$

where we have defined the antisymmetric matrix elements

$$\langle pq|\hat{v}|rs\rangle_{AS} = \langle pq|\hat{v}|rs\rangle - \langle pq|\hat{v}|sr\rangle.$$

We can also define a three-body operator

$$\hat{V}_3 = \frac{1}{36}\sum_{pqrstu} \langle pqr|\hat{v}_3|stu\rangle_{AS} a_p^\dagger a_q^\dagger a_r^\dagger a_u a_t a_s$$

with the antisymmetrized matrix element

$$\langle pqr|\hat{v}_3|stu\rangle_{AS} = \langle pqr|\hat{v}_3|stu\rangle + \langle pqr|\hat{v}_3|tus\rangle + \langle pqr|\hat{v}_3|ust\rangle - \langle pqr|\hat{v}_3|sut\rangle - \langle pqr|\hat{v}_3|tsu\rangle - \langle pqr|\hat{v}_3|uts\rangle. \tag{8.11}$$

$$\hat{H}_0 = \sum_{pq} \langle p|\hat{h}_0|q\rangle a_p^\dagger a_q,$$

$$\hat{H}_0 = \sum_{pq} \langle p|\hat{h}_0|q\rangle \left\{a_p^\dagger a_q\right\} + \sum_i \langle i|\hat{h}_0|i\rangle.$$

$$\hat{H}_I = \frac{1}{4}\sum_{pqrs} \langle pq|\hat{v}|rs\rangle a_p^\dagger a_q^\dagger a_s a_r,$$

$$\hat{H}_I = \frac{1}{4}\sum_{pqrs} \langle pq|\hat{v}|rs\rangle \left\{a_p^\dagger a_q^\dagger a_s a_r\right\} + \sum_{pqi} \langle pi|\hat{v}|qi\rangle \left\{a_p^\dagger a_q\right\} + \frac{1}{2}\sum_{ij} \langle ij|\hat{v}|ij\rangle.$$

Explain again the meaning of the various symbols.

$$\hat{H}_3 = \frac{1}{36}\sum_{\substack{pqr\\stu}} \langle pqr|\hat{v}_3|stu\rangle a_p^\dagger a_q^\dagger a_r^\dagger a_u a_t a_s,$$

and specify the contributions to the twobody, onebody and the scalar part.

This is a homogeneous system and the one-particle wave functions are given by plane wave functions normalized to a volume Ω for a box with length L (the limit $L \to \infty$ is to be taken after we have computed various expectation values)

$$\psi_{\mathbf{k}\sigma}(\mathbf{r}) = \frac{1}{\sqrt{\Omega}} \exp(i\mathbf{kr})\xi_\sigma$$

where $\mathbf{k}$ is the wave number and ξ_σ is a spin function for either spin up or down

$$\xi_{\sigma=+1/2} = \begin{pmatrix} 1 \\ 0 \end{pmatrix} \qquad \xi_{\sigma=-1/2} = \begin{pmatrix} 0 \\ 1 \end{pmatrix}.$$

We assume that we have periodic boundary conditions which limit the allowed wave numbers to

$$k_i = \frac{2\pi n_i}{L} \qquad i = x,y,z \qquad n_i = 0, \pm 1, \pm 2, \ldots$$

We assume first that the electrons interact via a central, symmetric and translationally invariant interaction $V(r_{12})$ with $r_{12} = |\mathbf{r}_1 - \mathbf{r}_2|$. The interaction is spin independent.

The total Hamiltonian consists then of kinetic and potential energy

$$\hat{H} = \hat{T} + \hat{V}.$$

The operator for the kinetic energy can be written as

$$\hat{T} = \sum_{\mathbf{k}\sigma} \frac{\hbar^2 k^2}{2m} a^{\dagger}_{\mathbf{k}\sigma} a_{\mathbf{k}\sigma}.$$

The Hamiltonian operator is given by

$$\hat{H} = \hat{H}_{el} + \hat{H}_b + \hat{H}_{el-b},$$

When using periodic boundary conditions, the discrete-momentum single-particle basis functions

$$\phi_{\mathbf{k}}(\mathbf{r}) = e^{i\mathbf{k}\cdot\mathbf{r}}/L^{d/2}$$

are associated with the single-particle energy

$$\varepsilon_{n_x,n_y} = \frac{\hbar^2}{2m}\left(\frac{2\pi}{L}\right)^2 \left(n_x^2 + n_y^2\right) \tag{8.12}$$

for two-dimensional sytems and

$$\varepsilon_{n_x,n_y,n_z} = \frac{\hbar^2}{2m}\left(\frac{2\pi}{L}\right)^2 \left(n_x^2 + n_y^2 + n_z^2\right) \tag{8.13}$$

for three-dimensional systems.

We choose the single-particle basis such that both the occupied and unoccupied single-particle spaces have a closed-shell structure. This means that all single-particle states corresponding to energies below a chosen cutoff are included in the basis. We study only the unpolarized spin phase, in which all orbitals are occupied with one spin-up and one spin-down electron.

The single-particle kinetic energy defined as

$$\frac{\hbar^2}{2m}\left(k_{n_x}^2 + k_{n_y}^2 k_{n_z}^2\right),$$

and

$$k_{n_i} = \frac{2\pi n_i}{L} \; n_i = 0, \pm 1, \pm 2, \ldots,$$

we can set up a similar table and obtain (assuming identical particles one and including spin up and spin down solutions) for energies less than or equal to $n_x^2 + n_y^2 + n_z^2 \leq 3$

$n_x^2+n_y^2+n_z^2$	n_x	n_y	n_z	$N_{\uparrow\downarrow}$
0	0	0	0	2
1	-1	0	0	
1	1	0	0	
1	0	-1	0	
1	0	1	0	
1	0	0	-1	
1	0	0	1	14
2	-1	-1	0	
2	-1	1	0	
2	1	-1	0	
2	1	1	0	
2	-1	0	-1	
2	-1	0	1	
2	1	0	-1	
2	1	0	1	
2	0	-1	-1	
2	0	-1	1	
2	0	1	-1	
2	0	1	1	38
3	-1	-1	-1	
3	-1	-1	1	
3	-1	1	-1	
3	-1	1	1	
3	1	-1	-1	
3	1	-1	1	
3	1	1	-1	
3	1	1	1	54

Continuing in this way we get for $n_x^2+n_y^2+n_z^2=4$ a total of 22 additional states, resulting in 76 as a new magic number. For the lowest six energy values the degeneracy in energy gives us 2, 14, 38, 54, 76 and 114 as magic numbers. These numbers will then define our Fermi level when we compute the energy in a Cartesian basis. When performing calculations based on many-body perturbation theory, Coupled cluster theory or other many-body methods, we need then to add states above the Fermi level in order to sum over single-particle states which are not occupied.

If we wish to study infinite nuclear matter with both protons and neutrons, the above magic numbers become $4, 28, 76, 108, 132, 228, \ldots$.

Every number of particles for filled shells defines also the number of particles to be used in a given calculation. Use the number of particles to define the density of the system

$$\rho = g\frac{k_F^3}{6\pi^2},$$

where you need to define k_F and the degeneracy g, which is two for one type of spin-$1/2$ particles and four for symmetric nuclear matter.

Use the density to find the length L of the box used with periodic boundary contributions, that is use the relation

$$V = L^3 = \frac{A}{\rho}.$$

You can use L to define the spacing to set up the spacing between varipus k-values, that is

$$\Delta k = \frac{2\pi}{L}.$$

Here, A can be the number of nucleons. If we deal with the electron gas only, this needs to be replaced by the number of electrons N.

The total Hamiltonian consists then of kinetic and potential energy

$$\hat{H} = \hat{T} + \hat{V}.$$

The operator for the kinetic energy can be written as

$$\hat{T} = \sum_{\mathbf{k}\sigma} \frac{\hbar^2 k^2}{2m} a^\dagger_{\mathbf{k}\sigma} a_{\mathbf{k}\sigma}.$$

As mentioned above, we will employ a plane wave basis for our calculations of infinite matter properties. With a cartesian basis it means that we can calculate directly the various matrix elements, as discussed in the previous subsection. However, a cartesian basis represents an approximation to the thermodynamical limit. In order to compare the stability of our basis with results from the thermodynamical limit, it is convenient to rewrite the nucleon-nucleon interaction in terms of a partial wave expansion. This will allow us to compute the Hartree-Fock energy of the ground state in the thermodynamical limit (with the caveat that we need to limit the number of partial waves). In order to find the expressions for the Hartree-Fock energy in a partial wave basis, we will find it convenient to rewrite our two-body force in terms of the relative and center-of-mass motion momenta.

The direct matrix element, with single-particle three-dimensional momenta $\mathbf{k}_i$, spin σ_i and isospin τ_i, is defined as

$$\langle \mathbf{k}_a \sigma_a \tau_a \mathbf{k}_b \sigma_b \tau_b | \hat{v} | \mathbf{k}_c \sigma_c \tau_c \mathbf{k}_d \sigma_d \tau_d \rangle,$$

or in a more compact form as $\langle \mathbf{ab}|\hat{v}|\mathbf{cd}\rangle$ where the boldfaced letters $\mathbf{a}$ etc represent the relevant quantum numbers, here momentum, spin and isospin. Introducing the relative momentum

$$\mathbf{k} = \frac{1}{2}(\mathbf{k}_a - \mathbf{k}_b),$$

and the center-of-mass momentum

$$\mathbf{K} = \mathbf{k}_a + \mathbf{k}_b,$$

we have

$$\langle \mathbf{k}_a \sigma_a \tau_a \mathbf{k}_b \sigma_b \tau_b | \hat{v} | \mathbf{k}_c \sigma_c \tau_c \mathbf{k}_d \sigma_d \tau_d \rangle = \langle \mathbf{k}\mathbf{K} \sigma_a \tau_a \sigma_b \tau_b | \hat{v} | \mathbf{k}'\mathbf{K}' \sigma_c \tau_c \sigma_d \tau_d \rangle.$$

The nucleon-nucleon interaction conserves the total momentum and is charge invariant, implying that the above uncoupled matrix element reads

$$\langle \mathbf{k}\mathbf{K} \sigma_a \tau_a \sigma_b \tau_b | \hat{v} | \mathbf{k}'\mathbf{K}' \sigma_c \tau_c \sigma_d \tau_d \rangle = \delta_{T_z, T_z'} \delta(\mathbf{K} - \mathbf{K}') \langle \mathbf{k} T_z S_z = (\sigma_a + \sigma_b) | \hat{v} | \mathbf{k}' T_z S_z' = (\sigma_c + \sigma_d) \rangle,$$

where we have defined the isospin projections $T_z = \tau_a + \tau_b$ and $T_z' = \tau_c + \tau_d$. Defining $\hat{v} = \hat{v}(\mathbf{k}, \mathbf{k}')$, we can rewrite the previous equation in a more compact form as

$$\delta_{T_z, T_z'} \delta(\mathbf{K} - \mathbf{K}') \langle \mathbf{k} T_z S_z = (\sigma_a + \sigma_b) | \hat{v} | \mathbf{k}' T_z S_z' = (\sigma_c + \sigma_d) \rangle = \delta_{T_z, T_z'} \delta(\mathbf{K} - \mathbf{K}') \langle T_z S_z | \hat{v}(\mathbf{k}, \mathbf{k}') | T_z S_z' \rangle.$$

These matrix elements can in turn be rewritten in terms of the total two-body quantum numbers for the spin S of two spin-1/2 fermions as

$$\langle \mathbf{k} T_z S_z | \hat{v}(\mathbf{k}, \mathbf{k}') | \mathbf{k}' T_z S_z' \rangle = \sum_{SS'} \langle \frac{1}{2}\sigma_a \frac{1}{2}\sigma_b | S S_z \rangle \langle \frac{1}{2}\sigma_c \frac{1}{2}\sigma_d | S' S_z' \rangle \langle \mathbf{k} T_z S S_z | \hat{v}(\mathbf{k}, \mathbf{k}') | \mathbf{k} T_z S' S_z' \rangle$$

The coefficients $\langle \frac{1}{2}\sigma_a \frac{1}{2}\sigma_b | S S_z \rangle$ are so-called Clebsch-Gordan recoupling coefficients. We will assume that our interactions break charge and isospin symmetry. We will refer to $T_z = 0$ as the *pn* (proton-neutron) channel, $T_z = -1$ as the *pp* (proton-proton) channel and $T_z = 1$ as the *nn* (neutron-neutron) channel.

The nucleon-nucleon force is often derived and analyzed theoretically in terms of a partial wave expansion. A state with linear momentum $\mathbf{k}$ can be written as

$$|\mathbf{k}\rangle = \sum_{l=0}^{\infty} \sum_{l_l=-l}^{L} \imath^l Y_l^{m_l}(\hat{k}|klm_l\rangle.$$

In terms of the relative and center-of-mass momenta $\mathbf{k}$ and $\mathbf{K}$, the potential in momentum space is related to the nonlocal operator $V(\mathbf{r},\mathbf{r}')$ by

$$\langle \mathbf{k}'\mathbf{K}'|\hat{v}|\mathbf{k}'\mathbf{K}\rangle = \int d\mathbf{r}d\mathbf{r}' e^{-\imath\mathbf{k}'\mathbf{r}'} V(\mathbf{r}',\mathbf{r}) e^{\imath\mathbf{k}\mathbf{r}} \delta(\mathbf{K},\mathbf{K}'). \tag{8.14}$$

We will assume that the interaction is spherically symmetric and use the partial wave expansion of the plane waves in terms of spherical harmonics. This means that we can separate the radial part of the wave function from its angular dependence. The wave function of the relative motion is described in terms of plane waves as

$$e^{\imath\mathbf{k}\mathbf{r}} = \langle \mathbf{r}|\mathbf{k}\rangle = 4\pi \sum_{lm} \imath^l j_l(kr) Y^*_{lm}(\hat{\mathbf{k}}) Y_{lm}(\hat{\mathbf{r}}), \tag{8.15}$$

where j_l is a spherical Bessel function and Y_{lm} the spherical harmonic. This partial wave basis is useful for defining the operator for the nucleon-nucleon interaction, which is symmetric with respect to rotations, parity and isospin transformations. These symmetries imply that the interaction is diagonal with respect to the quantum numbers of total angular momentum J, spin S and isospin T. Using the above plane wave expansion, and coupling to final J, S and T we get

$$\langle \mathbf{k}'|V|\mathbf{k}\rangle = (4\pi)^2 \sum_{JM} \sum_{lm} \sum_{l'm'} \imath^{l+l'} Y^*_{lm}(\hat{\mathbf{k}}) Y_{l'm'}(\hat{\mathbf{k}}') \mathscr{C}^{l'SJ}_{m'M_SM} \mathscr{C}^{lSJ}_{mM_SM} \langle k'l'STJM|V|klSTJM\rangle, \tag{8.16}$$

where we have defined

$$\langle k'l'STJM|V|klSTJM\rangle = \int j_{l'}(k'r') \langle l'STJM|V(r',r)|lSTJM\rangle j_l(kr) r'^2 dr' r^2 dr. \tag{8.17}$$

We have omitted the momentum of the center-of-mass motion $\mathbf{K}$ and the corresponding orbital momentum L, since the interaction is diagonal in these variables. The potentials we will employ in this work, like those of the Bonn group, are all non-local potentials defined in momentum space, and we will therefore not need the last equation.

8.3 Hartree-Fock theory

Hartree-Fock (HF) theory is an algorithm for finding an approximative expression for the ground state of a given Hamiltonian. The basic ingredients are Define a single-particle basis $\{\psi_\alpha\}$ so that

$$\hat{h}^{\mathrm{HF}}\psi_\alpha = \varepsilon_\alpha \psi_\alpha$$

with the Hartree-Fock Hamiltonian defined as

$$\hat{h}^{\mathrm{HF}} = \hat{t} + \hat{u}_{\mathrm{ext}} + \hat{u}^{\mathrm{HF}}$$

The term $\hat{u}^{\mathrm{HF}}$ is a single-particle potential to be determined by the HF algorithm.
The HF algorithm means to choose $\hat{u}^{\mathrm{HF}}$ in order to have

$$\langle \hat{H}\rangle = E^{\mathrm{HF}} = \langle \Phi_0|\hat{H}|\Phi_0\rangle$$

that is to find a local minimum with a Slater determinant Φ_0 being the ansatz for the ground state. The variational principle ensures that $E^{\mathrm{HF}} \geq E_0$, with E_0 the exact ground state energy.

We will show that the Hartree-Fock Hamiltonian $\hat{h}^{\mathrm{HF}}$ equals our definition of the operator $\hat{f}$ discussed in connection with the new definition of the normal-ordered Hamiltonian (see later lectures), that is we have, for a specific matrix element

$$\langle p|\hat{h}^{\mathrm{HF}}|q\rangle = \langle p|\hat{f}|q\rangle = \langle p|\hat{t}+\hat{u}_{\mathrm{ext}}|q\rangle + \sum_{i\leq F}\langle pi|\hat{V}|qi\rangle_{AS},$$

meaning that

$$\langle p|\hat{u}^{\mathrm{HF}}|q\rangle = \sum_{i\leq F}\langle pi|\hat{V}|qi\rangle_{AS}.$$

The so-called Hartree-Fock potential $\hat{u}^{\mathrm{HF}}$ brings an explicit medium dependence due to the summation over all single-particle states below the Fermi level F. It brings also in an explicit dependence on the two-body interaction (in nuclear physics we can also have complicated three- or higher-body forces). The two-body interaction, with its contribution from the other bystanding fermions, creates an effective mean field in which a given fermion moves, in addition to the external potential $\hat{u}_{\mathrm{ext}}$ which confines the motion of the fermion. For systems like nuclei, there is no external confining potential. Nuclei are examples of self-bound systems, where the binding arises due to the intrinsic nature of the strong force. For nuclear systems thus, there would be no external one-body potential in the Hartree-Fock Hamiltonian.

Another possibility is to expand the single-particle functions in a known basis and vary the coefficients, that is, the new single-particle wave function is written as a linear expansion in terms of a fixed chosen orthogonal basis (for example the well-known harmonic oscillator functions or the hydrogen-like functions etc). We define our new Hartree-Fock single-particle basis by performing a unitary transformation on our previous basis (labelled with greek indices) as

$$\psi_p^{HF} = \sum_{\lambda} C_{p\lambda}\phi_{\lambda}. \tag{8.18}$$

In this case we vary the coefficients $C_{p\lambda}$. If the basis has infinitely many solutions, we need to truncate the above sum. We assume that the basis ϕ_{λ} is orthogonal. A unitary transformation keeps the orthogonality, as discussed in exercise 1 below.

It is normal to choose a single-particle basis defined as the eigenfunctions of parts of the full Hamiltonian. The typical situation consists of the solutions of the one-body part of the Hamiltonian, that is we have

$$\hat{h}_0\phi_{\lambda} = \varepsilon_{\lambda}\phi_{\lambda}.$$

The single-particle wave functions $\phi_{\lambda}(\mathbf{r})$, defined by the quantum numbers λ and $\mathbf{r}$ are defined as the overlap

$$\phi_{\lambda}(\mathbf{r}) = \langle \mathbf{r}|\lambda\rangle.$$

In our discussions hereafter we will use our definitions of single-particle states above and below the Fermi (F) level given by the labels $ijkl\cdots \leq F$ for so-called single-hole states and $abcd\cdots > F$ for so-called particle states. For general single-particle states we employ the labels $pqrs\ldots$.

$$E[\Phi] = \sum_{\mu=1}^{A}\langle \mu|h|\mu\rangle + \frac{1}{2}\sum_{\mu=1}^{A}\sum_{\nu=1}^{A}\langle \mu\nu|\hat{v}|\mu\nu\rangle_{AS},$$

we found the expression for the energy functional in terms of the basis function $\phi_{\lambda}(\mathbf{r})$. We then varied the above energy functional with respect to the basis functions $|\mu\rangle$. Now we are interested in defining a new basis defined in terms of a chosen basis as defined in Eq. (refeq:newbasis). We can then rewrite the energy functional as

$$E[\Phi^{HF}] = \sum_{i=1}^{A}\langle i|h|i\rangle + \frac{1}{2}\sum_{ij=1}^{A}\langle ij|\hat{v}|ij\rangle_{AS}, \tag{8.19}$$

where Φ^{HF} is the new Slater determinant defined by the new basis of Eq. (refeq:newbasis).

Using Eq. (8.18) we can rewrite Eq. (8.19) as

$$E[\Psi] = \sum_{i=1}^{A}\sum_{\alpha\beta} C_{i\alpha}^{*}C_{i\beta}\langle\alpha|h|\beta\rangle + \frac{1}{2}\sum_{ij=1}^{A}\sum_{\alpha\beta\gamma\delta} C_{i\alpha}^{*}C_{j\beta}^{*}C_{i\gamma}C_{j\delta}\langle\alpha\beta|\hat{v}|\gamma\delta\rangle_{AS}. \tag{8.20}$$

We wish now to minimize the above functional. We introduce again a set of Lagrange multipliers, noting that since $\langle i|j\rangle = \delta_{i,j}$ and $\langle\alpha|\beta\rangle = \delta_{\alpha,\beta}$, the coefficients $C_{i\gamma}$ obey the relation

$$\langle i|j\rangle = \delta_{i,j} = \sum_{\alpha\beta} C_{i\alpha}^{*}C_{i\beta}\langle\alpha|\beta\rangle = \sum_{\alpha} C_{i\alpha}^{*}C_{i\alpha},$$

which allows us to define a functional to be minimized that reads

$$F[\Phi^{HF}] = E[\Phi^{HF}] - \sum_{i=1}^{A}\varepsilon_i\sum_{\alpha} C_{i\alpha}^{*}C_{i\alpha}. \tag{8.21}$$

Minimizing with respect to $C_{i\alpha}^{*}$, remembering that the equations for $C_{i\alpha}^{*}$ and $C_{i\alpha}$ can be written as two independent equations, we obtain

$$\frac{d}{dC_{i\alpha}^{*}}\left[E[\Phi^{HF}] - \sum_{j}\varepsilon_j\sum_{\alpha} C_{j\alpha}^{*}C_{j\alpha}\right] = 0,$$

which yields for every single-particle state i and index α (recalling that the coefficients $C_{i\alpha}$ are matrix elements of a unitary (or orthogonal for a real symmetric matrix) matrix) the following Hartree-Fock equations

$$\sum_{\beta} C_{i\beta}\langle\alpha|h|\beta\rangle + \sum_{j=1}^{A}\sum_{\beta\gamma\delta} C_{j\beta}^{*}C_{j\delta}C_{i\gamma}\langle\alpha\beta|\hat{v}|\gamma\delta\rangle_{AS} = \varepsilon_i^{HF}C_{i\alpha}.$$

We can rewrite this equation as (changing dummy variables)

$$\sum_{\beta}\left\{\langle\alpha|h|\beta\rangle + \sum_{j}^{A}\sum_{\gamma\delta} C_{j\gamma}^{*}C_{j\delta}\langle\alpha\gamma|\hat{v}|\beta\delta\rangle_{AS}\right\}C_{i\beta} = \varepsilon_i^{HF}C_{i\alpha}.$$

Note that the sums over greek indices run over the number of basis set functions (in principle an infinite number).

Defining

$$h_{\alpha\beta}^{HF} = \langle\alpha|h|\beta\rangle + \sum_{j=1}^{A}\sum_{\gamma\delta} C_{j\gamma}^{*}C_{j\delta}\langle\alpha\gamma|\hat{v}|\beta\delta\rangle_{AS},$$

we can rewrite the new equations as

$$\sum_{\gamma} h_{\alpha\beta}^{HF}C_{i\beta} = \varepsilon_i^{HF}C_{i\alpha}. \tag{8.22}$$

The latter is nothing but a standard eigenvalue problem. Compared with Eq. (refeq:hartreefockcoordinatespace), we see that we do not need to compute any integrals in an iterative procedure for solving the equations. It suffices to tabulate the matrix elements $\langle\alpha|h|\beta\rangle$ and $\langle\alpha\gamma|\hat{v}|\beta\delta\rangle_{AS}$ once and for all. Successive iterations require thus only a look-up in tables over one-body and two-body matrix

elements. These details will be discussed below when we solve the Hartree-Fock equations numerical.

Our Hartree-Fock matrix is thus

$$\hat{h}^{HF}_{\alpha\beta} = \langle\alpha|\hat{h}_0|\beta\rangle + \sum_{j=1}^{A}\sum_{\gamma\delta} C^*_{j\gamma}C_{j\delta}\langle\alpha\gamma|\hat{v}|\beta\delta\rangle_{AS}.$$

The Hartree-Fock equations are solved in an iterative waym starting with a guess for the coefficients $C_{j\gamma} = \delta_{j,\gamma}$ and solving the equations by diagonalization till the new single-particle energies $\varepsilon_i^{\mathrm{HF}}$ do not change anymore by a prefixed quantity.

Normally we assume that the single-particle basis $|\beta\rangle$ forms an eigenbasis for the operator $\hat{h}_0$, meaning that the Hartree-Fock matrix becomes

$$\hat{h}^{HF}_{\alpha\beta} = \varepsilon_\alpha\delta_{\alpha,\beta} + \sum_{j=1}^{A}\sum_{\gamma\delta} C^*_{j\gamma}C_{j\delta}\langle\alpha\gamma|\hat{v}|\beta\delta\rangle_{AS}.$$

The Hartree-Fock eigenvalue problem

$$\sum_\beta \hat{h}^{HF}_{\alpha\beta}C_{i\beta} = \varepsilon_i^{\mathrm{HF}}C_{i\alpha},$$

can be written out in a more compact form as

$$\hat{h}^{HF}\hat{C} = \varepsilon^{\mathrm{HF}}\hat{C}.$$

The Hartree-Fock equations are, in their simplest form, solved in an iterative way, starting with a guess for the coefficients $C_{i\alpha}$. We label the coefficients as $C^{(n)}_{i\alpha}$, where the subscript n stands for iteration n. To set up the algorithm we can proceed as follows:

We start with a guess $C^{(0)}_{i\alpha} = \delta_{i,\alpha}$. Alternatively, we could have used random starting values as long as the vectors are normalized. Another possibility is to give states below the Fermi level a larger weight. The Hartree-Fock matrix simplifies then to (assuming that the coefficients $C_{i\alpha}$ are real)

$$\hat{h}^{HF}_{\alpha\beta} = \varepsilon_\alpha\delta_{\alpha,\beta} + \sum_{j=1}^{A}\sum_{\gamma\delta} C^{(0)}_{j\gamma}C^{(0)}_{j\delta}\langle\alpha\gamma|\hat{v}|\beta\delta\rangle_{AS}.$$

Solving the Hartree-Fock eigenvalue problem yields then new eigenvectors $C^{(1)}_{i\alpha}$ and eigenvalues $\varepsilon_i^{HF(1)}$. With the new eigenvalues we can set up a new Hartree-Fock potential

$$\sum_{j=1}^{A}\sum_{\gamma\delta} C^{(1)}_{j\gamma}C^{(1)}_{j\delta}\langle\alpha\gamma|\hat{v}|\beta\delta\rangle_{AS}.$$

The diagonalization with the new Hartree-Fock potential yields new eigenvectors and eigenvalues. This process is continued till for example

$$\frac{\sum_p|\varepsilon_i^{(n)} - \varepsilon_i^{(n-1)}|}{m} \leq \lambda,$$

where λ is a user prefixed quantity ($\lambda \sim 10^{-8}$ or smaller) and p runs over all calculated single-particle energies and m is the number of single-particle states.

We can rewrite the ground state energy by adding and subtracting $\hat{u}^{HF}(x_i)$

$$E_0^{HF} = \langle\Phi_0|\hat{H}|\Phi_0\rangle = \sum_{i\leq F}^{A}\langle i|\hat{h}_0 + \hat{u}^{HF}|j\rangle + \frac{1}{2}\sum_{i\leq F}^{A}\sum_{j\leq F}^{A}[\langle ij|\hat{v}|ij\rangle - \langle ij|\hat{v}|ji\rangle] - \sum_{i\leq F}^{A}\langle i|\hat{u}^{HF}|i\rangle,$$

which results in

$$E_0^{HF} = \sum_{i\leq F}^{A} \varepsilon_i^{HF} + \frac{1}{2}\sum_{i\leq F}^{A}\sum_{j\leq F}^{A} [\langle ij|\hat{v}|ij\rangle - \langle ij|\hat{v}|ji\rangle] - \sum_{i\leq F}^{A}\langle i|\hat{u}^{HF}|i\rangle.$$

Our single-particle states $ijk\ldots$ are now single-particle states obtained from the solution of the Hartree-Fock equations.

Using our definition of the Hartree-Fock single-particle energies we obtain then the following expression for the total ground-state energy

$$E_0^{HF} = \sum_{i\leq F}^{A} \varepsilon_i - \frac{1}{2}\sum_{i\leq F}^{A}\sum_{j\leq F}^{A} [\langle ij|\hat{v}|ij\rangle - \langle ij|\hat{v}|ji\rangle].$$

8.3.1 Introducing our first ansatz for the ground state

8.3.2 Slater determinants as basis states

The simplest possible choice for many-body wavefunctions are **product** wavefunctions. That is

$$\Psi(x_1,x_2,x_3,\ldots,x_A) \approx \phi_1(x_1)\phi_2(x_2)\phi_3(x_3)\ldots$$

because we are really only good at thinking about one particle at a time. Such product wavefunctions, without correlations, are easy to work with; for example, if the single-particle states $\phi_i(x)$ are orthonormal, then the product wavefunctions are easy to orthonormalize.

Similarly, computing matrix elements of operators are relatively easy, because the integrals factorize.

The price we pay is the lack of correlations, which we must build up by using many, many product wavefunctions.

Because we have fermions, we are required to have antisymmetric wavefunctions, that is

$$\Psi(x_1,x_2,x_3,\ldots,x_A) = -\Psi(x_2,x_1,x_3,\ldots,x_A)$$

etc. This is accomplished formally by using the determinantal formalism

$$\Psi(x_1,x_2,\ldots,x_A) = \frac{1}{\sqrt{A!}}\det\begin{vmatrix} \phi_1(x_1) & \phi_1(x_2) & \ldots & \phi_1(x_A) \\ \phi_2(x_1) & \phi_2(x_2) & \ldots & \phi_2(x_A) \\ \vdots & & & \\ \phi_A(x_1) & \phi_A(x_2) & \ldots & \phi_A(x_A) \end{vmatrix}$$

Product wavefunction + antisymmetry (Pauli principle) = Slater determinant.

Properties of the determinant (interchange of any two rows or any two columns yields a change in sign; thus no two rows and no two columns can be the same) lead to the following consequence of the Pauli principle:

- No two particles can be at the same place (two columns the same); and
- No two particles can be in the same state (two rows the same).

As a practical matter, however, Slater determinants beyond $N = 4$ quickly become unwieldy. Thus we turn to the **occupation representation** or **second quantization** to simplify calculations.

The occupation representation, using fermion **creation** and **annihilation** operators, is compact and efficient. It is also abstract and, at first encounter, not easy to internalize. It is inspired by other operator formalism, such as the ladder operators for the harmonic oscillator or for angular momentum, but unlike those cases, the operators **do not have coordinate space representations**.

Instead, one can think of fermion creation/annihilation operators as a game of symbols that compactly reproduces what one would do, albeit clumsily, with full coordinate-space Slater determinants.

We start with a set of orthonormal single-particle states $\{\phi_i(x)\}$. (Note: this requirement, and others, can be relaxed, but leads to a more involved formalism.) **Any** orthonormal set will do.

To each single-particle state $\phi_i(x)$ we associate a creation operator $\hat{a}_i^\dagger$ and an annihilation operator $\hat{a}_i$.

When acting on the vacuum state $|0\rangle$, the creation operator $\hat{a}_i^\dagger$ causes a particle to occupy the single-particle state $\phi_i(x)$:

$$\phi_i(x) \rightarrow \hat{a}_i^\dagger|0\rangle$$

But with multiple creation operators we can occupy multiple states:

$$\phi_i(x)\phi_j(x')\phi_k(x'') \rightarrow \hat{a}_i^\dagger\hat{a}_j^\dagger\hat{a}_k^\dagger|0\rangle.$$

Now we impose antisymmetry, by having the fermion operators satisfy **anticommutation relations**:

$$\hat{a}_i^\dagger\hat{a}_j^\dagger + \hat{a}_j^\dagger\hat{a}_i^\dagger = [\hat{a}_i^\dagger, \hat{a}_j^\dagger]_+ = \{\hat{a}_i^\dagger, \hat{a}_j^\dagger\} = 0$$

so that

$$\hat{a}_i^\dagger\hat{a}_j^\dagger = -\hat{a}_j^\dagger\hat{a}_i^\dagger$$

Because of this property, automatically $\hat{a}_i^\dagger\hat{a}_i^\dagger = 0$, enforcing the Pauli exclusion principle. Thus when writing a Slater determinant using creation operators,

$$\hat{a}_i^\dagger\hat{a}_j^\dagger\hat{a}_k^\dagger\ldots|0\rangle$$

each index $i, j, k, \ldots$ must be unique.

8.3.3 The Breuckner G-matrix

The Brueckner G-matrix has historically been an important ingredient in many-body calculations of nuclear systems. In this section, we will briefly survey the philosophy behind the G-matrix.

Historically, the G-matrix was developed in microscopic nuclear matter calculations using realistic nucleon-nucleon (NN) interactions. It is an ingenuous as well as an interesting method to overcome the difficulties caused by the strong, short-range repulsive core contained in all modern models for the NN interaction. The G-matrix method was originally developed by Brueckner, and further developed by Goldstone and Bethe, Brandow and Petschek. In the literature it is generally referred to as the Brueckner theory or the Brueckner-Bethe-Goldstone theory.

Suppose we want to calculate the nuclear matter ground-state energy E_0 using the non-relativistic Schrödinger equation

$$H\Psi_0(A) = E_0(A)\Psi_0(A), \tag{8.23}$$

with $H = T + V$ where A denotes the number of particles, T is the kinetic energy and V is the nucleon-nucleon (NN) potential. Models for the NN interaction are discussed in the chapter on nuclear forces. The corresponding unperturbed problem is

$$H_0\psi_0(A) = W_0(A)\psi_0(A). \tag{8.24}$$

Here H_0 is just kinetic energy T and ψ_0 is a Slater determinant representing the Fermi sea, where all orbits through the Fermi momentum k_F are filled. We write

$$E_0 = W_0 + \Delta E_0, \tag{8.25}$$

where ΔE_0 is the ground-state energy shift or correlation energy as it was defined in many-body perturbation theory. If we know how to calculate ΔE_0, then we know E_0, since W_0 is easily obtained. In the limit $A \to \infty$, the quantities E_0 and ΔE_0 themselves are not well defined, but the ratios E_0/A and $\Delta E_0/A$ are. The nuclear-matter binding energy per nucleon is commonly denoted by BE/A, which is just $-E_0/A$. In passing, we note that the empirical value for symmetric nuclear matter (proton number Z=neutron number N) is ≈ 16 MeV. There exists a formal theory for the calculation of ΔE_0. According to the well-known Goldstone linked-diagram theory, the energy shift ΔE_0 is given exactly by the diagrammatic expansion shown in Fig. **??**. This theory, is a linked-cluster perturbation expansion for the ground state energy of a many-body system, and applies equally well to both nuclear matter and closed-shell nuclei such as the doubly magic nucleus ^{40}Ca. We will not discuss the Goldstone expansion, but rather discuss briefly how it is used in calculations.

Using the standard diagram rules (see the discussion on coupled-cluster theory and many-body perturbation theory), the various diagrams contained in the above figure can be readily calculated (in an uncoupled scheme)

$$(i) = \frac{(-)^{n_h+n_l}}{2^{n_{ep}}} \sum_{ij\leq k_F} \langle ij|\hat{v}|ij\rangle_{AS}, \tag{8.26}$$

with $n_h = n_l = 2$ and $n_{ep} = 1$. As discussed in connection with the diagram rules in the many-body perturbation theory chapter, n_h denotes the number of hole lines, n_l the number of closed fermion loops and n_{ep} is the number of so-called equivalent pairs. The factor $1/2^{n_{ep}}$ is needed since we want to count a pair of particles only once. We will carry this factor $1/2$ with us in the equations below. The subscript AS denotes the antisymmetrized and normalized matrix element

$$\langle ij|\hat{v}|ij\rangle_{AS} = \langle ij|\hat{v}|ij\rangle - \langle ji|\hat{v}|ij\rangle. \tag{8.27}$$

Similarly, diagrams (ii) and (iii) read

$$(ii) = \frac{(-)^{2+2}}{2^2} \sum_{ij\leq k_F} \sum_{ab>k_F} \frac{\langle ij|\hat{v}|ab\rangle_{AS}\langle ab|\hat{v}|ij\rangle_{AS}}{\varepsilon_i + \varepsilon_j - \varepsilon_a - \varepsilon_b}, \tag{8.28}$$

and

$$(iii) = \frac{(-)^{2+2}}{2^3} \sum_{k_i,k_j\leq k_F} \sum_{abcdk_F} \frac{\langle ij|\hat{v}|ab\rangle_{AS}\langle ab|\hat{v}|cd\rangle_{AS}\langle cd|\hat{v}|ij\rangle_{AS}}{(\varepsilon_i + \varepsilon_j - \varepsilon_a - \varepsilon_b)(\varepsilon_i + \varepsilon_j - \varepsilon_c - \varepsilon_d)}. \tag{8.29}$$

In the above, ε denotes the sp energies defined by H_0. The steps leading to the above expressions for the various diagrams are rather straightforward. Though, if we wish to compute the matrix elements for the interaction v, a serious problem arises. Typically, the matrix elements will contain a term (see the next section for the formal details) $V(|\mathbf{r}|)$, which represents the interaction potential V between two nucleons, where $\mathbf{r}$ is the internucleon distance. All modern models for V have a strong short-range repulsive core. Hence, matrix elements in-

volving $V(|\mathbf{r}|)$, will result in large (or infinitely large for a potential with a hard core) and repulsive contributions to the ground-state energy. Thus, the diagrammatic expansion for the ground-state energy in terms of the potential $V(|\mathbf{r}|)$ becomes meaningless.

One possible solution to this problem is provided by the well-known Brueckner theory or the Brueckner G-matrix, or just the G-matrix. In fact, the G-matrix is an almost indispensable tool in almost every microscopic nuclear structure calculation. Its main idea may be paraphrased as follows. Suppose we want to calculate the function $f(x) = x/(1+x)$. If x is small, we may expand the function $f(x)$ as a power series $x+x^2+x^3+\dots$ and it may be adequate to just calculate the first few terms. In other words, $f(x)$ may be calculated using a low-order perturbation method. But if x is large (or infinitely large), the above power series is obviously meaningless. However, the exact function $x/(1+x)$ is still well defined in the limit of x becoming very large.

These arguments suggest that one should sum up the diagrams (i), (ii), (iii) in fig. **??** and the similar ones to all orders, instead of computing them one by one. Denoting this all-order sum as $1/2\tilde{G}_{ijij}$, where we have introduced the shorthand notation $\tilde{G}_{ijij} = \langle k_i k_j|\tilde{G}|k_i k_j\rangle_{AS}$ (and similarly for $\tilde{v}$), we have that

$$\frac{1}{2}\tilde{G}_{ijij} = \frac{1}{2}\hat{v}_{ijij} + \sum_{ab>k_F}\frac{1}{2}\hat{v}_{ijab}\frac{1}{\varepsilon_i+\varepsilon_j-\varepsilon_a-\varepsilon_b} \times\left[\frac{1}{2}\hat{v}_{abij} + \sum_{cd>k_F}\frac{1}{2}\hat{v}_{abcd}\frac{1}{\varepsilon_i+\varepsilon_j-\varepsilon_c-\varepsilon_d}\frac{1}{2}V_{cdij}+\dots\right]. \tag{8.30}$$

The factor $1/2$ is the same as that discussed above, namely we want to count a pair of particles only once. The quantity inside the brackets is just $1/2\tilde{G}_{mnij}$ and the above equation can be rewritten as an integral equation

$$\tilde{G}_{ijij} = \tilde{V}_{ijij} + \sum_{ab>F}\frac{1}{2}\hat{v}_{ijab}\frac{1}{\varepsilon_i+\varepsilon_j-\varepsilon_a-\varepsilon_b}\tilde{G}_{abij}. \tag{8.31}$$

Note that $\tilde{G}$ is the antisymmetrized G-matrix since the potential $\tilde{v}$ is also antisymmetrized. This means that $\tilde{G}$ obeys

$$\tilde{G}_{ijij} = -\tilde{G}_{jiij} = -\tilde{G}_{ijji}. \tag{8.32}$$

The $\tilde{G}$-matrix is defined as

$$\tilde{G}_{ijij} = G_{ijij} - G_{jiij}, \tag{8.33}$$

and the equation for G is

$$G_{ijij} = V_{ijij} + \sum_{ab>k_F} V_{ijab}\frac{1}{\varepsilon_i+\varepsilon_j-\varepsilon_a-\varepsilon_b}G_{abij}, \tag{8.34}$$

which is the familiar G-matrix equation. The above matrix is specifically designed to treat a class of diagrams contained in ΔE_0, of which typical contributions were shown in fig. **??**. In fact the sum of the diagrams in fig. **??** is equal to $1/2(G_{ijij}-G_{jiij})$.

Let us now define a more general G-matrix as

$$G_{ijij} = V_{ijij} + \sum_{mn>0} V_{ijmn}\frac{Q(mn)}{\omega-\varepsilon_m-\varepsilon_n}G_{mnij}, \tag{8.35}$$

which is an extension of Eq. (8.34). Note that Eq. (8.34) has $\varepsilon_i+\varepsilon_j$ in the energy denominator, whereas in the latter equation we have a general energy variable ω in the denominator. Furthermore, in Eq. (8.34) we have a restricted sum over mn, while in Eq. (8.35) we sum over all ab and we have introduced a weighting factor $Q(ab)$. In Eq. (8.35) $Q(ab)$ corresponds to

the choice

$$Q(a,b) = \begin{cases} 1, & min(a,b) > k_F \\ 0, & \text{else.} \end{cases}, \tag{8.36}$$

where $Q(ab)$ is usually referred to as the G-matrix Pauli exclusion operator. The role of Q is to enforce a selection of the intermediate states allowed in the G-matrix equation. The above Q requires that the intermediate particles a and b must be both above the Fermi surface defined by F. We may enforce a different requirement by using a summation over intermediate states different from that in Eq. (8.35). An example is the Pauli operator for the model-space Brueckner-Hartree-Fock method discussed below.

Before ending this section, let us rewrite the G-matrix equation in a more compact form. The sp energies ε and wave functions are defined by the unperturbed hamiltonian H_0 as

$$H_0|\psi_a\psi_b = (\varepsilon_a + \varepsilon_b)|\psi_a\psi_b. \tag{8.37}$$

The G-matrix equation can then be rewritten in the following compact form

$$G(\omega) = V + V\frac{\hat{Q}}{\omega - H_0}G(\omega), \tag{8.38}$$

with $\hat{Q} = \sum_{ab}|\psi_a\psi_b\rangle\langle\psi_a\psi_b|$. In terms of diagrams, G corresponds to an all-order sum of the "ladder-type" interactions between two particles with the intermediate states restricted by Q.

The G-matrix equation has a very simple form. But its calculation is rather complicated, particularly for finite nuclear systems such as the nucleus ^{18}O. There are a number of complexities. To mention a few, the Pauli operator Q may not commute with the unperturbed hamiltonian H_0 and we have to make the replacement

$$\frac{Q}{\omega - H_0} \rightarrow Q\frac{1}{\omega - QH_0Q}Q.$$

The determination of the starting energy ω is also another problem.

In a medium such as nuclear matter we must account for the fact that certain states are not available as intermediate states in the calculation of the G-matrix. Following the discussion above this is achieved by introducing the medium dependent Pauli operator Q. Further, the energy ω of the incoming particles, given by a pure kinetic term in a scattering problem between two unbound particles (for example two colliding protons), must be modified so as to allow for medium corrections. How to evaluate the Pauli operator for nuclear matter is, however, not straightforward. Before discussing how to evaluate the Pauli operator for nuclear matter, we note that the G-matrix is conventionally given in terms of partial waves and the coordinates of the relative and center-of-mass motion. If we assume that the G-matrix is diagonal in α (α is a shorthand notation for J, S, L and T), we write the equation for the G-matrix as a coupled-channels equation in the relative and center-of-mass system

$$G^{\alpha}_{ll'}(kk'K\omega) = V^{\alpha}_{ll'}(kk') + \sum_{l''}\int \frac{d^3q}{(2\pi)^3}V^{\alpha}_{ll''}(kq)\frac{Q(q,K)}{\omega - H_0}G^{\alpha}_{l''l'}(qk'K\omega). \tag{8.39}$$

This equation is similar in structure to the scattering equations discussed in connection with nuclear forces (see the chapter on models for nuclear forces), except that we now have introduced the Pauli operator Q and a medium dependent two-particle energy ω. The notations in this equation follow those of the chapter on nuclear forces where we discuss the solution of the scattering matrix T. The numerical details on how to solve the above G-matrix equation through matrix inversion techniques are discussed below Note however that the G-matrix may not be diagonal in α. This is due to the fact that the Pauli operator Q is not diagonal in

the above representation in the relative and center-of-mass system. The Pauli operator depends on the angle between the relative momentum and the center of mass momentum. This angle dependence causes Q to couple states with different relative angular momentua $\mathscr{J}$, rendering a partial wave decomposition of the G-matrix equation rather difficult. The angle dependence of the Pauli operator can be eliminated by introducing the angle-average Pauli operator, where one replaces the exact Pauli operator Q by its average $\bar{Q}$ over all angles for fixed relative and center-of-mass momenta. The choice of Pauli operator is decisive to the determination of the sp spectrum. Basically, to first order in the reaction matrix G, there are three commonly used sp spectra, all defined by the solution of the following equations

$$\varepsilon_m = \varepsilon(k_m) = t_m + u_m = \frac{k_m^2}{2M_N} + u_m, \tag{8.40}$$

and

$$u_m = \sum_{h \leq k_F} \langle mh| G(\omega = \varepsilon_m + \varepsilon_h) |mh\rangle_{AS} \quad k_m \leq k_M, \tag{8.41}$$

$$\tag{8.42}$$

$$u_m = 0, k_m > k_M. \tag{8.43}$$

For notational economy, we set $|\mathbf{k}_m| = k_m$. Here we employ antisymmetrized matrix elements (AS), and k_M is a cutoff on the momentum. Further, t_m is the sp kinetic energy and similarly u_m is the sp potential. The choice of cutoff k_M is actually what determines the three commonly used sp spectra. In the conventional BHF approach one employs $k_M = k_F$, which leads to a Pauli operator Q_{BHF} (in the laboratory system) given by

$$Q_{\text{BHF}}(k_m, k_n) = \begin{cases} 1, \, min(k_m, k_n) > k_F \\ 0, \qquad \text{else.} \end{cases}, \tag{8.44}$$

or, since we will define an angle-average Pauli operator in the relative and center-of-mass system, we have

$$\bar{Q}_{\text{BHF}}(k, K) = \begin{cases} 0, & k \leq \sqrt{k_F^2 - K^2/4} \\ 1, & k \geq k_F + K/2 \\ \frac{K^2/4 + k^2 - k_F^2}{kK} & \text{else,} \end{cases} \tag{8.45}$$

with k_F the momentum at the Fermi surface.

The BHF choice sets $u_k = 0$ for $k > k_F$, which leads to an unphysical, large gap at the Fermi surface, typically of the order of $50 - 60$ MeV. To overcome the gap problem, Mahaux and collaborators introduced a continuous sp spectrum for all values of k. The divergencies which then may occur in Eq. (8.39) are taken care of by introducing a principal value integration in Eq. (8.39), to retain only the real part contribution to the G-matrix.

To define the energy denominators we will also make use of the angle-average approximation. The angle dependence is handled by the so-called effective mass approximation. The single-particle energies in nuclear matter are assumed to have the simple quadratic form

$$\begin{aligned} \varepsilon(k_m) &= \frac{\hbar^2 k_m^2}{2M_N^*} + \Delta, \quad k_m \leq k_F \\ &= \frac{\hbar^2 k_m^2}{2M_N}, \qquad k_m > k_F, \end{aligned} \tag{8.46}$$

where M_N^* is the effective mass of the nucleon and M_N is the bare nucleon mass. For particle states above the Fermi sea we choose a pure kinetic energy term, whereas for hole states, the

terms M_N^* and Δ, the latter being an effective single-particle potential related to the G-matrix, are obtained through the self-consistent Brueckner-Hartree-Fock procedure. The sp potential is obtained through the same angle-average approximation

$$U(k_m) = \sum_{l\alpha}(2T+1)(2J+1)\left\{\frac{8}{\pi}\int_0^{(k_F-k_m)/2} k^2 dk G_{ll}^{\alpha}(k,\bar{K}_1) + \frac{1}{\pi k_m}\int_{(k_F-k_m)/2}^{(k_F+k_m)/2} kdk(k_F^2-(k_m-2k)^2)G_{ll}^{\alpha}(k,\bar{K}_2)\right\}, \tag{8.47}$$

where we have defined

$$\bar{K}_1^2 = 4(k_m^2+k^2), \tag{8.48}$$

and

$$\bar{K}_2^2 = 4(k_m^2+k^2)-(2k+k_m-k_F)(2k+k_1+k_F). \tag{8.49}$$

This self-consistency scheme consists in choosing adequate initial values of the effective mass and Δ. The obtained G-matrix is in turn used to obtain new values for M_N^* and Δ. This procedure continues until these parameters vary little.

8.4 Full Configuration Interaction Theory

We have defined the ansatz for the ground state as

$$|\Phi_0\rangle = \left(\prod_{i\leq F}\hat{a}_i^{\dagger}\right)|0\rangle,$$

where the index i defines different single-particle states up to the Fermi level. We have assumed that we have N fermions. A given one-particle-one-hole ($1p1h$) state can be written as

$$|\Phi_i^a\rangle = \hat{a}_a^{\dagger}\hat{a}_i|\Phi_0\rangle,$$

while a $2p2h$ state can be written as

$$|\Phi_{ij}^{ab}\rangle = \hat{a}_a^{\dagger}\hat{a}_b^{\dagger}\hat{a}_j\hat{a}_i|\Phi_0\rangle,$$

and a general $ApAh$ state as

$$|\Phi_{ijk\dots}^{abc\dots}\rangle = \hat{a}_a^{\dagger}\hat{a}_b^{\dagger}\hat{a}_c^{\dagger}\dots\hat{a}_k\hat{a}_j\hat{a}_i|\Phi_0\rangle.$$

We use letters $ijkl\dots$ for states below the Fermi level and $abcd\dots$ for states above the Fermi level. A general single-particle state is given by letters $pqrs\dots$.

We can then expand our exact state function for the ground state as

$$|\Psi_0\rangle = C_0|\Phi_0\rangle + \sum_{ai}C_i^a|\Phi_i^a\rangle + \sum_{abij}C_{ij}^{ab}|\Phi_{ij}^{ab}\rangle + \dots = (C_0+\hat{C})|\Phi_0\rangle,$$

where we have introduced the so-called correlation operator

$$\hat{C} = \sum_{ai}C_i^a\hat{a}_a^{\dagger}\hat{a}_i + \sum_{abij}C_{ij}^{ab}\hat{a}_a^{\dagger}\hat{a}_b^{\dagger}\hat{a}_j\hat{a}_i + \dots$$

Since the normalization of Ψ_0 is at our disposal and since C_0 is by hypothesis non-zero, we may arbitrarily set $C_0 = 1$ with corresponding proportional changes in all other coefficients. Using this so-called intermediate normalization we have

$$\langle\Psi_0|\Phi_0\rangle = \langle\Phi_0|\Phi_0\rangle = 1,$$

resulting in

$$|\Psi_0\rangle = (1+\hat{C})|\Phi_0\rangle.$$

We rewrite

$$|\Psi_0\rangle = C_0|\Phi_0\rangle + \sum_{ai} C_i^a|\Phi_i^a\rangle + \sum_{abij} C_{ij}^{ab}|\Phi_{ij}^{ab}\rangle + \dots,$$

in a more compact form as

$$|\Psi_0\rangle = \sum_{PH} C_H^P \Phi_H^P = \left(\sum_{PH} C_H^P \hat{A}_H^P\right)|\Phi_0\rangle,$$

where H stands for $0,1,\dots,n$ hole states and P for $0,1,\dots,n$ particle states. Our requirement of unit normalization gives

$$\langle\Psi_0|\Psi_0\rangle = \sum_{PH}|C_H^P|^2 = 1,$$

and the energy can be written as

$$E = \langle\Psi_0|\hat{H}|\Psi_0\rangle = \sum_{PP'HH'} C_H^{*P}\langle\Phi_H^P|\hat{H}|\Phi_{H'}^{P'}\rangle C_{H'}^{P'}.$$

Normally

$$E = \langle\Psi_0|\hat{H}|\Psi_0\rangle = \sum_{PP'HH'} C_H^{*P}\langle\Phi_H^P|\hat{H}|\Phi_{H'}^{P'}\rangle C_{H'}^{P'},$$

is solved by diagonalization setting up the Hamiltonian matrix defined by the basis of all possible Slater determinants. A diagonalization is equivalent to finding the variational minimum of

$$\langle\Psi_0|\hat{H}|\Psi_0\rangle - \lambda\langle\Psi_0|\Psi_0\rangle,$$

where λ is a variational multiplier to be identified with the energy of the system.

The minimization process results in

$$\delta\left[\langle\Psi_0|\hat{H}|\Psi_0\rangle - \lambda\langle\Psi_0|\Psi_0\rangle\right] =$$

$$\sum_{P'H'}\left\{\delta[C_H^{*P}]\langle\Phi_H^P|\hat{H}|\Phi_{H'}^{P'}\rangle C_{H'}^{P'} + C_H^{*P}\langle\Phi_H^P|\hat{H}|\Phi_{H'}^{P'}\rangle\delta[C_{H'}^{P'}] - \lambda(\delta[C_H^{*P}]C_{H'}^{P'} + C_H^{*P}\delta[C_{H'}^{P'}]\right\} = 0.$$

Since the coefficients $\delta[C_H^{*P}]$ and $\delta[C_{H'}^{P'}]$ are complex conjugates it is necessary and sufficient to require the quantities that multiply with $\delta[C_H^{*P}]$ to vanish.

This leads to

$$\sum_{P'H'}\langle\Phi_H^P|\hat{H}|\Phi_{H'}^{P'}\rangle C_{H'}^{P'} - \lambda C_H^P = 0,$$

for all sets of P and H.

If we then multiply by the corresponding C_H^{*P} and sum over PH we obtain

$$\sum_{PP'HH'} C_H^{*P}\langle\Phi_H^P|\hat{H}|\Phi_{H'}^{P'}\rangle C_{H'}^{P'} - \lambda\sum_{PH}|C_H^P|^2 = 0,$$

leading to the identification $\lambda = E$. This means that we have for all PH sets

$$\sum_{P'H'}\langle\Phi_H^P|\hat{H} - E|\Phi_{H'}^{P'}\rangle = 0. \tag{8.50}$$

An alternative way to derive the last equation is to start from

$$(\hat{H}-E)|\Psi_0\rangle = (\hat{H}-E)\sum_{P'H'} C_{H'}^{P'}|\Phi_{H'}^{P'}\rangle = 0,$$

and if this equation is successively projected against all Φ_H^P in the expansion of Ψ, we end up with Eq. (8.50).

One solves this equation normally by diagonalization. If we are able to solve this equation exactly (that is numerically exactly) in a large Hilbert space (it will be truncated in terms of the number of single-particle states included in the definition of Slater determinants), it can then serve as a benchmark for other many-body methods which approximate the correlation operator $\hat{C}$.

8.4.1 Example of a Hamiltonian matrix

Suppose, as an example, that we have six fermions below the Fermi level. This means that we can make at most $6p-6h$ excitations. If we have an infinity of single particle states above the Fermi level, we will obviously have an infinity of say $2p-2h$ excitations. Each such way to configure the particles is called a **configuration**. We will always have to truncate in the basis of single-particle states. This gives us a finite number of possible Slater determinants. Our Hamiltonian matrix would then look like (where each block can have a large dimensionalities):

	$0p-0h$	$1p-1h$	$2p-2h$	$3p-3h$	$4p-4h$	$5p-5h$	$6p-6h$
$0p-0h$	x	x	x	0	0	0	0
$1p-1h$	x	x	x	x	0	0	0
$2p-2h$	x	x	x	x	x	0	0
$3p-3h$	0	x	x	x	x	x	0
$4p-4h$	0	0	x	x	x	x	x
$5p-5h$	0	0	0	x	x	x	x
$6p-6h$	0	0	0	0	x	x	x

with a two-body force. Why are there non-zero blocks of elements? If we use a Hartree-Fock basis, this corresponds to a particular unitary transformation where matrix elements of the type $\langle 0p-0h|\hat{H}|1p-1h\rangle = \langle \Phi_0|\hat{H}|\Phi_i^a\rangle = 0$ and our Hamiltonian matrix becomes

	$0p-0h$	$1p-1h$	$2p-2h$	$3p-3h$	$4p-4h$	$5p-5h$	$6p-6h$
$0p-0h$	$\tilde{x}$	0	$\tilde{x}$	0	0	0	0
$1p-1h$	0	$\tilde{x}$	$\tilde{x}$	$\tilde{x}$	0	0	0
$2p-2h$	$\tilde{x}$	$\tilde{x}$	$\tilde{x}$	$\tilde{x}$	$\tilde{x}$	0	0
$3p-3h$	0	$\tilde{x}$	$\tilde{x}$	$\tilde{x}$	$\tilde{x}$	$\tilde{x}$	0
$4p-4h$	0	0	$\tilde{x}$	$\tilde{x}$	$\tilde{x}$	$\tilde{x}$	$\tilde{x}$
$5p-5h$	0	0	0	$\tilde{x}$	$\tilde{x}$	$\tilde{x}$	$\tilde{x}$
$6p-6h$	0	0	0	0	$\tilde{x}$	$\tilde{x}$	$\tilde{x}$

If we do not make any truncations in the possible sets of Slater determinants (many-body states) we can make by distributing A nucleons among n single-particle states, we call such a calculation for

- Full configuration interaction theory

If we make truncations, we have different possibilities

- The standard nuclear shell-model. Here we define an effective Hilbert space with respect to a given core. The calculations are normally then performed for all many-body states that can be constructed from the effective Hilbert spaces. This approach requires a properly defined effective Hamiltonian

- We can truncate in the number of excitations. For example, we can limit the possible Slater determinants to only $1p-1h$ and $2p-2h$ excitations. This is called a configuration interaction calculation at the level of singles and doubles excitations, or just CISD.
- We can limit the number of excitations in terms of the excitation energies. If we do not define a core, this defines normally what is called the no-core shell-model approach.

What happens if we have a three-body interaction and a Hartree-Fock basis?

Full configuration interaction theory calculations provide in principle, if we can diagonalize numerically, all states of interest. The dimensionality of the problem explodes however quickly.

The total number of Slater determinants which can be built with say N neutrons distributed among n single particle states is

$$\binom{n}{N} = \frac{n!}{(n-N)!N!}.$$

For a model space which comprises the first for major shells only $0s$, $0p$, $1s0d$ and $1p0f$ we have 40 single particle states for neutrons and protons. For the eight neutrons of oxygen-16 we would then have

$$\binom{40}{8} = \frac{40!}{(32)!8!} \sim 10^9,$$

and multiplying this with the number of proton Slater determinants we end up with approximately witha dimensionality d of $d \sim 10^{18}$.

This number can be reduced if we look at specific symmetries only. However, the dimensionality explodes quickly!

- For Hamiltonian matrices of dimensionalities which are smaller than $d \sim 10^5$, we would use so-called direct methods for diagonalizing the Hamiltonian matrix
- For larger dimensionalities iterative eigenvalue solvers like Lanczos' method are used. The most efficient codes at present can handle matrices of $d \sim 10^{10}$.

8.4.2 A non-practical way of solving the eigenvalue problem

For reasons to come (links with Coupled-Cluster theory and Many-Body perturbation theory), we will rewrite Eq. (8.50) as a set of coupled non-linear equations in terms of the unknown coefficients C_H^P. To obtain the eigenstates and eigenvalues in terms of non-linear equations is not a very practical approach. However, it serves the scope of linking FCI theory with approximative solutions to the many-body problem.

To see this, we look at the contributions arising from

$$\langle \Phi_H^P| = \langle \Phi_0|$$

in Eq. (8.50), that is we multiply with $\langle \Phi_0|$ from the left in

$$(\hat{H}-E)\sum_{P'H'} C_{H'}^{P'}|\Phi_{H'}^{P'}\rangle = 0.$$

If we assume that we have a two-body operator at most, Slater's rule gives then an equation for the correlation energy in terms of C_i^a and C_{ij}^{ab} only. We get then

$$\langle \Phi_0|\hat{H}-E|\Phi_0\rangle + \sum_{ai}\langle \Phi_0|\hat{H}-E|\Phi_i^a\rangle C_i^a + \sum_{abij}\langle \Phi_0|\hat{H}-E|\Phi_{ij}^{ab}\rangle C_{ij}^{ab} = 0,$$

or

$$E - E_0 = \Delta E = \sum_{ai} \langle \Phi_0 | \hat{H} | \Phi_i^a \rangle C_i^a + \sum_{abij} \langle \Phi_0 | \hat{H} | \Phi_{ij}^{ab} \rangle C_{ij}^{ab},$$

where the energy E_0 is the reference energy and ΔE defines the so-called correlation energy. The single-particle basis functions could be the results of a Hartree-Fock calculation or just the eigenstates of the non-interacting part of the Hamiltonian.

In our notes on Hartree-Fock calculations, we have already computed the matrix $\langle \Phi_0 | \hat{H} | \Phi_i^a \rangle$ and $\langle \Phi_0 | \hat{H} | \Phi_{ij}^{ab} \rangle$. If we are using a Hartree-Fock basis, then the matrix elements $\langle \Phi_0 | \hat{H} | \Phi_i^a \rangle = 0$ and we are left with a *correlation energy* given by

$$E - E_0 = \Delta E^{HF} = \sum_{abij} \langle \Phi_0 | \hat{H} | \Phi_{ij}^{ab} \rangle C_{ij}^{ab}.$$

Inserting the various matrix elements we can rewrite the previous equation as

$$\Delta E = \sum_{ai} \langle i | \hat{f} | a \rangle C_i^a + \sum_{abij} \langle ij | \hat{v} | ab \rangle C_{ij}^{ab}.$$

This equation determines the correlation energy but not the coefficients C. We need more equations. Our next step is to set up

$$\langle \Phi_i^a | \hat{H} - E | \Phi_0 \rangle + \sum_{bj} \langle \Phi_i^a | \hat{H} - E | \Phi_j^b \rangle C_j^b + \sum_{bcjk} \langle \Phi_i^a | \hat{H} - E | \Phi_{jk}^{bc} \rangle C_{jk}^{bc} + \sum_{bcdjkl} \langle \Phi_i^a | \hat{H} - E | \Phi_{jkl}^{bcd} \rangle C_{jkl}^{bcd} = 0,$$

as this equation will allow us to find an expression for the coefficents C_i^a since we can rewrite this equation as

$$\langle i | \hat{f} | a \rangle + \langle \Phi_i^a | \hat{H} | \Phi_i^a \rangle C_i^a + \sum_{bj \neq ai} \langle \Phi_i^a | \hat{H} | \Phi_j^b \rangle C_j^b + \sum_{bcjk} \langle \Phi_i^a | \hat{H} | \Phi_{jk}^{bc} \rangle C_{jk}^{bc} + \sum_{bcdjkl} \langle \Phi_i^a | \hat{H} | \Phi_{jkl}^{bcd} \rangle C_{jkl}^{bcd} = E C_i^a.$$

We see that on the right-hand side we have the energy E. This leads to a non-linear equation in the unknown coefficients. These equations are normally solved iteratively (that is we can start with a guess for the coefficients C_i^a). A common choice is to use perturbation theory for the first guess, setting thereby

$$C_i^a = \frac{\langle i | \hat{f} | a \rangle}{\varepsilon_i - \varepsilon_a}.$$

The observant reader will however see that we need an equation for C_{jk}^{bc} and C_{jkl}^{bcd} as well. To find equations for these coefficients we need then to continue our multiplications from the left with the various Φ_H^P terms.

For C_{jk}^{bc} we need then

$$\langle \Phi_{ij}^{ab} | \hat{H} - E | \Phi_0 \rangle + \sum_{kc} \langle \Phi_{ij}^{ab} | \hat{H} - E | \Phi_k^c \rangle C_k^c +$$

$$\sum_{cdkl} \langle \Phi_{ij}^{ab} | \hat{H} - E | \Phi_{kl}^{cd} \rangle C_{kl}^{cd} + \sum_{cdeklm} \langle \Phi_{ij}^{ab} | \hat{H} - E | \Phi_{klm}^{cde} \rangle C_{klm}^{cde} + \sum_{cdefklmn} \langle \Phi_{ij}^{ab} | \hat{H} - E | \Phi_{klmn}^{cdef} \rangle C_{klmn}^{cdef} = 0,$$

and we can isolate the coefficients C_{kl}^{cd} in a similar way as we did for the coefficients C_i^a. A standard choice for the first iteration is to set

$$C_{ij}^{ab} = \frac{\langle ij | \hat{v} | ab \rangle}{\varepsilon_i + \varepsilon_j - \varepsilon_a - \varepsilon_b}.$$

At the end we can rewrite our solution of the Schroedinger equation in terms of n coupled equations for the coefficients C_H^P. This is a very cumbersome way of solving the equation.

However, by using this iterative scheme we can illustrate how we can compute the various terms in the wave operator or correlation operator $\hat{C}$. We will later identify the calculation of the various terms C_H^P as parts of different many-body approximations to full CI. In particular, we can relate this non-linear scheme with Coupled Cluster theory and many-body perturbation theory.

8.4.3 Summarizing FCI and bringing in approximative methods

If we can diagonalize large matrices, FCI is the method of choice since:

- It gives all eigenvalues, ground state and excited states
- The eigenvectors are obtained directly from the coefficients C_H^P which result from the diagonalization
- We can compute easily expectation values of other operators, as well as transition probabilities
- Correlations are easy to understand in terms of contributions to a given operator beyond the Hartree-Fock contribution. This is the standard approach in many-body theory.

The correlation energy is defined as, with a two-body Hamiltonian,

$$\Delta E = \sum_{ai} \langle i|\hat{f}|a\rangle C_i^a + \sum_{abij} \langle ij|\hat{v}|ab\rangle C_{ij}^{ab}.$$

The coefficients C result from the solution of the eigenvalue problem. The energy of say the ground state is then

$$E = E_{ref} + \Delta E,$$

where the so-called reference energy is the energy we obtain from a Hartree-Fock calculation, that is

$$E_{ref} = \langle \Phi_0|\hat{H}|\Phi_0\rangle.$$

However, as we have seen, even for a small case like the four first major shells and a nucleus like oxygen-16, the dimensionality becomes quickly intractable. If we wish to include single-particle states that reflect weakly bound systems, we need a much larger single-particle basis. We need thus approximative methods that sum specific correlations to infinite order.

Popular methods are

- Many-body perturbation theory (in essence a Taylor expansion)
- Coupled cluster theory (coupled non-linear equations)
- Green's function approaches (matrix inversion)
- Similarity group transformation methods (coupled ordinary differential equations

All these methods start normally with a Hartree-Fock basis as the calculational basis.

8.4.4 Building a many-body basis

Here we will discuss how we can set up a single-particle basis which we can use in the various parts of our projects, from the simple pairing model to infinite nuclear matter. We will use here the simple pairing model to illustrate in particular how to set up a single-particle basis. We will also use this do discuss standard FCI approaches like:

1. Standard shell-model basis in one or two major shells
2. Full CI in a given basis and no truncations
3. CISD and CISDT approximations
4. No-core shell model and truncation in excitation energy

An important step in an FCI code is to construct the many-body basis.

While the formalism is independent of the choice of basis, the **effectiveness** of a calculation will certainly be basis dependent.

Furthermore there are common conventions useful to know.

First, the single-particle basis has angular momentum as a good quantum number. You can imagine the single-particle wavefunctions being generated by a one-body Hamiltonian, for example a harmonic oscillator. Modifications include harmonic oscillator plus spin-orbit splitting, or self-consistent mean-field potentials, or the Woods-Saxon potential which mocks up the self-consistent mean-field. For nuclei, the harmonic oscillator, modified by spin-orbit splitting, provides a useful language for describing single-particle states.

Each single-particle state is labeled by the following quantum numbers:

- Orbital angular momentum l
- Intrinsic spin s = 1/2 for protons and neutrons
- Angular momentum $j = l \pm 1/2$
- z-component j_z (or m)
- Some labeling of the radial wavefunction, typically n the number of nodes in the radial wavefunction, but in the case of harmonic oscillator one can also use the principal quantum number N, where the harmonic oscillator energy is $(N+3/2)\hbar\omega$. For our nuclear matter projects, you will need to change the quantum numbers to those relevant for calculations

in three-dimensional cartesian basis, see the relevante lectures.

In this format one labels states by $n(l)_j$, with (l) replaced by a letter: s for $l = 0$, p for $l = 1$, d for $l = 2$, f for $l = 3$, and thenceforth alphabetical.

In practice the single-particle space has to be severely truncated. This truncation is typically based upon the single-particle energies, which is the effective energy from a mean-field potential.

Sometimes we freeze the core and only consider a valence space. For example, one may assume a frozen ^{4}He core, with two protons and two neutrons in the $0s_{1/2}$ shell, and then only allow active particles in the $0p_{1/2}$ and $0p_{3/2}$ orbits.

Another example is a frozen ^{16}O core, with eight protons and eight neutrons filling the $0s_{1/2}$, $0p_{1/2}$ and $0p_{3/2}$ orbits, with valence particles in the $0d_{5/2}, 1s_{1/2}$ and $0d_{3/2}$ orbits.

Sometimes we refer to nuclei by the valence space where their last nucleons go. So, for example, we call ^{12}C a p-shell nucleus, while ^{26}Al is an sd-shell nucleus and ^{56}Fe is a pf-shell nucleus.

There are different kinds of truncations.

- For example, one can start with 'filled' orbits (almost always the lowest), and then allow one, two, three... particles excited out of those filled orbits. These are called 1p-1h, 2p-2h, 3p-3h excitations.
- Alternately, one can state a maximal orbit and allow all possible configurations with particles occupying states up to that maximum. This is called *full configuration*.
- Finally, for particular use in nuclear physics, there is the *energy* truncation, also called the $N\hbar\Omega$ or N_{max} truncation.

Here one works in a harmonic oscillator basis, with each major oscillator shell assigned a principal quantum number $N = 0, 1, 2, 3, ...$ The $N\hbar\Omega$ or N_{max} truncation: Any configuration is

given an noninteracting energy, which is the sum of the single-particle harmonic oscillator energies. (Thus this ignores spin-orbit splitting.)

Excited state are labeled relative to the lowest configuration by the number of harmonic oscillator quanta.

This truncation is useful because if one includes *all* configuration up to some N_{max}, and has a translationally invariant interaction, then the intrinsic motion and the center-of-mass motion factor. In other words, we can know exactly the center-of-mass wavefunction.

In almost all cases, the many-body Hamiltonian is rotationally invariant. This means it commutes with the operators $\hat{J}^2, \hat{J}_z$ and so eigenstates will have good J, M. Furthermore, the eigenenergies do not depend upon the orientation M.

Therefore we can choose to construct a many-body basis which has fixed M; this is called an M-scheme basis.

Alternately, one can construct a many-body basis which has fixed J, or a J-scheme basis.

The Hamiltonian matrix will have smaller dimensions (a factor of 10 or more) in the J-scheme than in the M-scheme. On the other hand, as we'll show in the next slide, the M-scheme is very easy to construct with Slater determinants, while the J-scheme basis states, and thus the matrix elements, are more complicated, almost always being linear combinations of M-scheme states. J-scheme bases are important and useful, but we'll focus on the simpler M-scheme.

The quantum number m is additive (because the underlying group is Abelian): if a Slater determinant $\hat{a}_i^\dagger \hat{a}_j^\dagger \hat{a}_k^\dagger \ldots |0\rangle$ is built from single-particle states all with good m, then the total

$$M = m_i + m_j + m_k + \ldots$$

This is *not* true of J, because the angular momentum group SU(2) is not Abelian.

The upshot is that

- It is easy to construct a Slater determinant with good total M;
- It is trivial to calculate M for each Slater determinant;
- So it is easy to construct an M-scheme basis with fixed total M.

Note that the individual M-scheme basis states will *not*, in general, have good total J. Because the Hamiltonian is rotationally invariant, however, the eigenstates will have good J. (The situation is muddied when one has states of different J that are nonetheless degenerate.)

Example: two $j = 1/2$ orbits

Index	n	l	j	m_j
1	0	0	1/2	-1/2
2	0	0	1/2	1/2
3	1	0	1/2	-1/2
4	1	0	1/2	1/2

Note that the order is arbitrary. There are $\binom{4}{2} = 6$ two-particle states, which we list with the total M:

Occupied	M
1,2	0
1,3	-1
1,4	0
2,3	0
2,4	1
3,4	0

and 1 each with $M = \pm 1$.

As another example, consider using only single particle states from the $0d_{5/2}$ space. They have the following quantum numbers

Index	n	l	j	m_j
1	0	2	5/2	-5/2
2	0	2	5/2	-3/2
3	0	2	5/2	-1/2
4	0	2	5/2	1/2
5	0	2	5/2	3/2
6	0	2	5/2	5/2

There are $\binom{6}{2} = 15$ two-particle states, which we list with the total M:

Occupied	M	Occupied	M	Occupied	M
1,2	-4	2,3	-2	3,5	1
1,3	-3	2,4	-1	3,6	2
1,4	-2	2,5	0	4,5	2
1,5	-1	2,6	1	4,6	3
1,6	0	3,4	0	5,6	4

8.5 Many-body perturbation theory

8.5.1 Many-body perturbation theory

We assume here that we are only interested in the ground state of the system and expand the exact wave function in term of a series of Slater determinants

$$|\Psi_0\rangle = |\Phi_0\rangle + \sum_{m=1}^{\infty} C_m |\Phi_m\rangle,$$

where we have assumed that the true ground state is dominated by the solution of the unperturbed problem, that is

$$\hat{H}_0|\Phi_0\rangle = W_0|\Phi_0\rangle.$$

The state $|\Psi_0\rangle$ is not normalized, rather we have used an intermediate normalization $\langle\Phi_0|\Psi_0\rangle = 1$ since we have $\langle\Phi_0|\Phi_0\rangle = 1$.

The Schroedinger equation is

$$\hat{H}|\Psi_0\rangle = E|\Psi_0\rangle,$$

and multiplying the latter from the left with $\langle\Phi_0|$ gives

$$\langle\Phi_0|\hat{H}|\Psi_0\rangle = E\langle\Phi_0|\Psi_0\rangle = E,$$

and subtracting from this equation

$$\langle\Psi_0|\hat{H}_0|\Phi_0\rangle = W_0\langle\Psi_0|\Phi_0\rangle = W_0,$$

and using the fact that the both operators $\hat{H}$ and $\hat{H}_0$ are hermitian results in

$$\Delta E = E - W_0 = \langle\Phi_0|\hat{H}_I|\Psi_0\rangle,$$

which is an exact result. We call this quantity the correlation energy.

This equation forms the starting point for all perturbative derivations. However, as it stands it represents nothing but a mere formal rewriting of Schroedinger's equation and is not of much practical use. The exact wave function $|\Psi_0\rangle$ is unknown. In order to obtain a perturbative expansion, we need to expand the exact wave function in terms of the interaction $\hat{H}_I$.

Here we have assumed that our model space defined by the operator $\hat{P}$ is one-dimensional, meaning that

$$\hat{P} = |\Phi_0\rangle\langle\Phi_0|,$$

and

$$\hat{Q} = \sum_{m=1}^{\infty} |\Phi_m\rangle\langle\Phi_m|.$$

We can thus rewrite the exact wave function as

$$|\Psi_0\rangle = (\hat{P}+\hat{Q})|\Psi_0\rangle = |\Phi_0\rangle + \hat{Q}|\Psi_0\rangle.$$

Going back to the Schrödinger equation, we can rewrite it as, adding and a subtracting a term $\omega|\Psi_0\rangle$ as

$$\left(\omega - \hat{H}_0\right)|\Psi_0\rangle = \left(\omega - E + \hat{H}_I\right)|\Psi_0\rangle,$$

where ω is an energy variable to be specified later.

We assume also that the resolvent of $\left(\omega - \hat{H}_0\right)$ exits, that is it has an inverse which defined the unperturbed Green's function as

$$\left(\omega - \hat{H}_0\right)^{-1} = \frac{1}{\left(\omega - \hat{H}_0\right)}.$$

We can rewrite Schroedinger's equation as

$$|\Psi_0\rangle = \frac{1}{\omega - \hat{H}_0}\left(\omega - E + \hat{H}_I\right)|\Psi_0\rangle,$$

and multiplying from the left with $\hat{Q}$ results in

$$\hat{Q}|\Psi_0\rangle = \frac{\hat{Q}}{\omega - \hat{H}_0}\left(\omega - E + \hat{H}_I\right)|\Psi_0\rangle,$$

which is possible since we have defined the operator $\hat{Q}$ in terms of the eigenfunctions of $\hat{H}$.

These operators commute meaning that

$$\hat{Q}\frac{1}{\left(\omega - \hat{H}_0\right)}\hat{Q} = \hat{Q}\frac{1}{\left(\omega - \hat{H}_0\right)} = \frac{\hat{Q}}{\left(\omega - \hat{H}_0\right)}.$$

With these definitions we can in turn define the wave function as

$$|\Psi_0\rangle = |\Phi_0\rangle + \frac{\hat{Q}}{\omega - \hat{H}_0}\left(\omega - E + \hat{H}_I\right)|\Psi_0\rangle.$$

This equation is again nothing but a formal rewrite of Schrödinger's equation and does not represent a practical calculational scheme. It is a non-linear equation in two unknown quantities, the energy E and the exact wave function $|\Psi_0\rangle$. We can however start with a guess for $|\Psi_0\rangle$ on the right hand side of the last equation.

The most common choice is to start with the function which is expected to exhibit the largest overlap with the wave function we are searching after, namely $|\Phi_0\rangle$. This can again be inserted in the solution for $|\Psi_0\rangle$ in an iterative fashion and if we continue along these lines we end up with

$$|\Psi_0\rangle = \sum_{i=0}^{\infty}\left\{\frac{\hat{Q}}{\omega - \hat{H}_0}\left(\omega - E + \hat{H}_I\right)\right\}^i|\Phi_0\rangle,$$

for the wave function and

$$\Delta E = \sum_{i=0}^{\infty} \langle \Phi_0 | \hat{H}_I \left\{ \frac{\hat{Q}}{\omega - \hat{H}_0} \left(\omega - E + \hat{H}_I \right) \right\}^i | \Phi_0 \rangle,$$

which is now a perturbative expansion of the exact energy in terms of the interaction $\hat{H}_I$ and the unperturbed wave function $|\Psi_0\rangle$.

In our equations for $|\Psi_0\rangle$ and ΔE in terms of the unperturbed solutions $|\Phi_i\rangle$ we have still an undetermined parameter ω and a dependecy on the exact energy E. Not much has been gained thus from a practical computational point of view.

In Brilluoin-Wigner perturbation theory it is customary to set $\omega = E$. This results in the following perturbative expansion for the energy ΔE

$$\Delta E = \sum_{i=0}^{\infty} \langle \Phi_0 | \hat{H}_I \left\{ \frac{\hat{Q}}{\omega - \hat{H}_0} \left(\omega - E + \hat{H}_I \right) \right\}^i | \Phi_0 \rangle =$$

$$\langle \Phi_0 | \left(\hat{H}_I + \hat{H}_I \frac{\hat{Q}}{E - \hat{H}_0} \hat{H}_I + \hat{H}_I \frac{\hat{Q}}{E - \hat{H}_0} \hat{H}_I \frac{\hat{Q}}{E - \hat{H}_0} \hat{H}_I + \dots \right) | \Phi_0 \rangle.$$

$$\Delta E = \sum_{i=0}^{\infty} \langle \Phi_0 | \hat{H}_I \left\{ \frac{\hat{Q}}{\omega - \hat{H}_0} \left(\omega - E + \hat{H}_I \right) \right\}^i | \Phi_0 \rangle =$$

$$\langle \Phi_0 | \left(\hat{H}_I + \hat{H}_I \frac{\hat{Q}}{E - \hat{H}_0} \hat{H}_I + \hat{H}_I \frac{\hat{Q}}{E - \hat{H}_0} \hat{H}_I \frac{\hat{Q}}{E - \hat{H}_0} \hat{H}_I + \dots \right) | \Phi_0 \rangle.$$

This expression depends however on the exact energy E and is again not very convenient from a practical point of view. It can obviously be solved iteratively, by starting with a guess for E and then solve till some kind of self-consistency criterion has been reached.

Actually, the above expression is nothing but a rewrite again of the full Schrödinger equation.

Defining $e = E - \hat{H}_0$ and recalling that $\hat{H}_0$ commutes with $\hat{Q}$ by construction and that $\hat{Q}$ is an idempotent operator $\hat{Q}^2 = \hat{Q}$. Using this equation in the above expansion for ΔE we can write the denominator

$$\hat{Q} \frac{1}{\hat{e} - \hat{Q}\hat{H}_I\hat{Q}} =$$

$$\hat{Q} \left[\frac{1}{\hat{e}} + \frac{1}{\hat{e}} \hat{Q}\hat{H}_I\hat{Q} \frac{1}{\hat{e}} + \frac{1}{\hat{e}} \hat{Q}\hat{H}_I\hat{Q} \frac{1}{\hat{e}} \hat{Q}\hat{H}_I\hat{Q} \frac{1}{\hat{e}} + \dots \right] \hat{Q}.$$

Inserted in the expression for ΔE leads to

$$\Delta E = \langle \Phi_0 | \hat{H}_I + \hat{H}_I \hat{Q} \frac{1}{E - \hat{H}_0 - \hat{Q}\hat{H}_I\hat{Q}} \hat{Q}\hat{H}_I | \Phi_0 \rangle.$$

In RS perturbation theory we set $\omega = W_0$ and obtain the following expression for the energy difference

$$\Delta E = \sum_{i=0}^{\infty} \langle \Phi_0 | \hat{H}_I \left\{ \frac{\hat{Q}}{W_0 - \hat{H}_0} \left(\hat{H}_I - \Delta E \right) \right\}^i | \Phi_0 \rangle =$$

$$\langle \Phi_0 | \left(\hat{H}_I + \hat{H}_I \frac{\hat{Q}}{W_0 - \hat{H}_0} (\hat{H}_I - \Delta E) + \hat{H}_I \frac{\hat{Q}}{W_0 - \hat{H}_0} (\hat{H}_I - \Delta E) \frac{\hat{Q}}{W_0 - \hat{H}_0} (\hat{H}_I - \Delta E) + \dots \right) | \Phi_0 \rangle.$$

Recalling that $\hat{Q}$ commutes with $\hat{H}_0$ and since ΔE is a constant we obtain that

$$\hat{Q}\Delta E | \Phi_0 \rangle = \hat{Q}\Delta E | \hat{Q}\Phi_0 \rangle = 0.$$

Inserting this results in the expression for the energy results in

$$\Delta E = \langle \Phi_0 | \left(\hat{H}_I + \hat{H}_I \frac{\hat{Q}}{W_0 - \hat{H}_0} \hat{H}_I + \hat{H}_I \frac{\hat{Q}}{W_0 - \hat{H}_0} (\hat{H}_I - \Delta E) \frac{\hat{Q}}{W_0 - \hat{H}_0} \hat{H}_I + \dots \right) | \Phi_0 \rangle.$$

We can now this expression in terms of a perturbative expression in terms of $\hat{H}_I$ where we iterate the last expression in terms of ΔE

$$\Delta E = \sum_{i=1}^{\infty} \Delta E^{(i)}.$$

We get the following expression for $\Delta E^{(i)}$

$$\Delta E^{(1)} = \langle \Phi_0 | \hat{H}_I | \Phi_0 \rangle,$$

which is just the contribution to first order in perturbation theory,

$$\Delta E^{(2)} = \langle \Phi_0 | \hat{H}_I \frac{\hat{Q}}{W_0 - \hat{H}_0} \hat{H}_I | \Phi_0 \rangle,$$

which is the contribution to second order.

$$\Delta E^{(3)} = \langle \Phi_0 | \hat{H}_I \frac{\hat{Q}}{W_0 - \hat{H}_0} \hat{H}_I \frac{\hat{Q}}{W_0 - \hat{H}_0} \hat{H}_I \Phi_0 \rangle - \langle \Phi_0 | \hat{H}_I \frac{\hat{Q}}{W_0 - \hat{H}_0} \langle \Phi_0 | \hat{H}_I | \Phi_0 \rangle \frac{\hat{Q}}{W_0 - \hat{H}_0} \hat{H}_I | \Phi_0 \rangle,$$

being the third-order contribution.

8.5.2 Interpreting the correlation energy and the wave operator

In the shell-model lectures we showed that we could rewrite the exact state function for say the ground state, as a linear expansion in terms of all possible Slater determinants. That is, we define the ansatz for the ground state as

$$|\Phi_0\rangle = \left(\prod_{i \leq F} \hat{a}_i^\dagger \right) |0\rangle,$$

where the index i defines different single-particle states up to the Fermi level. We have assumed that we have N fermions. A given one-particle-one-hole ($1p1h$) state can be written as

$$|\Phi_i^a\rangle = \hat{a}_a^\dagger \hat{a}_i |\Phi_0\rangle,$$

while a $2p2h$ state can be written as

$$|\Phi_{ij}^{ab}\rangle = \hat{a}_a^\dagger \hat{a}_b^\dagger \hat{a}_j \hat{a}_i |\Phi_0\rangle,$$

and a general $ApAh$ state as

$$|\Phi_{ijk\dots}^{abc\dots}\rangle = \hat{a}_a^\dagger \hat{a}_b^\dagger \hat{a}_c^\dagger \dots \hat{a}_k \hat{a}_j \hat{a}_i |\Phi_0\rangle.$$

We use letters $ijkl\dots$ for states below the Fermi level and $abcd\dots$ for states above the Fermi level. A general single-particle state is given by letters $pqrs\dots$.

We can then expand our exact state function for the ground state as

$$|\Psi_0\rangle = C_0 |\Phi_0\rangle + \sum_{ai} C_i^a |\Phi_i^a\rangle + \sum_{abij} C_{ij}^{ab} |\Phi_{ij}^{ab}\rangle + \dots = (C_0 + \hat{C}) |\Phi_0\rangle,$$

where we have introduced the so-called correlation operator

$$\hat{C} = \sum_{ai} C_i^a \hat{a}_a^\dagger \hat{a}_i + \sum_{abij} C_{ij}^{ab} \hat{a}_a^\dagger \hat{a}_b^\dagger \hat{a}_j \hat{a}_i + \dots$$

Since the normalization of Ψ_0 is at our disposal and since C_0 is by hypothesis non-zero, we may arbitrarily set $C_0 = 1$ with corresponding proportional changes in all other coefficients. Using this so-called intermediate normalization we have

$$\langle \Psi_0 | \Phi_0 \rangle = \langle \Phi_0 | \Phi_0 \rangle = 1,$$

resulting in

$$|\Psi_0\rangle = (1 + \hat{C})|\Phi_0\rangle.$$

In a shell-model calculation, the unknown coefficients in $\hat{C}$ are the eigenvectors which result from the diagonalization of the Hamiltonian matrix.

How can we use perturbation theory to determine the same coefficients? Let us study the contributions to second order in the interaction, namely

$$\Delta E^{(2)} = \langle \Phi_0 | \hat{H}_I \frac{\hat{Q}}{W_0 - \hat{H}_0} \hat{H}_I | \Phi_0 \rangle.$$

The intermediate states given by $\hat{Q}$ can at most be of a $2p-2h$ nature if we have a two-body Hamiltonian. This means that second order in the perturbation theory can have $1p-1h$ and $2p-2h$ at most as intermediate states. When we diagonalize, these contributions are included to infinite order. This means that higher-orders in perturbation theory bring in more complicated correlations.

If we limit the attention to a Hartree-Fock basis, then we have that $\langle \Phi_0 | \hat{H}_I | 2p-2h \rangle$ is the only contribution and the contribution to the energy reduces to

$$\Delta E^{(2)} = \frac{1}{4} \sum_{abij} \langle ij|\hat{v}|ab\rangle \frac{\langle ab|\hat{v}|ij\rangle}{\varepsilon_i + \varepsilon_j - \varepsilon_a - \varepsilon_b}.$$

If we compare this to the correlation energy obtained from full configuration interaction theory with a Hartree-Fock basis, we found that

$$E - E_0 = \Delta E = \sum_{abij} \langle ij|\hat{v}|ab\rangle C_{ij}^{ab},$$

where the energy E_0 is the reference energy and ΔE defines the so-called correlation energy.

We see that if we set

$$C_{ij}^{ab} = \frac{1}{4} \frac{\langle ab|\hat{v}|ij\rangle}{\varepsilon_i + \varepsilon_j - \varepsilon_a - \varepsilon_b},$$

we have a perfect agreement between FCI and MBPT. However, FCI includes such $2p-2h$ correlations to infinite order. In order to make a meaningful comparison we would at least need to sum such correlations to infinite order in perturbation theory.

Summing up, we can see that

- MBPT introduces order-by-order specific correlations and we make comparisons with exact calculations like FCI
- At every order, we can calculate all contributions since they are well-known and either tabulated or calculated on the fly.
- MBPT is a non-variational theory and there is no guarantee that higher orders will improve the convergence.
- However, since FCI calculations are limited by the size of the Hamiltonian matrices to diagonalize (today's most efficient codes can attach dimensionalities of ten billion basis

states, MBPT can function as an approximative method which gives a straightforward (but tedious) calculation recipe.
- MBPT has been widely used to compute effective interactions for the nuclear shell-model.
- But there are better methods which sum to infinite order important correlations. Coupled cluster theory is one of these methods.

8.6 Coupled cluster theory

8.7 Introduction

Coester and Kummel first developed the ideas that led to coupled-cluster theory in the late 1950s. The basic idea is that the correlated wave function of a many-body system $|\Psi\rangle$ can be formulated as an exponential of correlation operators T acting on a reference state $|\Phi\rangle$

$$|\Psi\rangle = \exp\left(-\hat{T}\right)|\Phi\rangle \ .$$

We will discuss how to define the operators later in this work. This simple ansatz carries enormous power. It leads to a non-perturbative many-body theory that includes summation of ladder diagrams , ring diagrams, and an infinite-order generalization of many-body perturbation theory..

Developments and applications of coupled-cluster theory took different routes in chemistry and nuclear physics. In quantum chemistry, coupled-cluster developments and applications have proven to be extremely useful, see for example the review by Barrett and Musial as well as the recent textbook by Shavitt and Barrett. Many previous applications to nuclear physics struggled with the repulsive character of the nuclear forces and limited basis sets used in the computations. Most of these problems have been overcome during the last decade and coupled-cluster theory is one of the computational methods of preference for doing nuclear physics, with applications ranging from light nuclei to medium-heavy nuclei, see for example the recent review by Hagen, Papenbrock, Hjorth-Jensen and Dean.

8.7.1 A non-practical way of solving the eigenvalue problem

Before we proceed with the derivation of the Coupled cluster equations, let us repeat some of the arguments we presented during our FCI lectures. In our FCI discussions, we rewrote the solution of the Schroedinger equation as a set of coupled equationsin the unknown coefficients C. Let us repeat some of these arguments. To obtain the eigenstates and eigenvalues in terms of non-linear equations is not a very practical approach. However, it serves the scope of linking FCI theory with approximative solutions to the many-body problem like Coupled cluster (CC) theory

If we assume that we have a two-body operator at most, the Slater-Condon rule gives then an equation for the correlation energy in terms of C_i^a and C_{ij}^{ab} only. We get then

$$\langle\Phi_0|\hat{H}-E|\Phi_0\rangle+\sum_{ai}\langle\Phi_0|\hat{H}-E|\Phi_i^a\rangle C_i^a+\sum_{abij}\langle\Phi_0|\hat{H}-E|\Phi_{ij}^{ab}\rangle C_{ij}^{ab}=0,$$

or

$$E-E_0=\Delta E=\sum_{ai}\langle\Phi_0|\hat{H}|\Phi_i^a\rangle C_i^a+\sum_{abij}\langle\Phi_0|\hat{H}|\Phi_{ij}^{ab}\rangle C_{ij}^{ab},$$

where the energy E_0 is the reference energy and ΔE defines the so-called correlation energy. The single-particle basis functions could be the results of a Hartree-Fock calculation or just the eigenstates of the non-interacting part of the Hamiltonian.

In our notes on Hartree-Fock calculations, we have already computed the matrix $\langle\Phi_0|\hat{H}|\Phi_i^a\rangle$ and $\langle\Phi_0|\hat{H}|\Phi_{ij}^{ab}\rangle$. If we are using a Hartree-Fock basis, then the matrix elements $\langle\Phi_0|\hat{H}|\Phi_i^a\rangle = 0$ and we are left with a *correlation energy* given by

$$E - E_0 = \Delta E^{HF} = \sum_{abij}\langle\Phi_0|\hat{H}|\Phi_{ij}^{ab}\rangle C_{ij}^{ab}.$$

Inserting the various matrix elements we can rewrite the previous equation as

$$\Delta E = \sum_{ai}\langle i|\hat{f}|a\rangle C_i^a + \sum_{abij}\langle ij|\hat{v}|ab\rangle C_{ij}^{ab}.$$

This equation determines the correlation energy but not the coefficients C. We need more equations. Our next step is to set up

$$\langle\Phi_i^a|\hat{H}-E|\Phi_0\rangle + \sum_{bj}\langle\Phi_i^a|\hat{H}-E|\Phi_j^b\rangle C_j^b + \sum_{bcjk}\langle\Phi_i^a|\hat{H}-E|\Phi_{jk}^{bc}\rangle C_{jk}^{bc} + \sum_{bcdjkl}\langle\Phi_i^a|\hat{H}-E|\Phi_{jkl}^{bcd}\rangle C_{jkl}^{bcd} = 0,$$

as this equation will allow us to find an expression for the coefficents C_i^a since we can rewrite this equation as

$$\langle i|\hat{f}|a\rangle + \langle\Phi_i^a|\hat{H}|\Phi_i^a\rangle C_i^a + \sum_{bj\neq ai}\langle\Phi_i^a|\hat{H}|\Phi_j^b\rangle C_j^b + \sum_{bcjk}\langle\Phi_i^a|\hat{H}|\Phi_{jk}^{bc}\rangle C_{jk}^{bc} + \sum_{bcdjkl}\langle\Phi_i^a|\hat{H}|\Phi_{jkl}^{bcd}\rangle C_{jkl}^{bcd} = EC_i^a.$$

We see that on the right-hand side we have the energy E. This leads to a non-linear equation in the unknown coefficients. These equations are normally solved iteratively (that is we can start with a guess for the coefficients C_i^a). A common choice is to use perturbation theory for the first guess, setting thereby

$$C_i^a = \frac{\langle i|\hat{f}|a\rangle}{\varepsilon_i - \varepsilon_a}.$$

The observant reader will however see that we need an equation for C_{jk}^{bc} and C_{jkl}^{bcd} as well. To find equations for these coefficients we need then to continue our multiplications from the left with the various Φ_H^P terms.

For C_{jk}^{bc} we need then

$$\langle\Phi_{ij}^{ab}|\hat{H}-E|\Phi_0\rangle + \sum_{kc}\langle\Phi_{ij}^{ab}|\hat{H}-E|\Phi_k^c\rangle C_k^c +$$

$$\sum_{cdkl}\langle\Phi_{ij}^{ab}|\hat{H}-E|\Phi_{kl}^{cd}\rangle C_{kl}^{cd} + \sum_{cdeklm}\langle\Phi_{ij}^{ab}|\hat{H}-E|\Phi_{klm}^{cde}\rangle C_{klm}^{cde} + \sum_{cdefklmn}\langle\Phi_{ij}^{ab}|\hat{H}-E|\Phi_{klmn}^{cdef}\rangle C_{klmn}^{cdef} = 0,$$

and we can isolate the coefficients C_{kl}^{cd} in a similar way as we did for the coefficients C_i^a. A standard choice for the first iteration is to set

$$C_{ij}^{ab} = \frac{\langle ij|\hat{v}|ab\rangle}{\varepsilon_i + \varepsilon_j - \varepsilon_a - \varepsilon_b}.$$

At the end we can rewrite our solution of the Schroedinger equation in terms of n coupled equations for the coefficients C_H^P. This is a very cumbersome way of solving the equation. However, by using this iterative scheme we can illustrate how we can compute the various terms in the wave operator or correlation operator $\hat{C}$. We will later identify the calculation of the various terms C_H^P as parts of different many-body approximations to full CI. In particular,

we can relate this non-linear scheme with Coupled Cluster theory and many-body perturbation theory.

8.7.2 Summarizing FCI and bringing in approximative methods

If we can diagonalize large matrices, FCI is the method of choice since:

- It gives all eigenvalues, ground state and excited states
- The eigenvectors are obtained directly from the coefficients C_H^P which result from the diagonalization
- We can compute easily expectation values of other operators, as well as transition probabilities
- Correlations are easy to understand in terms of contributions to a given operator beyond the Hartree-Fock contribution. This is the standard approach in many-body theory.

The correlation energy is defined as, with a two-body Hamiltonian,

$$\Delta E = \sum_{ai} \langle i|\hat{f}|a\rangle C_i^a + \sum_{abij} \langle ij|\hat{v}|ab\rangle C_{ij}^{ab}.$$

The coefficients C result from the solution of the eigenvalue problem. The energy of say the ground state is then

$$E = E_{ref} + \Delta E,$$

where the so-called reference energy is the energy we obtain from a Hartree-Fock calculation, that is

$$E_{ref} = \langle \Phi_0|\hat{H}|\Phi_0\rangle.$$

However, as we have seen, even for a small case like the four first major shells and a nucleus like oxygen-16, the dimensionality becomes quickly intractable. If we wish to include single-particle states that reflect weakly bound systems, we need a much larger single-particle basis. We need thus approximative methods that sum specific correlations to infinite order.

Popular methods are

- Many-body perturbation theory (in essence a Taylor expansion)
- Coupled cluster theory (coupled non-linear equations)
- Green's function approaches (matrix inversion)
- Similarity group transformation methods (coupled ordinary differential equations)

All these methods start normally with a Hartree-Fock basis as the calculational basis.

8.7.3 A quick tour of Coupled Cluster theory

The ansatz for the wavefunction (ground state) is given by

$$|\Psi\rangle = |\Psi_{CC}\rangle = e^{\hat{T}}|\Phi_0\rangle = \left(\sum_{n=1}^{A} \frac{1}{n!}\hat{T}^n\right)|\Phi_0\rangle,$$

where A represents the maximum number of particle-hole excitations and $\hat{T}$ is the cluster operator defined as

$$\hat{T} = \hat{T}_1 + \hat{T}_2 + \ldots + \hat{T}_A$$
$$\hat{T}_n = \left(\frac{1}{n!}\right)^2 \sum_{\substack{i_1,i_2,\ldots i_n \\ a_1,a_2,\ldots a_n}} t_{i_1 i_2 \ldots i_n}^{a_1 a_2 \ldots a_n} a_{a_1}^\dagger a_{a_2}^\dagger \ldots a_{a_n}^\dagger a_{i_n} \ldots a_{i_2} a_{i_1}.$$

The energy is given by

$$E_{\mathrm{CC}} = \langle \Phi_0 | \overline{H} | \Phi_0 \rangle,$$

where $\overline{H}$ is a similarity transformed Hamiltonian

$$\overline{H} = e^{-\hat{T}} \hat{H}_N e^{\hat{T}}$$
$$\hat{H}_N = \hat{H} - \langle \Phi_0 | \hat{H} | \Phi_0 \rangle.$$

The coupled cluster energy is a function of the unknown cluster amplitudes $t_{i_1 i_2 \ldots i_n}^{a_1 a_2 \ldots a_n}$, given by the solutions to the amplitude equations

$$0 = \langle \Phi_{i_1 \ldots i_n}^{a_1 \ldots a_n} | \overline{H} | \Phi_0 \rangle.$$

The similarity transformed Hamiltonian $\overline{H}$ is expanded using the Baker-Campbell-Hausdorff expression,

$$\overline{H} = \hat{H}_N + \left[\hat{H}_N, \hat{T}\right] + \frac{1}{2}\left[\left[\hat{H}_N, \hat{T}\right], \hat{T}\right] + \ldots$$
$$\frac{1}{n!}\left[\ldots\left[\hat{H}_N, \hat{T}\right], \ldots \hat{T}\right] + \ldots$$

and simplified using the connected cluster theorem

$$\overline{H} = \hat{H}_N + \left(\hat{H}_N \hat{T}\right)_c + \frac{1}{2}\left(\hat{H}_N \hat{T}^2\right)_c + \cdots + \frac{1}{n!}\left(\hat{H}_N \hat{T}^n\right)_c + \ldots$$

A much used approximation is to truncate the cluster operator $\hat{T}$ at the $n = 2$ level. This defines the so-called singes and doubles approximation to the Coupled Cluster wavefunction, normally shortened to CCSD..

The coupled cluster wavefunction is now given by

$$|\Psi_{CC}\rangle = e^{\hat{T}_1 + \hat{T}_2} |\Phi_0\rangle$$

where

$$\hat{T}_1 = \sum_{ia} t_i^a a_a^\dagger a_i$$
$$\hat{T}_2 = \frac{1}{4} \sum_{ijab} t_{ij}^{ab} a_a^\dagger a_b^\dagger a_j a_i.$$

The amplutudes t play a role similar to the coefficients C in the shell-model calculations. They are obtained by solving a set of non-linear equations similar to those discussed above in connection withe FCI discussion.

If we truncate our equations at the CCSD level, it corresponds to performing a transformation of the Hamiltonian matrix of the following type for a six particle problem (with a two-body Hamiltonian):

	$0p-0h$	$1p-1h$	$2p-2h$	$3p-3h$	$4p-4h$	$5p-5h$	$6p-6h$
$0p-0h$	$\tilde{x}$	$\tilde{x}$	$\tilde{x}$	0	0	0	0
$1p-1h$	0	$\tilde{x}$	$\tilde{x}$	$\tilde{x}$	0	0	0
$2p-2h$	0	$\tilde{x}$	$\tilde{x}$	$\tilde{x}$	$\tilde{x}$	0	0
$3p-3h$	0	$\tilde{x}$	$\tilde{x}$	$\tilde{x}$	$\tilde{x}$	$\tilde{x}$	0
$4p-4h$	0	0	$\tilde{x}$	$\tilde{x}$	$\tilde{x}$	$\tilde{x}$	$\tilde{x}$
$5p-5h$	0	0	0	$\tilde{x}$	$\tilde{x}$	$\tilde{x}$	$\tilde{x}$
$6p-6h$	0	0	0	0	$\tilde{x}$	$\tilde{x}$	$\tilde{x}$

In our FCI discussion the correlation energy is defined as, with a two-body Hamiltonian,

$$\Delta E = \sum_{ai} \langle i|\hat{f}|a\rangle C_i^a + \sum_{abij} \langle ij|\hat{v}|ab\rangle C_{ij}^{ab}.$$

In Coupled cluster theory it becomes (irrespective of level of truncation of T)

$$\Delta E = \sum_{ai} \langle i|\hat{f}|a\rangle t_i^a + \sum_{abij} \langle ij|\hat{v}|ab\rangle t_{ij}^{ab}.$$

Coupled cluster theory has several interesting computational features and is the method of choice in quantum chemistry. The method was originally proposed by Coester and Kummel, two nuclear physicists (way back in the fifties). It came back in full strength in nuclear physics during the last decade.

There are several interesting features:

- With a truncation like CCSD or CCSDT, we can include to infinite order correlations like $2p-2h$.
- We can include a large basis of single-particle states, not possible in standard FCI calculations

However, Coupled Cluster theory is

- non-variational
- if we want to find properties of excited states, additional calculations via for example equation of motion methods are needed
- if correlations are strong, a single-reference ansatz may not be the best starting point
- we cannot quantify properly the error we make when truncations are made in the cluster operator

8.7.4 The CCD approximation

We will now approximate the cluster operator $\hat{T}$ to include only $2p-2h$ correlations. This leads to the so-called CCD approximation, that is

$$\hat{T} \approx \hat{T}_2 = \frac{1}{4} \sum_{abij} t_{ij}^{ab} a_a^\dagger a_b^\dagger a_j a_i,$$

meaning that we have

$$|\Psi_0\rangle \approx |\Psi_{CCD}\rangle = \exp\left(\hat{T}_2\right)|\Phi_0\rangle.$$

Inserting these equations in the expression for the computation of the energy we have, with a Hamiltonian defined with respect to a general vacuum (see the exercises in the second quantization part)

$$\hat{H} = \hat{H}_N + E_{\text{ref}},$$

with

$$\hat{H}_N = \sum_{pq} \langle p|\hat{f}|q\rangle a_p^\dagger a_q + \frac{1}{4}\sum_{pqrs}\langle pq|\hat{v}|rs\rangle a_p^\dagger a_q^\dagger a_s a_r,$$

we obtain that the energy can be written as

$$\langle \Phi_0|\exp-\left(\hat{T}_2\right)\hat{H}_N\exp\left(\hat{T}_2\right)|\Phi_0\rangle = \langle\Phi_0|\hat{H}_N(1+\hat{T}_2)|\Phi_0\rangle = E_{CCD}.$$

This quantity becomes

$$E_{CCD} = E_{\rm ref} + \frac{1}{4}\sum_{abij}\langle ij|\hat{v}|ab\rangle t_{ij}^{ab},$$

where the latter is the correlation energy from this level of approximation of CC theory. Similarly, the expression for the amplitudes reads

$$\langle \Phi_{ij}^{ab}|\exp-\left(\hat{T}_2\right)\hat{H}_N\exp\left(\hat{T}_2\right)|\Phi_0\rangle = 0.$$

These equations can be reduced to (after several applications of Wick's theorem) to, for all $i>j$ and all $a>b$,

$$\begin{aligned}
0 = \langle ab|\hat{v}|ij\rangle + (\varepsilon_a+\varepsilon_b-\varepsilon_i-\varepsilon_j)t_{ij}^{ab} \\
+\frac{1}{2}\sum_{cd}\langle ab|\hat{v}|cd\rangle t_{ij}^{cd} + \frac{1}{2}\sum_{kl}\langle kl|\hat{v}|ij\rangle t_{kl}^{ab} + \hat{P}(ij|ab)\sum_{kc}\langle kb|\hat{v}|cj\rangle t_{ik}^{ac} \\
+\frac{1}{4}\sum_{klcd}\langle kl|\hat{v}|cd\rangle t_{ij}^{cd}t_{kl}^{ab} + \hat{P}(ij)\sum_{klcd}\langle kl|\hat{v}|cd\rangle t_{ik}^{ac}t_{jl}^{bd} \\
-\frac{1}{2}\hat{P}(ij)\sum_{klcd}\langle kl|\hat{v}|cd\rangle t_{ik}^{dc}t_{lj}^{ab} - \frac{1}{2}\hat{P}(ab)\sum_{klcd}\langle kl|\hat{v}|cd\rangle t_{lk}^{ac}t_{ij}^{db},
\end{aligned} \tag{8.51}$$

where we have defined

$$\hat{P}(ab) = 1-\hat{P}_{ab},$$

where $\hat{P}_{ab}$ interchanges two particles occupying the quantum numbers a and b. The operator $\hat{P}(ij|ab)$ is defined as

$$\hat{P}(ij|ab) = (1-\hat{P}_{ij})(1-\hat{P}_{ab}).$$

Recall also that the unknown amplitudes t_{ij}^{ab} represent anti-symmetrized matrix elements, meaning that they obey the same symmetry relations as the two-body interaction, that is

$$t_{ij}^{ab} = -t_{ji}^{ab} = -t_{ij}^{ba} = t_{ji}^{ba}.$$

The two-body matrix elements are also anti-symmetrized, meaning that

$$\langle ab|\hat{v}|ij\rangle = -\langle ab|\hat{v}|ji\rangle = -\langle ba|\hat{v}|ij\rangle = \langle ba|\hat{v}|ji\rangle.$$

The non-linear equations for the unknown amplitudes t_{ij}^{ab} are solved iteratively. We discuss the implementation of these equations below.

Approximations to the full CCD equations.

It is useful to make approximations to the equations for the amplitudes. The standard method for solving these equations is to set up an iterative scheme where method's like Newton's method or similar root searching methods are used to find the amplitudes. Itreative solvers need a guess for the amplitudes. A good starting point is to use the correlated wave operator from perturbation theory to first order in the interaction. This means that we define the zeroth

approximation to the amplitudes as

$$t^{(0)} = \frac{\langle ab|\hat{v}|ij\rangle}{(\varepsilon_i + \varepsilon_j - \varepsilon_a - \varepsilon_b)},$$

leading to our first approximation for the correlation energy at the CCD level to be equal to second-order perturbation theory without $1p-1h$ excitations, namely

$$\Delta E^{(0)}_{\mathrm{CCD}} = \frac{1}{4}\sum_{abij}\frac{\langle ij|\hat{v}|ab\rangle\langle ab|\hat{v}|ij\rangle}{(\varepsilon_i + \varepsilon_j - \varepsilon_a - \varepsilon_b)}.$$

With this starting point, we are now ready to solve Eq. (8.51) iteratively. Before we attack the full equations, it is however instructive to study a truncated version of the equations. We will first study the following approximation where we take away all terms except the linear terms that involve the single-particle energies and the the two-particle intermediate excitations, that is

$$0 = \langle ab|\hat{v}|ij\rangle + (\varepsilon_a + \varepsilon_b - \varepsilon_i - \varepsilon_j)t^{ab}_{ij} + \frac{1}{2}\sum_{cd}\langle ab|\hat{v}|cd\rangle t^{cd}_{ij}. \tag{8.52}$$

Setting the single-particle energies for the hole states equal to an energy variable $\omega = \varepsilon_i + \varepsilon_j$, Eq. (8.52) reduces to the well-known equations for the so-called G-matrix, widely used in infinite matter and finite nuclei studies. The equation can then be reordered and solved by matrix inversion. To see this let us define the following quantity

$$\tau^{ab}_{ij} = (\omega - \varepsilon_a - \varepsilon_b)t^{ab}_{ij},$$

and inserting

$$1 = \frac{(\omega - \varepsilon_c - \varepsilon_d)}{(\omega - \varepsilon_c - \varepsilon_d)},$$

in the intermediate sums over cd in Eq. (8.52), we can rewrite the latter equation as

$$\tau^{ab}_{ij}(\omega) = \langle ab|\hat{v}|ij\rangle + \frac{1}{2}\sum_{cd}\langle ab|\hat{v}|cd\rangle\frac{1}{\omega - \varepsilon_c - \varepsilon_d}\tau^{cd}_{ij}(\omega),$$

where we have indicated an explicit energy dependence. This equation, transforming a two-particle configuration into a single index, can be transformed into a matrix inversion problem. Solving the equations for a fixed energy ω allows us to compare directly with results from Green's function theory when only two-particle intermediate states are included.

To solve Eq. (8.52), we would thus start with a guess for the unknown amplitudes, typically using the wave operator defined by first order in perturbation theory, leading to a zeroth approximation to the energy given by second-order perturbation theory for the correlation energy. A simple approach to the solution of Eq. (8.52), is to thus to

1. Start with a guess for the amplitudes and compute the zeroth approximation to the correlation energy
2. Use the ansatz for the amplitudes to solve Eq. (8.52) via for example your root-finding method of choice (Newton's method or modifications thereof can be used) and continue these iterations till the correlation energy does not change more than a prefixed quantity λ; $\Delta E^{(i)}_{\mathrm{CCD}} - \Delta E^{(i-1)}_{\mathrm{CCD}} \leq \lambda$.
3. It is common during the iterations to scale the amplitudes with a parameter α, with $\alpha \in (0,1]$ as $t^{(i)} = \alpha t^{(i)} + (1-\alpha)t^{(i-1)}$.

The next approximation is to include the two-hole term in Eq. (8.51), a term which allow us to make a link with Green's function theory with two-particle and two-hole correlations. This

means that we solve

$$0 = \langle ab|\hat{v}|ij\rangle + (\varepsilon_a + \varepsilon_b - \varepsilon_i - \varepsilon_j)\, t_{ij}^{ab} + \frac{1}{2}\sum_{cd}\langle ab|\hat{v}|cd\rangle t_{ij}^{cd} + \frac{1}{2}\sum_{kl}\langle kl|\hat{v}|ij\rangle t_{kl}^{ab}. \tag{8.53}$$

This equation is solved the same way as we would do for Eq. (8.52). The final step is then to include all terms in Eq. (8.51).

8.8 Developing a numerical project

This section will focus on writing a working CCD code from scratch. If you are familiar with writing quantum many-body physics codes, feel free to skip ahead as we are going to go into some detail about implementing CCD as a computer code now. As we saw earlier, the CCD equations can be written as

$$\begin{aligned}(\varepsilon_i + \varepsilon_j - \varepsilon_a - \varepsilon_b)\, t_{ij}^{ab} &= \langle ab|\hat{v}|ij\rangle \\ &+ \frac{1}{2}\sum_{cd}\langle ab|\hat{v}|cd\rangle t_{ij}^{cd} + \frac{1}{2}\sum_{kl}\langle kl|\hat{v}|ij\rangle t_{kl}^{ab} + \hat{P}(ij|ab)\sum_{kc}\langle kb|\hat{v}|cj\rangle t_{ik}^{ac} \\ &+ \frac{1}{4}\sum_{klcd}\langle kl|\hat{v}|cd\rangle t_{ij}^{cd} t_{kl}^{ab} + \hat{P}(ij)\sum_{klcd}\langle kl|\hat{v}|cd\rangle t_{ik}^{ac} t_{jl}^{bd} \\ &- \frac{1}{2}\hat{P}(ij)\sum_{klcd}\langle kl|\hat{v}|cd\rangle t_{ik}^{dc} t_{lj}^{ab} - \frac{1}{2}\hat{P}(ab)\sum_{klcd}\langle kl|\hat{v}|cd\rangle t_{lk}^{ac} t_{ij}^{db},\end{aligned} \tag{8.54}$$

for all $i < j$ and all $a < b$, using the standard notation that $a, b, \ldots$ are particle states and $i, j, \ldots$ are hole states. With the CCD correlation energy given by

$$\Delta E_{CCD} = \frac{1}{4}\sum_{ijab}\langle ij|\hat{v}|ab\rangle\, t_{ij}^{ab}. \tag{8.55}$$

One way to solve these equations, is to write equation (8.54) as a series of iterative nonlinear algebraic equations.

$$\begin{aligned}t_{ij}^{ab(n+1)} &= \frac{1}{\varepsilon_{ij}^{ab}}\Bigg(\langle ab|\hat{v}|ij\rangle \\ &+ \frac{1}{2}\sum_{cd}\langle ab|\hat{v}|cd\rangle t_{ij}^{cd(n)} + \frac{1}{2}\sum_{kl}\langle kl|\hat{v}|ij\rangle t_{kl}^{ab(n)} + \hat{P}(ij|ab)\sum_{kc}\langle kb|\hat{v}|cj\rangle t_{ik}^{ac(n)} \\ &+ \frac{1}{4}\sum_{klcd}\langle kl|\hat{v}|cd\rangle t_{ij}^{cd(n)} t_{kl}^{ab(n)} + \hat{P}(ij)\sum_{klcd}\langle kl|\hat{v}|cd\rangle t_{ik}^{ac(n)} t_{jl}^{bd(n)} \\ &- \frac{1}{2}\hat{P}(ij)\sum_{klcd}\langle kl|\hat{v}|cd\rangle t_{ik}^{dc(n)} t_{lj}^{ab(n)} - \frac{1}{2}\hat{P}(ab)\sum_{klcd}\langle kl|\hat{v}|cd\rangle t_{lk}^{ac(n)} t_{ij}^{db(n)}\Bigg),\end{aligned} \tag{8.56}$$

for all $i < j$ and all $a < b$, where $\varepsilon_{ij}^{ab} = (\varepsilon_i + \varepsilon_j - \varepsilon_a - \varepsilon_b)$, and $t_{ij}^{ab(n)}$ is the t amplitude for the nth iteration of the series. This way, given some starting guess $t_{ij}^{ab(0)}$, we can generate subsequent t amplitudes that converges to some value. Discussion of the mathematical details regarding convergence will be tabled for later; for now we will talk about implementing these equations into a computer program and assume convergence. In pseudocode, the function that updates the t amplitudes looks like

```
CCD_Update()
for i ∈ {0, N_fermi − 1} do
```

```
for j ∈ {0, N_fermi − 1} do
    for a ∈ {N_fermi, N_sp − 1} do
        for b ∈ {N_fermi, N_sp − 1} do
            sum ← TBME[index(a, b, i, j)]
            for c ∈ {N_fermi, N_sp − 1} do
                for d ∈ {N_fermi, N_sp − 1} do
                    sum ← sum + 0.5 ∗ ME[index(a, b, c, d)] ∗ t_amplitudes_old[index(c, d, i, j)]
                end for
            end for
            ...
            sum ← sum + (all other terms)
            ...
            energy_denom = SP_energy[i]+SP_energy[j]-SP_energy[a]-SP_energy[b]
            t_amplitudes[index(a, b, i, j)] = sum/energy_denom
        end for
    end for
end for
end for
```

Where N_{fermi} is the fermi level and N_{sp} is the total number of single particle (s.p.) states, indexed from 0 to $N_{sp}-1$. At the most basic level, the CCD equations are just the addition of many products containing t_{ij}^{ab} amplitudes and two-body matrix elements (TBMEs) $\langle ij|\hat{v}|ab\rangle$, so a lot of care should be placed into how we store these objects. These are both objects with four indices, so a sensible first implementation of the CCD equations would be to create two 4-D arrays to store the objects. However, it is often more convenient to work with simple 1-D arrays instead. *index*() is a function that maps the four indices onto one index so that a 1-D array can be used. An example of such a function is:

```
function index(p, q, r, s)
    return p ∗ N_sp^3 + q ∗ N_sp^2 + r ∗ N_sp + s
end function
```

Because elements with repeated indices vanish, $t_{ii}^{ab} = t_{ij}^{aa} = 0$ and $\langle pp|\hat{v}|rs\rangle = \langle pq|\hat{v}|rr\rangle = 0$, data structures using this index function will contain many elements that are automatically zero, so we will discuss more efficient storage strategies later. Notice also that we are looping over all i, j, a, b, rather than the restricted indices. This means that we are doing redundant work, but it is simpler to code up, and we will want to unrestrict these indices later anyways.

The goal of this code is to calculate the correlation energy, ΔE_{CCD}, so after each iteration of our equation, we use our newest t amplitudes to update this value,

$$\Delta E_{CCD}^{(n)} = \frac{1}{4}\sum_{ijab}\langle ij|\hat{v}|ab\rangle\, t_{ij}^{ab(n)}. \tag{8.57}$$

We check that our result is converged by checking that to see if the most recent iteration has changed the correlation energy by less than some tolerance threshold η,

$$\eta > |\Delta E_{CCD}^{(n+1)} - \Delta E_{CCD}^{(n)}|. \tag{8.58}$$

The basic structure of the iterative process will look like:

```
while (abs(energy_Diff) > tolerance) do
    CCD_Update()
    correlation_Energy ← CCD_Corr_Energy()
    energy_Diff ← correlation_Energy - correlation_Energy_old
    correlation_Energy_old ← correlation_Energy
```

t_amplitudes_old ← t_amplitudes
end while

Prior to this algorithm, the t amplitudes should be initalized, $t_{ij}^{ab(0)}$. A particularly convenient choice is to set $t_{ij}^{ab(0)} = 0$. Notice that if this starting point is used, then

$$t_{ij}^{ab(1)} = \frac{\langle ab|\hat{v}|ij\rangle}{\varepsilon_{ij}^{ab}} \tag{8.59}$$

$$\Delta E_{CCD}^{(1)} = \frac{1}{4}\sum_{ijab}\frac{\langle ab|\hat{v}|ij\rangle}{\varepsilon_{ij}^{ab}}, \tag{8.60}$$

which is the result from MBPT2. This is a useful, as one iteration of the CCD equations can be ran, and checked against MBPT2 to give some confidence that everything is working so far. To check that everything is working, it is useful to run the code using a minimal example. A simple pairing model Hamiltonian is a nice place to start.

$$\hat{H}_0 = \xi\sum_{p\sigma}(p-1)a_{p\sigma}^{\dagger}a_{p\sigma} \tag{8.61}$$

$$\hat{V} = -\frac{1}{2}g\sum_{pq}a_{p+}^{\dagger}a_{p-}^{\dagger}a_{q-}a_{q+} \tag{8.62}$$

which represents a basic pairing model with p levels each with a spin degeneracy of 2. The form of the coupled cluster equations in (Eq) uses single-particle states that are eigenstates of the Hartree-Fock operator, $(\hat{u}+\hat{u}_{\rm HF}|p\rangle = \varepsilon_p|p\rangle$. In the pairing model, this condition is already fulfilled. All we have to do is define the lowest N_{fermi} states as holes then redefine the single-particle energies,

$$\varepsilon_q = h_{qq} + \sum_i \langle qi||qi\rangle\,. \tag{8.63}$$

To be more specific, let's look at this pairing model with 4 particles and 8 single-particle states. These states (with $\xi = 1.0$) could be labeled as such with

State Label	p	$2s_z$	E	type
0	1	1	-g/2	hole
1	1	-1	-g/2	hole
2	2	1	1-g/2	hole
3	2	-1	1-g/2	hole
4	3	1	2	particle
5	3	-1	2	particle
6	4	1	3	particle
7	4	-1	3	particle

Here are some more results for specific values of g that can be used for benchmarking.

g	E_{ref}	ΔE_{MBPT2}	ΔE_{CCD}
-1.0	3	-0.46667	-0.21895*
-0.5	2.5	-0.08874	-0.06306
0.0	2	0	0
0.5	1.5	-0.06239	-0.08336
1.0	1	-0.21905	-0.36956

The $g = -1.0$ case diverges without implementing iterative mixing. Sometimes iterative solvers run into oscillating solutions, and mixing can help the iterations break this cycle.

$$t^{(i)} = \alpha t^{(i)}_{no\_mixing} + (1-\alpha) t^{(i-1)} \tag{8.64}$$

In the case of this simple pairing model, it is easy to calculate ΔE_{MBPT2} by hand, which is useful to check the code's calcuation of this value, as well as the first CCD iteration.

$$\Delta E_{MBPT2} = \frac{1}{4}\sum_{abij} \frac{\langle ij||ab\rangle \langle ab||ij\rangle}{\varepsilon^{ab}_{ij}} = \sum_{a<b,i<j} \frac{\langle ij||ab\rangle \langle ab||ij\rangle}{\varepsilon^{ab}_{ij}} \tag{8.65}$$

For our pairing example:

$$\Delta E_{MBPT2} = \frac{\langle 01||45\rangle^2}{\varepsilon^{45}_{01}} + \frac{\langle 01||67\rangle^2}{\varepsilon^{67}_{01}} + \frac{\langle 23||45\rangle^2}{\varepsilon^{45}_{23}} + \frac{\langle 23||67\rangle^2}{\varepsilon^{67}_{23}}$$

$$\Delta E_{MBPT2} = -\frac{g^2}{4}\left(\frac{1}{4+g} + \frac{1}{6+g} + \frac{1}{2+g} + \frac{1}{4+g}\right),$$

which is a nice expression which can be used to check the results for any value of g.

Once a working pairing model has been implemented, improvements can start to be made, all the while using the pairing model to make sure that the code is still working and giving correct answers. Realistic systems will be much larger than this small pairing example.

One limitation that will be ran into while trying to do realistic CCD calculations is that of memory. The 4-indexed TBMEs and t-amplitudes have to store a lot of elements, and the size of these arrays can quite become larger than that of the available memory on the machine. If calculation wants to use 500 s.p. basis states, then a structure like $\langle pq|v|rs\rangle$ will have length 500 for each of its four indices, which means it will have $500^4 = 625 * 10^8$ elements. To get a handle on how much memory is used, consider the elements as double-precision floating point type. One double takes up 8 bytes of memory. So this array would take up $8 * 625 * 10^8$ bytes = $5000 * 10^8$ bytes = 500 Gbytes of memory. Most personal computers in 2016 have 4-8 Gbytes of RAM, so this calculation would be way out of reach. There are supercomputers that can handle applications using 500 Gbytes of memory, but we can quickly reduce the total memory required by applying some physical arguments. In addition to vanishing elements with repeated indices, mentioned above, elements that do not obey certain symmetries are also zero. Almost all realistic two-body forces preserve some quantities due to symmetries in the interaction. For example, an interaction with rotational symmetry will conserve angular momentum. This means that a two-body ket state $|rs\rangle$, which has some set of quantum numbers, will retain quantum numbers corresponding to the interaction symmetries after being acted on by $\hat{v}$. This state is then projected onto $|pq\rangle$ with its own set of quantum numbers. Thus $\langle pq|v|rs\rangle$ is only non-zero if $|pq\rangle$ and $|rs\rangle$ share the same quantum numbers that are preserved by $\hat{v}$. In addition, because the cluster operators represent excitations due to the interaction, t^{ab}_{ij} is only non-zero if $|ij\rangle$ has the same relevant quantum numbers as $|ab\rangle$.

To take advantage of this, these two-body ket states can be organized into "channels" of shared quantum numbers. In the case of the pairing model, the interaction preserves the total spin projection of a two-body state, $S_z = s_{z1} + s_{z2}$. The single particle states can have spin of +1/2 or -1/2, so there can be three two-body channels with $S_z = -1, 0, +1$. These channels can then be indexed with a unique label in a similar way to the single particle index scheme. In more complicated systems, there will be many more channels involving multiple symmetries, so it is useful to create a data structure that stores the relevant two-body quantum numbers to keep track of the labeling scheme.

Now it is more efficient to use two-dimensional array data structures, where the first index refers to the channel number and the second refers to the element withing that channel. So to access matrix elements or t amplitudes, you can loop over the channels first, then the indices within that channel. To get an idea of the savings using this block diagonal structure, let's

look at a case with a plane wave basis, with three momentum and one spin quantum numbers, with an interaction that conserves linear momentum in all three dimensions, as well as the total spin projection. Using 502 basis states, the TBME's require about 0.23 Gb of memory in block diagonal form, which is an enormous saving from the 500 Gb mentions earlier in the naïve storage scheme.

Since the calculation of all of these zeros can now be avoided, improvements in speed as memory will now follow. To get a handle on how example these CCD calculations are we need only to look at the most expensive sum in equation 8.54. This corresponds to the sum over $klcd$. Since this sum is repeated for all $i < j$ and $a < b$, that means these equations will scale as $\mathcal{O}(n_p^4 n_h^4)$. However, (as we saw earlier?), they can be rewritten using intermediates as

$$\begin{aligned} 0 = \langle ab|\hat{v}|ij\rangle + \hat{P}(ab)\sum_c \langle b|\chi|c\rangle \langle ac|t|ij\rangle - \hat{P}(ij)\sum_k \langle k|\chi|j\rangle \langle ab|t|ik\rangle \\ + \frac{1}{2}\sum_{cd} \langle ab|\chi|cd\rangle \langle cd|t|ij\rangle + \frac{1}{2}\sum_{kl} \langle ab|t|kl\rangle \langle kl|\chi|ij\rangle \\ + \hat{P}(ij)\hat{P}(ab)\sum_{kc} \langle ac|t|ik\rangle \langle kb|\chi|cj\rangle \end{aligned} \tag{8.66}$$

for all i, j, a, b, the reason why these indices are now unrestricted will be explained later. Where the intermediates χ are

$$\langle b|\chi|c\rangle = \langle b|f|c\rangle - \frac{1}{2}\sum_{kld} \langle bd|t|kl\rangle \langle kl|v|cd\rangle \tag{8.67}$$

$$\langle k|\chi|j\rangle = \langle k|f|j\rangle + \frac{1}{2}\sum_{cdl} \langle kl|v|cd\rangle \langle cd|t|jl\rangle \tag{8.68}$$

$$\langle kl|\chi|ij\rangle = \langle kl|v|ij\rangle + \frac{1}{2}\sum_{cd} \langle kl|v|cd\rangle \langle cd|t|ij\rangle \tag{8.69}$$

$$\langle kb|\chi|cj\rangle = \langle kb|v|cj\rangle + \frac{1}{2}\sum_{dl} \langle kl|v|cd\rangle \langle db|t|lj\rangle \tag{8.70}$$

$$\langle ab|\chi|cd\rangle = \langle ab|v|cd\rangle \tag{8.71}$$

Maybe demonstrate how these equations are equal here?

Now the CCD equations will scale as $\mathcal{O}(n_h^2 n_p^4)$ which is quite a bit better than before. This is of course at the cost of computing the intermediates at the beginning of each iteration, which the most expensive one, $\langle kb|\chi|cj\rangle$, will scale as $\mathcal{O}(n_h^3 n_p^3)$. To further speed these computations up, we see that these sums can be written as matrix-matrix multiplication. It is not obvious how to write all of these sums in such a way, but it is useful to first remember that to write out the multiplication of matices $\hat{C} = \hat{A} * \hat{B}$ is

$$C_{ij} = \sum_k A_{ik} * B_{kj}. \tag{8.72}$$

Notice that equation (8.69) can be written as

$$\langle K|\chi|I\rangle = \langle K|v|I\rangle + \frac{1}{2}\sum_C \langle K|v|C\rangle \langle C|t|I\rangle$$

by mapping the two index pairs $kl \to K, ij \to I, cd \to C$. So now the sum looks like a matrix-matrix multiplication. This is useful because there are packages like BLAS (Basic Linear

Algebra Subprograms) which have extremely fast implementations of matrix-matrix multiplication.

Now that we have a working CCD program, we can move on to more realistic cases. One such case is infinite nuclear matter using a plane-wave basis. These states are solutions to the free-particle Hamiltonian,

$$\frac{-\hbar^2}{2m}\nabla^2\phi(\mathbf{x}) = \varepsilon\,\phi(\mathbf{x}). \tag{8.73}$$

For a finite basis, we approximate the problem by constructing a box with sides of length L, which quantizes the momentum, and impose periodic boundary conditions in each direction.

$$\phi(x_i) = \phi(x_i + L) \tag{8.74}$$

$$\phi_{\mathbf{k}}(\mathbf{x}) = \frac{1}{\sqrt{L^3}}e^{i\mathbf{k}\cdot\mathbf{x}}, \qquad \mathbf{k} = \frac{2\pi\mathbf{n}}{L}, \qquad n_i \tag{8.75}$$

The first step in calculating infinite matter is to construct a model space by finding every single-particle state relevant to a given problem. In our case, this amounts to looping over the quantum numbers for spin, isospin, and the three momentum directions. To control the model space size, the momentum can be truncated to give a cubic space, where $n_i \leq n_{\max}$, or a spherical space, where $n_x^2 + n_y^2 + n_z^2 \leq N_{\max}$. The number of single-particle states in a cubic space increases rapidly with $n_{\max}$ compared to the spherical case with $N_{\max}$. For example, in pure neutron matter a cubic space with $n_{\max} = 3$ has 668 states while the spherical space with $N_{\max} = 17$ has 610 states. Therefore, the spherical case will be used for the rest of the calculations here. The loop increases in energy by counting the number of shells, so states can be 'filled' by labeling the first P proton and N neutron states as holes. The following loop is for pure neutron matter and requires the number of neutrons, N and density, $\rho = N/L^3$, as input. Symmetric nuclear matter requires an extra loop over isospin.

```
n = 0
for shell ∈ {0,...,N_max} do
  for −√N_max ≤ n_x ≤ √N_max do
    for −√N_max ≤ n_y ≤ √N_max do
      for −√N_max ≤ n_z ≤ √N_max do
        for s_z ∈ {−1/2, 1/2} do
          if n_x^2 + n_y^2 + n_z^2 = shell then
            Energy = 4π^2ħ^2/2m × shell
            if n < N then
              type = "hole"
            else
              type = "particle"
            end if
            STATES ← (n, n_x, n_y, n_z, s_z, Energy, type)
            n ← n + 1
          end if
        end for
      end for
    end for
  end for
end for
```

The next step is to build every two-body state in the model space and separate them by their particle/hole character and combined quantum numbers. While each single-particle state was unique, two-body states can share quantum numbers with members of a particular two-body channel. These channels allow us to remove matrix elements and cluster amplitudes that vio-

late the symmetries of the interaction and greatly reduces the size and speed of the calculation. Our structures will depend on direct two-body channels, T, where the quantum numbers are added and cross two-body channels, X, where the quantum numbers are subtracted. Before filling the channels, it's helpful to order them with an index function which returns a unique index for a given set of two-body quantum numbers. Without an index function, one has to loop over all the channels for each two-body state which adds a substantial amount of time to this algorithm. An example of an index function for the direct channels in symmetric nuclear matter is, for $N_x = n_{x,1} + n_{x,2}$, $N_y = n_{y,1} + n_{y,2}$, $N_z = n_{z,1} + n_{z,2}$, $S_z = s_{z,1} + s_{z,2}$, $T_z = t_{z,1} + t_{z,2}$, $m = 2\lfloor\sqrt{N_{\max}}\rfloor$, and $M = 2m+1$,

$$\mathrm{Ind}\left(N_x, N_y, N_z, S_z, T_z\right) = 2\left(N_x+m\right)M^3 + 2\left(N_y+m\right)M^2 + 2\left(N_z+m\right)M + 2\left(S_z+1\right) + \left(T_z+1\right). \quad (8.76)$$

This function, which can also be used for the cross-channel index function, is well suited for a cubic model space but can be applied in either case. An additional restriction for two-body states is that they must be composed of two different states to satisfy the Pauli-exclusion principle.

for sp1 $\in$ *STATES* **do**
  for sp2 $\in$ *STATES* **do**
    if $sp1 \neq sp2$ **then**
      $N_i \leftarrow n_{i,1} + n_{i,2}$
      $S_z \leftarrow s_{z,1} + s_{z,2}$
      $T_z \leftarrow t_{z,1} + t_{z,2}$
      i_dir $\leftarrow \mathrm{Ind}\left(N_x, N_y, N_z, S_z, T_z\right)$
      $T \leftarrow$ (sp1, sp2, i_dir)
      $N_i' \leftarrow n_{i,1} - n_{i,2}$
      $S_z' \leftarrow s_{z,1} - s_{z,2}$
      $T_z' \leftarrow t_{z,1} - t_{z,2}$
      i_cross $\leftarrow \mathrm{Ind}\left(N_x', N_y', N_z', S_z', T_z'\right)$
      $X \leftarrow$ (sp1, sp2, i_cross)
    end if
  end for
end for

From the cross channels, one can construct the cross channel compliments, X', where $X\left(pq\right) \equiv X'\left(qp\right)$. Also from the direct channels, one can construct one-body, and correspondint three-body, channels for each single-particle state, K by finding every combination of two two-body states within a direct channel that contains that single particle state, $T\left(pq\right) = T\left(rs\right) \Rightarrow K_p \leftarrow \left(qrs\right)$.

for Chan $\in T$ **do**
  for tb1 $\in$ Chan **do**
    for tb2 $\in$ Chan **do**
      $K \leftarrow \mathrm{tb1}_1$
      $K_{\mathrm{tb1}_1} \leftarrow \mathrm{tb1}_2, \mathrm{tb2}_1, \mathrm{tb2}_2$
    end for
  end for
end for

These different sctructures can be further categorized by a two-body state's particle-hole character, $\langle pp|t|hh\rangle, \langle hh|v|hh\rangle, \langle pp|v|pp\rangle, \langle hh|v|pp\rangle$, and $\langle hp|v|hp\rangle$, which greatly simplifies the matrix-matrix multiplications of the CCD iterations by indexing the summed variables in a systematic way. Summations are constructed by placeing two structures next to each other in such a way that the inner, summed indices are of the same channel. The resulting structure is indexed by the outer channels.

$$\langle b|\chi|c\rangle = \langle b|f|c\rangle - \frac{1}{2}\sum_{kld}\langle bd|t|kl\rangle\langle kl|v|cd\rangle \rightarrow f_c^b(K(b),K(c)) - \frac{1}{2}t_{kl}^{bd}(K(b),K_b(kld))\cdot v_{cd}^{kl}(K_c(kld),K(c)) \tag{8.77}$$

$$\langle k|\chi|j\rangle = \langle k|f|j\rangle + \frac{1}{2}\sum_{cdl}\langle kl|v|cd\rangle\langle cd|t|jl\rangle \rightarrow f_j^k(K(k),K(j)) + \frac{1}{2}v_{cd}^{kl}(K(k),K_k(cdl))\cdot t_{jl}^{cd}(K_j(cdl),K(j)) \tag{8.78}$$

$$\langle kl|\chi|ij\rangle = \langle kl|v|ij\rangle + \frac{1}{2}\sum_{cd}\langle kl|v|cd\rangle\langle cd|t|ij\rangle \rightarrow v_{ij}^{kl}(T(kl),T(ij)) + \frac{1}{2}v_{cd}^{kl}(T(kl),T(cd))\cdot t_{ij}^{cd}(T(cd),T(ij)) \tag{8.79}$$

$$\langle kb|\chi|cj\rangle = \langle kb|v|cj\rangle + \frac{1}{2}\sum_{dl}\langle kl|v|cd\rangle\langle db|t|lj\rangle \rightarrow v_{cj}^{kb}(X(kc),X(jb)) + \frac{1}{2}v_{cd}^{kl}(X(kc),X(dl))\cdot t_{lj}^{db}(X(dl),X(jb)) \tag{8.80}$$

$$\langle ab|\chi|cd\rangle = \langle ab|v|cd\rangle \rightarrow v_{cd}^{ab}(T(ab),T(cd)) \tag{8.81}$$

$$\sum_c\langle b|\chi|c\rangle\langle ac|t|ij\rangle \rightarrow \chi_c^b(K(b),K(c))\cdot t_{ij}^{ac}(K(c),K_c(ija)) \tag{8.82}$$

$$\sum_k\langle k|\chi|j\rangle\langle ab|t|ik\rangle \rightarrow \chi_j^k(K(j),K(k))\cdot t_{ik}^{ab}(K(c),K_c(ija)) \tag{8.83}$$

$$\sum_{cd}\langle ab|\chi|cd\rangle\langle cd|t|ij\rangle \rightarrow \chi_{cd}^{ab}(T(ab),T(cd))\cdot t_{ij}^{cd}(T(cd),T(ij)) \tag{8.84}$$

$$\sum_{kl}\langle ab|t|kl\rangle\langle kl|\chi|ij\rangle \rightarrow t_{kl}^{ab}(T(ab),T(kl))\cdot\chi_{ij}^{kl}(T(kl),T(ij)) \tag{8.85}$$

$$\sum_{kc}\langle ac|t|ik\rangle\langle kb|\chi|cj\rangle = \sum_{kc}\langle ai^{-1}|t|kc^{-1}\rangle\langle kc^{-1}|\chi|jb^{-1}\rangle \rightarrow t_{ik}^{ac}(X(ia),X(kc))\cdot\chi_{cj}^{kb}(X(kc),X(jb)) \tag{8.86}$$

The interaction we will use for these calculations is a semirealistic nucleon-nucleon potential known as the Minnesota potential which has the form, $V_\alpha(r) = V_\alpha e^{-\alpha r^2}$. The spin and isospin dependence of the Minnesota potential is given by,

$$V(r) = \frac{1}{2}\left(V_R + \frac{1}{2}(1+P_{12}^\sigma)V_T + \frac{1}{2}(1-P_{12}^\sigma)V_S\right)(1-P_{12}^\sigma P_{12}^\tau), \tag{8.87}$$

where $P_{12}^\sigma = \frac{1}{2}(1+\sigma_1\cdot\sigma_2)$ and $P_{12}^\tau = \frac{1}{2}(1+\tau_1\cdot\tau_2)$ are the spin and isospin exchange operators, respectively. When this potential is integrated over space, the result depends only on the magnitude of the momentum transfer, $\mathbf{q} = \frac{1}{2}(\mathbf{k}_p - \mathbf{k}_q - \mathbf{k}_r + \mathbf{k}_s)$, as well as the spin and isospin dependencies,

$$\langle pq|V_\alpha|rs\rangle = \frac{V_\alpha}{L^3}\left(\frac{\pi}{\alpha}\right)^{3/2} e^{\frac{-q^2}{4\alpha}}\delta_{\mathbf{k}_p+\mathbf{k}_q,\mathbf{k}_r+\mathbf{k}_s} \tag{8.88}$$

α	V_α	κ_α
R	200 MeV	1.487 fm^{-2}
T	178 MeV	0.639 fm^{-2}
S	91.85 MeV	0.465 fm^{-2}

We approximated our problem with periodic boundary conditions, $\phi(x_i) = \phi(x_i+L)$, but we could have chosen anti-periodic boundary conditions, $\phi(x_i) = -\phi(x_i+L)$. The difference between these two shows how the correlation energy contains finite-size effects. One solution to this problem is by integrating over solutions between periodic and anti-periodic conditions,

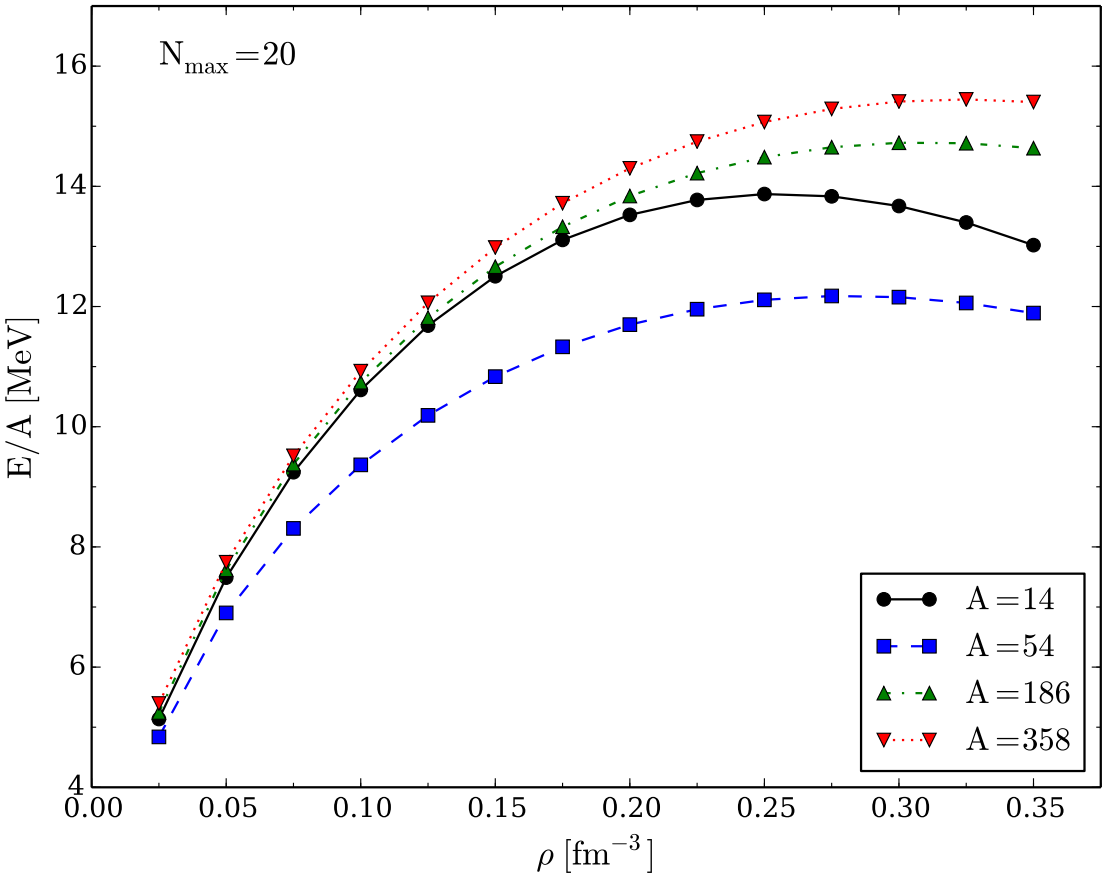

Fig. 8.1 Energy per particle of pure neutron matter computed in the CCD approximation with the Minnesota potential for different numbers of particles with $N_{max} = 20$.

known as twist-averaging. First, we multiply the single-particle states by a phase for each direction, characterized by a twist-angle, θ_i.

$$\phi_{\mathbf{k}}(\mathbf{x}+\mathbf{L}) \rightarrow e^{i\theta}\phi_{\mathbf{k}}(\mathbf{x}) \tag{8.89}$$

$\theta_i = 0$ for PBC and $\theta_i = \pi$ for APBC

$$\mathbf{k} \rightarrow \mathbf{k} + \frac{\theta}{L} \tag{8.90}$$

$$\varepsilon_{\mathbf{k}} \rightarrow \varepsilon_{\mathbf{k}} + \frac{\pi}{L}\mathbf{k}\cdot\theta + \frac{\pi^2}{L^2} \tag{8.91}$$

Adding these phases changes the single-particle energies, the correction of which disappear as $L \rightarrow \infty$, depending on θ and thus changes the shell structure so that hole states can jump up to particle states and vis a versa. So it's necessary to fill hole states separately for each θ. Integration over some quantitiy is approximated by a weighted sum, such as Gauss-Legendre quadrature, over the quantity for each set of twist angles.

Build mesh points and weights for each direction i: $\{\theta_i, w_i\}$
$E_{\text{twist}} = 0$
for $(\theta_x, w_x) \in \{\theta_x, w_x\}$ **do**
  for $(\theta_y, w_y) \in \{\theta_y, w_y\}$ **do**

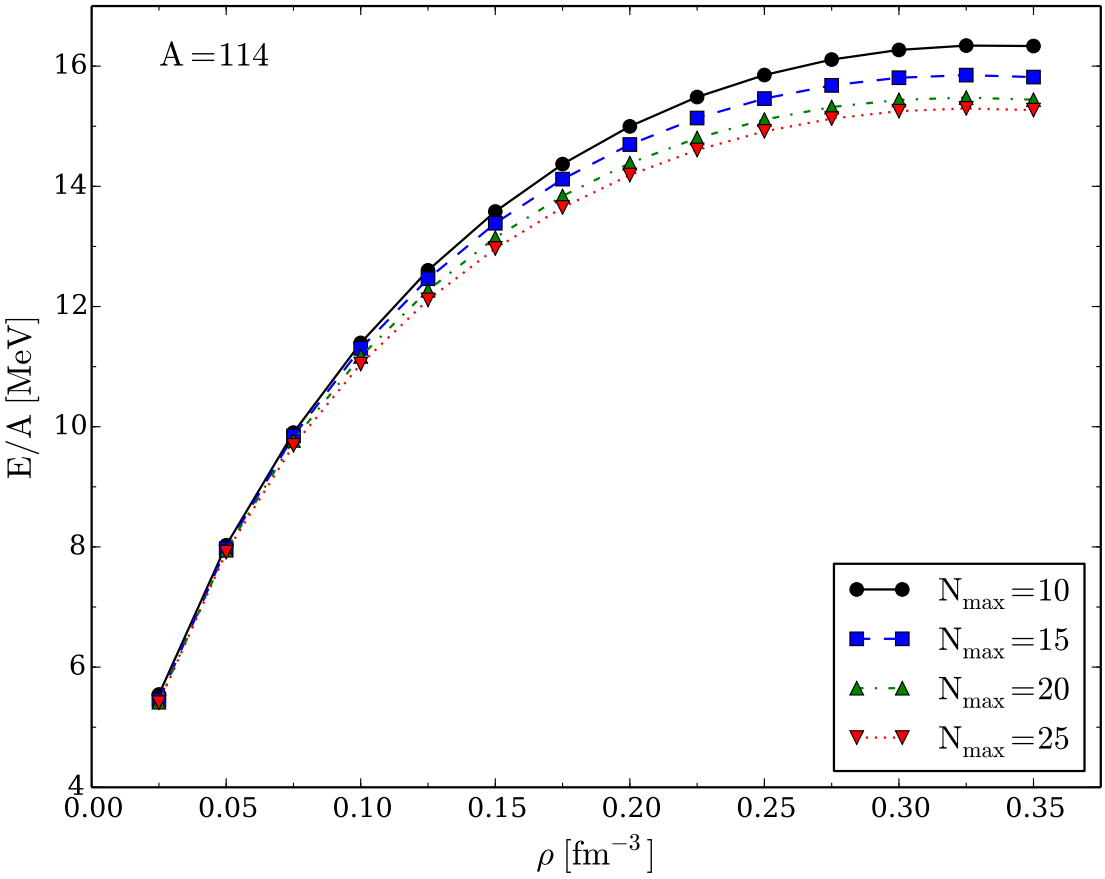

Fig. 8.2 Energy per particle of pure neutron matter computed in the CCD approximation with the Minnesota potential for different model space sizes with A = 20.

for $(\theta_z, w_z) \in \{\theta_z, w_z\}$ **do**
Build Basis States with $k_i \rightarrow k_i + \frac{\theta_i}{L}$
Order States by Energy and Fill Holes
Get Result E (T,HF,CCD)
$E_{\text{twist}} = E_{\text{twist}} + \frac{1}{\pi^3} w_x w_y w_z E$
end for
end for
end for

This technique gives results which depend much less on the particle number, but requires a full calculation for each set of twist angles, which can grow very quickly. For example, using 10 twist angles in each direction requires 1000 calculations. To see the effects of twist averaging, it's easy to calculate the kinetic energy per particle and the Hartree-Fock energy per particle, which avoids the full CCD calculation. These calculations can be compared to the exact values for infinite matter, which are calculated by integrating the the relevent values up to the fermi surface.

$$\mathrm{T_{inf}} = \frac{3\hbar^2 k_f^2}{10m} \tag{8.92}$$

$$\mathrm{HF_{inf}} = \frac{1}{(2\pi)^6}\frac{L^3}{2\rho}\int_0^{k_f} d\mathbf{k}_1 \int_0^{k_f} d\mathbf{k}_2 \, \langle \mathbf{k}_1\mathbf{k}_2|\hat{v}|\mathbf{k}_1\mathbf{k}_2\rangle \tag{8.93}$$

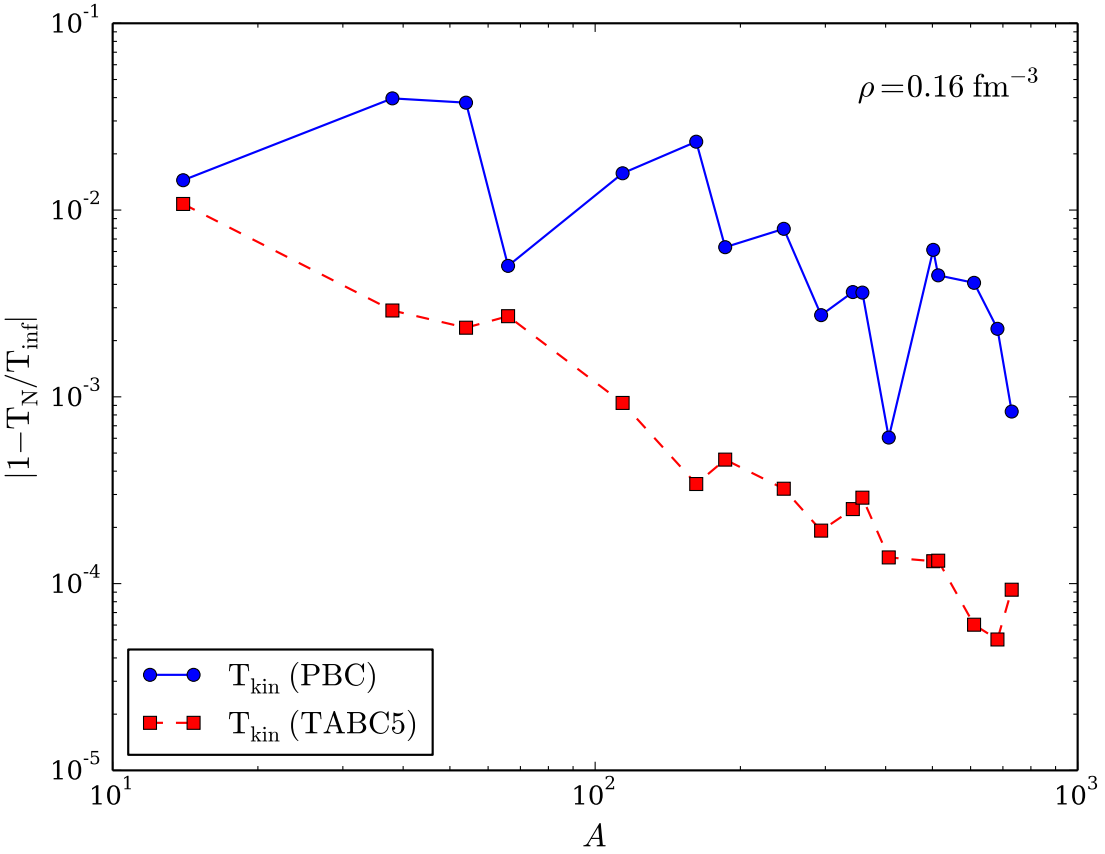

Fig. 8.3 Finite-size effects in the kinetic energy of pure neutron matter computed with the Minnesota potential as a function of the number of particles for both periodic boundary conditions and twist-averaged boundary conditions.

8.9 Conclusions

8.10 Exercises

8.1.

Acknowledgements If you want to include acknowledgments of assistance and the like at the end of an individual chapter please use the `acknowledgement` environment – it will automatically render Springer's preferred layout.

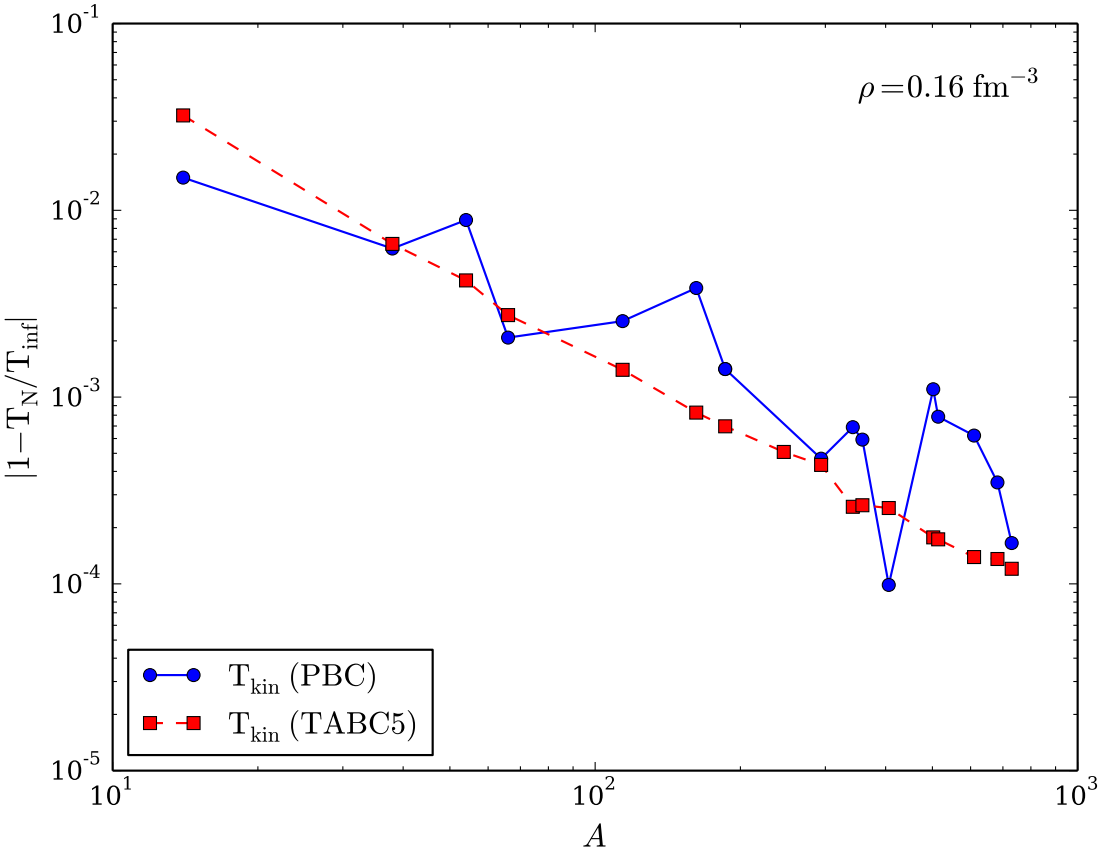

Fig. 8.4 Finite-size effects in the Hartree-Fock energy of pure neutron matter computed with the Minnesota potential as a function of the number of particles for both periodic boundary conditions and twist-averaged boundary conditions.

Chapter 9
Variational and diffusion Monte Carlo approaches to the nuclear few- and many-body problem

Francesco Pederiva

Abstract Each chapter should be preceded by an abstract (10–15 lines long) that summarizes the content. The abstract will appear *online* at www.SpringerLink.com and be available with unrestricted access. This allows unregistered users to read the abstract as a teaser for the complete chapter. As a general rule the abstracts will not appear in the printed version of your book unless it is the style of your particular book or that of the series to which your book belongs.

Please use the 'starred' version of the new Springer abstract command for typesetting the text of the online abstracts (cf. source file of this chapter template abstract) and include them with the source files of your manuscript. Use the plain abstract command if the abstract is also to appear in the printed version of the book.

9.1 The Nuclear few- and many-body problem

9.2 Methods for bound states based on the variational principle I:The No Core Shell Model (NCSM)

9.3 Methods for bound states based on the variational principle II:The Hyperspherical Harmonics (HH) method

9.4 Methods for reactions involving continuum states I:Perturbation induced reactions and integral transforms

9.5 Methods for reactions involving continuum states II:The continuum state problem reduced to a bound state problem

Acknowledgements If you want to include acknowledgments of assistance and the like at the end of an individual chapter please use the acknowledgement environment – it will automatically render Springer's preferred layout.

Francesco Pederiva
Name of institution and address, e-mail: name@email.address

Chapter 10
In-medium SRG approaches to infinite nuclear matter

Scott K. Bogner, Heiko Hergert, Titus Morris, Nathan Parzuchowski, and Fei Yuan

Abstract Each chapter should be preceded by an abstract (10–15 lines long) that summarizes the content. The abstract will appear *online* at `www.SpringerLink.com` and be available with unrestricted access. This allows unregistered users to read the abstract as a teaser for the complete chapter. As a general rule the abstracts will not appear in the printed version of your book unless it is the style of your particular book or that of the series to which your book belongs.

Please use the 'starred' version of the new Springer `abstract` command for typesetting the text of the online abstracts (cf. source file of this chapter template `abstract`) and include them with the source files of your manuscript. Use the plain `abstract` command if the abstract is also to appear in the printed version of the book.

10.1 Introduction

10.2 The similarity renormalization group approach

10.3 In-medium SRG studies of infinite matter

Acknowledgements If you want to include acknowledgments of assistance and the like at the end of an individual chapter please use the `acknowledgement` environment – it will automatically render Springer's preferred layout.

Scott Bogner
Department of Physics and Astronomy and National Superconducting Cyclotron Laboratory, Michigan State University, East Lansing, Michigan USA, e-mail: `bogner@nscl.msu.edu`,

Heiko Hergert
Department of Physics and Astronomy and National Superconducting Cyclotron Laboratory, Michigan State University, East Lansing, Michigan USA, e-mail: `hergert@nscl.msu.edu`,

Titus Morris
Department of Physics and Astronomy and National Superconducting Cyclotron Laboratory, Michigan State University, East Lansing, Michigan USA, e-mail: `morrist@nscl.msu.edu`,

Nathan Parzuchowski
Department of Physics and Astronomy and National Superconducting Cyclotron Laboratory, Michigan State University, East Lansing, Michigan USA, e-mail: `parzuchowski@frib.msu.edu`,

Fei Yuan
Department of Physics and Astronomy and National Superconducting Cyclotron Laboratory, Michigan State University, East Lansing, Michigan USA, e-mail: `parzuchowski@frib.msu.edu`

Chapter 11
Concluding remarks and perspectives

Morten Hjorth-Jensen, Maria Paola Lombardo, and Ubirajara van Kolck

Abstract Here Morten the Roman-Viking (who has never admitted his Norse roots) goes finally berserk in a classical Norse way and and Bira, clad in his befitting apologetic suit, presents himself as the true messiah of EFT and shouts stand up all ye infidels and hail the master. Halleluja and amen. Maria Paola is left speechless and runs for shelter somewhere in lovely Frascati (we envy her).

11.1 Concluding remarks

11.2 Perspectives

Morten Hjorth-Jensen
Department of Physics and Astronomy and National Superconducting Cyclotron Laboratory, Michigan State University, East Lansing, Michigan USA and Department of Physics, University of Oslo, Oslo, Norway, e-mail: hjensen@msu.edu,

Maria Paola Lombardo
Name and address of institution(s), e-mail: mariapaola.lombardo@lnf.infn.it,

Ubirajara van Kolck
Name and address of institution(s), e-mail: vankolck@ipno.in2p3.fr

References

1. R.P. Feynman, A.R. Hibbs, *Quantum Mechanics and Path Integrals* (McGraw-Hill, 1965)
2. N. Metropolis, A.W. Rosenbluth, M.N. Rosenbluth, A.H. Teller, E. Teller, J. Chem. Phys. **21**, 1087 (1953). DOI 10.1063/1.1699114
3. M. Creutz, B. Freedman, Annals Phys. **132**, 427 (1981). DOI 10.1016/0003-4916(81)90074-9
4. E.V. Shuryak, O.V. Zhirov, Nucl. Phys. **B242**, 393 (1984). DOI 10.1016/0550-3213(84)90401-2
5. E.V. Shuryak, Nucl. Phys. **B302**, 621 (1988). DOI 10.1016/0550-3213(88)90191-5
6. T. Schäfer, Instantons and Monte Carlo methods in quantum mechanics (2004). ArXive:hep-lat/0411010
7. M. Jarrell, J.E. Gubernatis, Phys. Rept. **269**, 133 (1996). DOI 10.1016/0370-1573(95)00074-7
8. M. Asakawa, T. Hatsuda, Y. Nakahara, Prog. Part. Nucl. Phys. **46**, 459 (2001). DOI 10.1016/S0146-6410(01)00150-8
9. C. Jarzynski, Physical Review Letters **78**, 2690 (1997). DOI 10.1103/PhysRevLett.78.2690
10. D.J. Gross, F. Wilczek, Phys.Rev.Lett. **30**, 1343 (1973). DOI 10.1103/PhysRevLett.30.1343
11. H.D. Politzer, Phys.Rev.Lett. **30**, 1346 (1973). DOI 10.1103/PhysRevLett.30.1346
12. S.R. Coleman, E.J. Weinberg, Phys.Rev. **D7**, 1888 (1973). DOI 10.1103/PhysRevD.7.1888
13. K. Nakamura, et al., J. Phys. **G37**, 075021 (2010). DOI 10.1088/0954-3899/37/7A/075021
14. M.G. Alford, A. Schmitt, K. Rajagopal, T. Schäfer, Rev. Mod. Phys. **80**, 1455 (2008). DOI 10.1103/RevModPhys.80.1455
15. A. Adams, L.D. Carr, T. Schäfer, P. Steinberg, J.E. Thomas, New J. Phys. **14**, 115009 (2012). DOI 10.1088/1367-2630/14/11/115009
16. P. Braun-Munzinger, V. Koch, T. Schäfer, J. Stachel, Phys. Rept. **621**, 76 (2016). DOI 10.1016/j.physrep.2015.12.003
17. M. Gell-Mann, R.J. Oakes, B. Renner, Phys. Rev. **175**, 2195 (1968). DOI 10.1103/PhysRev.175.2195
18. S.R. Coleman, E. Witten, Phys. Rev. Lett. **45**, 100 (1980). DOI 10.1103/PhysRevLett.45.100
19. G. 't Hooft, NATO Sci. Ser. B **59**, 135 (1980)
20. E.V. Shuryak, Sov. Phys. JETP **47**, 212 (1978). [Zh. Eksp. Teor. Fiz.74,408(1978)]
21. E.V. Shuryak, Phys. Lett. **B78**, 150 (1978). DOI 10.1016/0370-2693(78)90370-2. [Yad. Fiz.28,796(1978)]
22. A.D. Linde, Phys. Lett. **B96**, 289 (1980). DOI 10.1016/0370-2693(80)90769-8
23. R.D. Pisarski, F. Wilczek, Phys. Rev. **D29**, 338 (1984). DOI 10.1103/PhysRevD.29.338
24. Y. Aoki, G. Endrodi, Z. Fodor, S.D. Katz, K.K. Szabo, Nature **443**, 675 (2006). DOI 10.1038/nature05120
25. A. Bazavov, et al., Phys. Rev. **D85**, 054503 (2012). DOI 10.1103/PhysRevD.85.054503
26. Y. Aoki, Z. Fodor, S.D. Katz, K.K. Szabo, Phys. Lett. **B643**, 46 (2006). DOI 10.1016/j.physletb.2006.10.021
27. Y. Aoki, S. Borsanyi, S. Durr, Z. Fodor, S.D. Katz, S. Krieg, K.K. Szabo, JHEP **06**, 088 (2009). DOI 10.1088/1126-6708/2009/06/088
28. A. Bazavov, et al., Phys. Rev. **D90**(9), 094503 (2014). DOI 10.1103/PhysRevD.90.094503
29. M.A. Stephanov, Prog. Theor. Phys. Suppl. **153**, 139 (2004)
30. Z. Fodor, S.D. Katz, JHEP **03**, 014 (2002)
31. C. Allton, S. Ejiri, S. Hands, O. Kaczmarek, F. Karsch, et al., Phys.Rev. **D66**, 074507 (2002). DOI 10.1103/PhysRevD.66.074507
32. F. Karsch, C.R. Allton, S. Ejiri, S.J. Hands, O. Kaczmarek, E. Laermann, C. Schmidt, Nucl. Phys. Proc. Suppl. **129**, 614 (2004). DOI 10.1016/S0920-5632(03)02659-8. [,614(2003)]
33. Z. Fodor, S. Katz, JHEP **0404**, 050 (2004). DOI 10.1088/1126-6708/2004/04/050
34. R.V. Gavai, S. Gupta, Phys. Rev. **D78**, 114503 (2008). DOI 10.1103/PhysRevD.78.114503
35. S. Datta, R.V. Gavai, S. Gupta, Nucl. Phys. **A904-905**, 883c (2013). DOI 10.1016/j.nuclphysa.2013.02.156
36. P. de Forcrand, O. Philipsen, Phys. Rev. Lett. **105**, 152001 (2010). DOI 10.1103/PhysRevLett.105.152001
37. M.A. Stephanov, K. Rajagopal, E.V. Shuryak, Phys. Rev. Lett. **81**, 4816 (1998)
38. G. Sauer, H. Chandra, U. Mosel, Nucl. Phys. **A264**, 221 (1976). DOI 10.1016/0375-9474(76)90429-2
39. J. Pochodzalla, et al., Phys. Rev. Lett. **75**, 1040 (1995). DOI 10.1103/PhysRevLett.75.1040
40. J.B. Elliott, P.T. Lake, L.G. Moretto, L. Phair, Phys. Rev. **C87**(5), 054622 (2013). DOI 10.1103/PhysRevC.87.054622
41. M.G. Alford, K. Rajagopal, F. Wilczek, Nucl. Phys. **B537**, 443 (1999). DOI 10.1016/S0550-3213(98)00668-3
42. T. Schäfer, Nucl. Phys. **B575**, 269 (2000). DOI 10.1016/S0550-3213(00)00063-8
43. T. Schäfer, F. Wilczek, Phys. Rev. Lett. **82**, 3956 (1999). DOI 10.1103/PhysRevLett.82.3956
44. T. Hatsuda, M. Tachibana, N. Yamamoto, G. Baym, Phys. Rev. Lett. **97**, 122001 (2006). DOI 10.1103/PhysRevLett.97.122001
45. M. Creutz, *Quarks, Gluons, and Lattices* (Cambridge University Press, 1983)
46. I. Montvay, G. Münster, *Quantum Fields on a Lattice* (Cambridge University Press, 1994)
47. J. Smit, *Introduction to Quantum Fields on a Lattice* (Cambridge University Press, 2002)

48. C. Gattringer, C.B. Lang, *Quantum Chromodynamics on the Lattice* (Springer, 2009)
49. H.W. Lin, H.B. Meyer, *Lattice QCD for Nuclear Physics* (Springer, 2014)
50. Z. Fodor, S.D. Katz, The Phase diagram of quantum chromodynamics (2009). ArXiv:0908.3341
51. H.T. Ding, F. Karsch, S. Mukherjee, Thermodynamics of strong-interaction matter from Lattice QCD (2015). ArXiv:1504.05274
52. K.G. Wilson, Phys. Rev. **D10**, 2445 (1974). DOI 10.1103/PhysRevD.10.2445. [,45(1974)]
53. F. Mezzadri, How to generate random matrices from the classical compact groups (2006). ArXiv:math-ph/0609050
54. A. Hasenfratz, P. Hasenfratz, Phys. Lett. **B93**, 165 (1980). DOI 10.1016/0370-2693(80)90118-5. [,241(1980)]
55. G.P. Lepage, in *Strong interactions at low and intermediate energies. Proceedings, 13th Annual Hampton University Graduate Studies, HUGS'98, Newport News, USA, May 26-June 12, 1998* (1998), pp. 49–90
56. U. Wolff, Phys. Rev. Lett. **62**, 361 (1989). DOI 10.1103/PhysRevLett.62.361
57. J.B. Kogut, L. Susskind, Phys. Rev. **D11**, 395 (1975). DOI 10.1103/PhysRevD.11.395
58. D.B. Kaplan, Phys. Lett. **B288**, 342 (1992). DOI 10.1016/0370-2693(92)91112-M
59. H. Neuberger, Phys. Lett. **B417**, 141 (1998). DOI 10.1016/S0370-2693(97)01368-3
60. M. Luscher, in *Modern perspectives in lattice QCD: Quantum field theory and high performance computing. Proceedings, International School, 93rd Session, Les Houches, France, August 3-28, 2009* (2010), pp. 331–399
61. E. Endress, C. Pena, K. Sivalingam, Comput. Phys. Commun. **195**, 35 (2015). DOI 10.1016/j.cpc.2015.04.017
62. V. Dick, F. Karsch, E. Laermann, S. Mukherjee, S. Sharma, Phys. Rev. **D91**(9), 094504 (2015). DOI 10.1103/PhysRevD.91.094504
63. M. Teper, Phys. Lett. **B171**, 86 (1986). DOI 10.1016/0370-2693(86)91004-X
64. M. Lüscher, JHEP **08**, 071 (2010). DOI 10.1007/JHEP08(2010)071,10.1007/JHEP03(2014)092. [Erratum: JHEP03,092(2014)]
65. A.A. Belavin, A.M. Polyakov, A.S. Schwartz, Yu.S. Tyupkin, Phys. Lett. **B59**, 85 (1975). DOI 10.1016/0370-2693(75)90163-X
66. T. Schäfer, E.V. Shuryak, Rev. Mod. Phys. **70**, 323 (1998). DOI 10.1103/RevModPhys.70.323
67. L. Del Debbio, L. Giusti, C. Pica, Phys. Rev. Lett. **94**, 032003 (2005). DOI 10.1103/PhysRevLett.94.032003
68. M. Ce, C. Consonni, G.P. Engel, L. Giusti, PoS **LATTICE2014**, 353 (2014)
69. E. Poppitz, T. Schäfer, M. Ünsal, JHEP **03**, 087 (2013). DOI 10.1007/JHEP03(2013)087
70. T. Banks, A. Casher, Nucl. Phys. **B169**, 103 (1980). DOI 10.1016/0550-3213(80)90255-2
71. P.H. Ginsparg, K.G. Wilson, Phys. Rev. **D25**, 2649 (1982). DOI 10.1103/PhysRevD.25.2649
72. A. Cherman, T. Schäfer, M. Unsal, Chiral Lagrangian from Duality and Monopole Operators in Compactified QCD (2016). ArXiv:1604.06108
73. M. Cristoforetti, F. Di Renzo, L. Scorzato, Phys. Rev. **D86**, 074506 (2012). DOI 10.1103/PhysRevD.86.074506
74. G. Aarts, L. Bongiovanni, E. Seiler, D. Sexty, JHEP **10**, 159 (2014). DOI 10.1007/JHEP10(2014)159
75. G. Aarts, E. Seiler, I.O. Stamatescu, Phys. Rev. **D81**, 054508 (2010). DOI 10.1103/PhysRevD.81.054508
76. D. Sexty, Phys. Lett. **B729**, 108 (2014). DOI 10.1016/j.physletb.2014.01.019
77. T. Kloiber, C. Gattringer, PoS **LATTICE2013**, 206 (2014)
78. T. Schäfer, D. Teaney, Rept. Prog. Phys. **72**, 126001 (2009). DOI 10.1088/0034-4885/72/12/126001
79. T. Schäfer, Ann. Rev. Nucl. Part. Sci. **64**, 125 (2014). DOI 10.1146/annurev-nucl-102313-025439
80. F. Karsch, H.W. Wyld, Phys. Rev. **D35**, 2518 (1987). DOI 10.1103/PhysRevD.35.2518
81. H.B. Meyer, Phys. Rev. **D76**, 101701 (2007). DOI 10.1103/PhysRevD.76.101701
82. H.B. Meyer, Phys. Rev. Lett. **100**, 162001 (2008). DOI 10.1103/PhysRevLett.100.162001
83. S. Sakai, A. Nakamura, PoS **LAT2007**, 221 (2007). DOI 10.1063/1.2729742. [AIP Conf. Proc.893,5(2007)]
84. G. Aarts, C. Allton, J. Foley, S. Hands, S. Kim, Phys. Rev. Lett. **99**, 022002 (2007). DOI 10.1103/PhysRevLett.99.022002
85. G. Aarts, PoS **LAT2007**, 001 (2007)
86. G. Aarts, C. Allton, J. Foley, S. Hands, S. Kim, Nucl. Phys. **A785**, 202 (2007). DOI 10.1016/j.nuclphysa.2006.11.148
87. H.B. Meyer, JHEP **08**, 031 (2008). DOI 10.1088/1126-6708/2008/08/031
88. P. Romatschke, D.T. Son, Phys. Rev. **D80**, 065021 (2009). DOI 10.1103/PhysRevD.80.065021
89. P.B. Arnold, G.D. Moore, L.G. Yaffe, JHEP **11**, 001 (2000). DOI 10.1088/1126-6708/2000/11/001
90. P. Kovtun, D.T. Son, A.O. Starinets, Phys. Rev. Lett. **94**, 111601 (2005). DOI 10.1103/PhysRevLett.94.111601
91. P. Romatschke, Int. J. Mod. Phys. **E19**, 1 (2010). DOI 10.1142/S0218301310014613
92. L. Rezzolla, O. Zanotti, *Relativistic Hydrodynamics* (Oxford University Press, 2013)

93. S. Jeon, U. Heinz, Int. J. Mod. Phys. **E24**(10), 1530010 (2015). DOI 10.1142/S0218301315300106
94. P. Colella, P.R. Woodward, J. Comp. Phys. **54**, 174 (1984)
95. J.M. Blondin, E.A. Lufkin, Astrophys. J. Supp. Ser. **88**, 589 (1993)
96. T. Schäfer, Phys. Rev. **A82**, 063629 (2010). DOI 10.1103/PhysRevA.82.063629
97. W. Florkowski, R. Ryblewski, Phys. Rev. **C83**, 034907 (2011). DOI 10.1103/PhysRevC.83.034907
98. M. Martinez, M. Strickland, Nucl. Phys. **A848**, 183 (2010). DOI 10.1016/j.nuclphysa.2010.08.011
99. M. Bluhm, T. Schäfer, Phys. Rev. **A92**(4), 043602 (2015). DOI 10.1103/PhysRevA.92.043602
100. M. Bluhm, T. Schäfer, Phys. Rev. Lett. **116**(11), 115301 (2016). DOI 10.1103/PhysRevLett.116.115301
101. P. Romatschke, M. Mendoza, S. Succi, Phys. Rev. **C84**, 034903 (2011). DOI 10.1103/PhysRevC.84.034903
102. J. Brewer, M. Mendoza, R.E. Young, P. Romatschke, Phys. Rev. **A93**(1), 013618 (2016). DOI 10.1103/PhysRevA.93.013618
103. L.P. Kadanoff, G. Baym, *Quantum Statistical Mechanics* (W. A. Benjamin, 1962)
104. G.F. Bertsch, S. Das Gupta, Phys. Rept. **160**, 189 (1988). DOI 10.1016/0370-1573(88)90170-6
105. T. Lepers, D. Davesne, S. Chiacchiera, M. Urban, Phys. Rev. **A82**, 023609 (2010). DOI 10.1103/PhysRevA.82.023609
106. S.A. Bass, et al., Prog. Part. Nucl. Phys. **41**, 255 (1998). DOI 10.1016/S0146-6410(98)00058-1. [Prog. Part. Nucl. Phys.41,225(1998)]
107. O. Buss, T. Gaitanos, K. Gallmeister, H. van Hees, M. Kaskulov, O. Lalakulich, A.B. Larionov, T. Leitner, J. Weil, U. Mosel, Phys. Rept. **512**, 1 (2012). DOI 10.1016/j.physrep.2011.12.001
108. W. Ehehalt, W. Cassing, Nucl. Phys. **A602**, 449 (1996). DOI 10.1016/0375-9474(96)00097-8
109. K. Geiger, B. Muller, Nucl. Phys. **B369**, 600 (1992). DOI 10.1016/0550-3213(92)90280-O
110. Z. Xu, C. Greiner, Phys. Rev. **C71**, 064901 (2005). DOI 10.1103/PhysRevC.71.064901
111. L.D. McLerran, R. Venugopalan, Phys. Rev. **D49**, 2233 (1994). DOI 10.1103/PhysRevD.49.2233
112. A.H. Mueller, D.T. Son, Phys. Lett. **B582**, 279 (2004). DOI 10.1016/j.physletb.2003.12.047
113. S. Mrowczynski, B. Schenke, M. Strickland, (2016)
114. J. Berges, A. Rothkopf, J. Schmidt, Phys. Rev. Lett. **101**, 041603 (2008). DOI 10.1103/PhysRevLett.101.041603
115. K. Dusling, T. Epelbaum, F. Gelis, R. Venugopalan, Nucl. Phys. **A850**, 69 (2011). DOI 10.1016/j.nuclphysa.2010.11.009
116. D.F. Litim, C. Manuel, Phys. Rept. **364**, 451 (2002). DOI 10.1016/S0370-1573(02)00015-7
117. S.K. Wong, Nuovo Cim. **A65**, 689 (1970). DOI 10.1007/BF02892134
118. C.R. Hu, B. Muller, Phys. Lett. **B409**, 377 (1997). DOI 10.1016/S0370-2693(97)00851-4
119. J.M. Maldacena, Int. J. Theor. Phys. **38**, 1113 (1999). DOI 10.1023/A:1026654312961. [Adv. Theor. Math. Phys.2,231(1998)]
120. D.T. Son, A.O. Starinets, Ann. Rev. Nucl. Part. Sci. **57**, 95 (2007). DOI 10.1146/annurev.nucl.57.090506.123120
121. S.S. Gubser, A. Karch, Ann. Rev. Nucl. Part. Sci. **59**, 145 (2009). DOI 10.1146/annurev.nucl.010909.083602
122. J. Casalderrey-Solana, H. Liu, D. Mateos, K. Rajagopal, U.A. Wiedemann, (2011)
123. O. DeWolfe, S.S. Gubser, C. Rosen, D. Teaney, Prog. Part. Nucl. Phys. **75**, 86 (2014). DOI 10.1016/j.ppnp.2013.11.001
124. G. Policastro, D.T. Son, A.O. Starinets, JHEP **09**, 043 (2002). DOI 10.1088/1126-6708/2002/09/043
125. D. Teaney, Phys. Rev. **D74**, 045025 (2006). DOI 10.1103/PhysRevD.74.045025
126. D.T. Son, A.O. Starinets, JHEP **03**, 052 (2006). DOI 10.1088/1126-6708/2006/03/052
127. P.M. Chesler, L.G. Yaffe, Phys. Rev. Lett. **106**, 021601 (2011). DOI 10.1103/PhysRevLett.106.021601
128. P.M. Chesler, L.G. Yaffe, JHEP **07**, 086 (2014). DOI 10.1007/JHEP07(2014)086
129. M. Rangamani, Class. Quant. Grav. **26**, 224003 (2009). DOI 10.1088/0264-9381/26/22/224003
130. A. Jaffe, E. Witten, Quantum Yang Mills Theory, Official Description of Millenium Prize Problems (2000). www.claymath.org
131. C. Fefferman, Existence and smoothness of the Navier-Stokes Equation, Official Description of Millenium Prize Problems (2000). www.claymath.org
132. C. Mouhot, C. Villani, Acta Mathematica **207**, 29 (2011). DOI 10.1007/s11511-011-0068-9
133. G. Perelman, The entropy formula for the Ricci flow and its geometric applications (2002). ArXiv:math/0211159 [math.DG]
134. C. Shen, Z. Qiu, H. Song, J. Bernhard, S. Bass, U. Heinz, Comput. Phys. Commun. **199**, 61 (2016). DOI 10.1016/j.cpc.2015.08.039
135. M. Creutz, Computers in Science & Engineering **March/April 2004**, 80 (2004)
136. S. Weinberg, Phys. Lett. **B251**, 288 (1990)
137. S. Weinberg, Nucl. Phys. **B363**, 3 (1991)
138. C. Ordonez, U. van Kolck, Phys. Lett. **B291**, 459 (1992)
139. C. Ordonez, L. Ray, U. van Kolck, Phys. Rev. Lett. **72**, 1982 (1994)

140. U. van Kolck, Phys. Rev. **C49**, 2932 (1994)
141. E. Epelbaum, W. Glöckle, U.G. Meißner, Phys. Lett. **B439**, 1 (1998)
142. E. Epelbaum, W. Glöckle, U.G. Meißner, Nucl. Phys. **A637**, 107 (1998)
143. P.F. Bedaque, U. van Kolck, Ann. Rev. Nucl. Part. Sci. **52**, 339 (2002)
144. E. Epelbaum, H.W. Hammer, U.G. Meißner, Rev. Mod. Phys. **81**, 1773 (2009)
145. D. Lee, Prog. Part. Nucl. Phys. **63**, 117 (2009)
146. J.E. Drut, A.N. Nicholson, J. Phys. G: Nucl. Part. Phys. **40**(4), 043101 (2013). DOI 10.1088/0954-3899/40/4/043101
147. J. Hubbard, Phys. Rev. Lett. **3**, 77 (1959)
148. R.L. Stratonovich, Soviet Phys. Doklady **2**, 416 (1958)
149. D.H. Weingarten, D.N. Petcher, Phys. Lett. **B99**, 333 (1981)
150. R.T. Scalettar, D.J. Scalapino, R.L. Sugar, Phys. Rev. **B34**, 7911 (1986)
151. S. Gottlieb, W. Liu, D. Toussaint, R.L. Renken, R.L. Sugar, Phys. Rev. **D35**, 2531 (1987)
152. S. Duane, A.D. Kennedy, B.J. Pendleton, D. Roweth, Phys. Lett. **B195**, 216 (1987)
153. H.M. Müller, S.E. Koonin, R. Seki, U. van Kolck, Phys. Rev. **C61**, 044320 (2000)
154. D. Lee, B. Borasoy, T. Schäfer, Phys. Rev. **C70**, 014007 (2004)
155. D. Lee, T. Schäfer, Phys. Rev. **C72**, 024006 (2005)
156. D. Lee, T. Schäfer, Phys. Rev. **C73**, 015201 (2006)
157. D. Lee, T. Schäfer, Phys. Rev. **C73**, 015202 (2006)
158. B. Borasoy, H. Krebs, D. Lee, U.G. Meißner, Nucl. Phys. **A768**, 179 (2006)
159. B. Borasoy, E. Epelbaum, H. Krebs, D. Lee, U.G. Meißner, Eur. Phys. J. **A31**, 105 (2007)
160. B. Borasoy, E. Epelbaum, H. Krebs, D. Lee, U.G. Meißner, Eur. Phys. J. **A35**, 343 (2008)
161. B. Borasoy, E. Epelbaum, H. Krebs, D. Lee, U.G. Meißner, Eur. Phys. J. **A35**, 357 (2008)
162. G. Wlazłowski, J.W. Holt, S. Moroz, A. Bulgac, K.J. Roche, Phys. Rev. Lett. **113**(18), 182503 (2014). DOI 10.1103/PhysRevLett.113.182503
163. E. Epelbaum, H. Krebs, D. Lee, U.G. Meißner, Eur. Phys. J. **A41**, 125 (2009)
164. E. Epelbaum, H. Krebs, D. Lee, U.G. Meißner, Phys. Rev. Lett. **104**, 142501 (2010)
165. E. Epelbaum, H. Krebs, D. Lee, U.G. Meißner, Phys. Rev. Lett. **106**, 192501 (2011). DOI 10.1103/PhysRevLett.106.192501
166. E. Epelbaum, H. Krebs, T. Lähde, D. Lee, U.G. Meißner, Phys. Rev. Lett. **109**, 252501 (2012). DOI 10.1103/PhysRevLett.109.252501
167. E. Epelbaum, H. Krebs, T.A. Lähde, D. Lee, U.G. Meißner, Phys. Rev. Lett. **110**, 112502 (2013). DOI 10.1103/PhysRevLett.110.112502
168. T.A. Lähde, E. Epelbaum, H. Krebs, D. Lee, U.G. Meißner, G. Rupak, Phys. Lett. **B732**, 110 (2014). DOI 10.1016/j.physletb.2014.03.023
169. E. Epelbaum, H. Krebs, T.A. Lähde, D. Lee, U.G. Meißner, G. Rupak, Phys. Rev. Lett. **112**(10), 102501 (2014). DOI 10.1103/PhysRevLett.112.102501
170. S. Elhatisari, et al., (2016)
171. G. Rupak, D. Lee, Phys. Rev. Lett. **111**(3), 032502 (2013). DOI 10.1103/PhysRevLett.111.032502
172. G. Rupak, P. Ravi, Phys. Lett. **B741**, 301 (2014). DOI 10.1016/j.physletb.2014.12.055
173. S. Elhatisari, D. Lee, G. Rupak, E. Epelbaum, H. Krebs, T.A. Lähde, T. Luu, U.G. Meißner, Nature **528**, 111 (2015). DOI 10.1038/nature16067
174. M. Lüscher, Commun. Math. Phys. **104**, 177 (1986)
175. M. Lüscher, Commun. Math. Phys. **105**, 153 (1986)
176. M. Lüscher, Nucl. Phys. **B354**, 531 (1991)
177. B. Borasoy, E. Epelbaum, H. Krebs, D. Lee, U.G. Meißner, Eur. Phys. J. **A34**, 185 (2007)
178. J. Carlson, V. Pandharipande, R. Wiringa, Nucl. Phys. A **424**(1), 47 (1984). DOI http://dx.doi.org/10.1016/0375-9474(84)90127-1. URL `http://www.sciencedirect.com/science/article/pii/0375947484901271`
179. B.N. Lu, T.A. Lähde, D. Lee, U.G. Meißner, (2015)
180. M. Pine, D. Lee, G. Rupak, Eur. Phys. J. **A49**, 151 (2013). DOI 10.1140/epja/i2013-13151-3
181. S. Elhatisari, D. Lee, Phys. Rev. **C90**(6), 064001 (2014). DOI 10.1103/PhysRevC.90.064001
182. A. Rokash, M. Pine, S. Elhatisari, D. Lee, E. Epelbaum, et al., (2015)
183. M. Creutz, Phys. Rev. **D38**, 1228 (1988)
184. M. Creutz, Found. Phys. **30**, 487 (2000)
185. J. Carlson, S. Gandolfi, F. Pederiva, S.C. Pieper, R. Schiavilla, K.E. Schmidt, R.B. Wiringa, Rev. Mod. Phys. **87**, 1067 (2015). DOI 10.1103/RevModPhys.87.1067